



**NEW GENERALIZED ALPHA PLANE FORMULATION FOR
NUMERICAL DIFFERENTIAL PROTECTION APPLICATIONS**

RÔMULO GONÇALVES BAINY

**PHD THESIS
ON ELECTRICAL ENGINEERING
ELECTRICAL ENGINEERING DEPARTMENT**

**TECHNOLOGY FACULTY
UNIVERSITY OF BRASÍLIA**

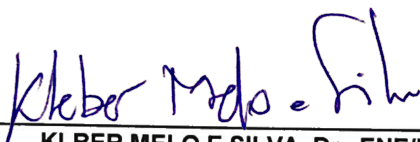
UNIVERSIDADE DE BRASÍLIA
FACULDADE DE TECNOLOGIA
DEPARTAMENTO DE ENGENHARIA ELÉTRICA

**NEW GENERALIZED ALPHA PLANE FORMULATION FOR
NUMERICAL DIFFERENTIAL PROTECTION
APPLICATIONS**

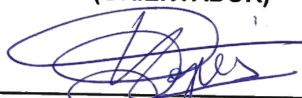
RÔMULO GONÇALVES BAINY

TESE DE DOUTORADO SUBMETIDA AO DEPARTAMENTO DE ENGENHARIA ELÉTRICA DA
FACULDADE DE TECNOLOGIA DA UNIVERSIDADE DE BRASÍLIA, COMO PARTE DOS
REQUISITOS NECESSÁRIOS PARA A OBTENÇÃO DO GRAU DE DOUTOR.

APROVADA POR:



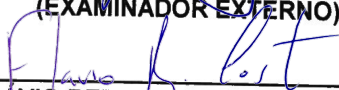
KLBER MELO E SILVA, Dr., ENE/UNB
(ORIENTADOR)



FELIPE VIGORINO LOPES, Dr., ENE/UNB
(EXAMINADOR INTERNO)



MÁRIO OLESKOVICZ, Dr., USP/EESC
(EXAMINADOR EXTERNO)



FLAVIO BEZERRA COSTA, Dr., UFRN
(EXAMINADOR EXTERNO)

Brasília, 22 de fevereiro de 2019.

FICHA CATALOGRÁFICA

BAINY, RÔMULO GONÇALVES

New Generalized Alpha Plane Formulation for Numerical Differential Protection Applications.
[Distrito Federal] 2019.

xi, 83p., 210 x 297 mm (ENE/FT/UnB, Doutor em Engenharia Elétrica).

Tese de Doutorado – Universidade de Brasília. Faculdade de Tecnologia.

Departamento de Engenharia Elétrica

1. Proteção Diferencial

3. Equipamento de Múltiplos terminais

5. Barramento

I. ENE/FT/UnB

2. Plano Alfa Generalizado

4. Linha de Transmissão

6. Transformador

II. Título (série)

REFERÊNCIA BIBLIOGRÁFICA

BAINY, R. G. (2019). New Generalized Alpha Plane Formulation for Numerical Differential Protection Applications, Tese de Doutorado em Engenharia Elétrica, Publicação PPGE-140/2019, Departamento de Engenharia Elétrica, Universidade de Brasília, Brasília, DF, 101p.

CESSÃO DE DIREITOS

AUTOR: Rômulo Gonçalves Bairy

TÍTULO: New Generalized Alpha Plane Formulation for Numerical Differential Protection Applications.

GRAU: Doutor ANO: 2019

É concedida à Universidade de Brasília permissão para reproduzir cópias desta tese de doutorado e para emprestar ou vender tais cópias somente para propósitos acadêmicos e científicos. O autor reserva outros direitos de publicação e nenhuma parte desse trabalho de graduação pode ser reproduzida sem autorização por escrito do autor.

Rômulo Gonçalves Bairy

Departamento de Eng. Elétrica (ENE) - FT

Universidade de Brasília (UnB)

Campus Darcy Ribeiro

CEP 70919-970 - Brasília - DF - Brasil

DEDICATION

*Dedicated to my beloved parents, brother and sister
who have provided me encouragement and support throughout my studies.*

Rémulo Bairy

ACKNOWLEDGEMENTS

I would like to thank my advisor Dr. Kleber M. e Silva for giving me the opportunity to work on this thesis. I am greatly indebted for his encouragement, support and guidance given during this project. It is an honor and pleasure to have him as my advisor.

I am greatly thankful to Dr. Felipe V. Lopes for his fruitful discussions and valuable suggestions throughout this project. His approach of solving complicated problems with simplified analysis helped greatly as an inspiration for my academic life.

I am thankful to my fiance Sione for sharing her knowledge and providing her valuable guidance during crucial parts of this thesis.

Financial support through a scholarship supported by the Brazilian Coordination for Improvement of Higher Education Personnel - Brazil (CAPES) is greatly acknowledged.

This Phd thesis is part of a sandwich program with Washington State University - USA (WSU) and financial supported by Brazilian National Council for Scientific and Technological Development - Brazil (CNPq) through a scholarship (204317/2017-7).

RESUMO

A presente tese propõe uma nova formulação de Plano Alfa Generalizado (PAG) para proteção diferencial de equipamentos de múltiplos terminais. Como ponto de partida, a nova formulação de PAG foi baseada em duas outras estratégias reportadas na literatura. Ademais, a solução proposta deve atender dois importantes requisitos: 1) trajetória transitória direta e segura. 2) Ponto de repouso em regime permanente de falta ajustável. Para tanto, dois ajustes foram criados, juntos eles definem uma circunferência com centro e raio ajustável a qual corresponde a uma região de repouso para defeitos internos. O controle refinado resultante dessas duas configurações é capaz de trazer benefícios para a proteção diferencial, como por exemplo um melhor controle das trajetórias no plano alfa. Com o objetivo de avaliar o PAG proposto, o software *Alternative Transients Program* foi utilizado para simular uma vasta gama de condições especiais em quatro sistemas diferentes. Para tanto uma linha de transmissão de dois e três terminais, uma configuração de barramento e um transformador de potência foram utilizados para testar o novo PAG. As simulações realizadas foram divididas em análises transitórias – nas quais avalia-se o comportamento da proteção durante situações de curto-circuito – e análises de sensibilidade paramétrica, nas quais investiga-se a influência de cada um dos parâmetros envolvidos no curto-circuito durante o regime permanente de falta. Os resultados obtidos revelam que o PAG proposto provê uma alternativa apropriada, eficiente e segura para linhas de transmissão, barramentos e transformadores.

Palavras-chave: Proteção diferencial, plano alfa generalizado, equipamento de múltiplos terminais, linha de transmissão, barramento, transformador.

ABSTRACT

This thesis proposes a new Generalized Alpha Plane (GAP) formulation for differential protection of multi-terminal devices. As a starting point, the proposed GAP formulation is based on other two GAP strategies found in literature. Additionally, two main requirements for the proposed solution are defined: 1) Smooth/secure transient path; 2) adjustable settlement point during fault steady-state. In order to do so, two settings are created, together they define a circumference with adjustable center and radius which corresponds to a settlement region for internal faults. The refined control enabled by the two settings are therefore capable to bring benefits to differential protection, such as better control of overall behavior in an alpha plane. Aiming to evaluate the proposed GAP, Alternative Transients Program was used to simulate a wide variety of conditions in four different systems. Therefore, a two-terminal and three-terminal transmission line, a busbar arrangement, and a power transformer were chosen to test the proposed GAP strategy. The performed simulations were divided into transient analysis – in which the performance of the proposed algorithm during fault situation – and massive data analysis, in which the influence of each variable is analyzed for the fault steady state value. The obtained results reveal that proposed GAP is an appropriate, efficient and safe alternative for transmission lines, busbars, and transformers protection.

Keywords: Differential protection, generalized alpha plane, multi-terminal device, transmission line, busbar, power transformer.

CONTENTS

Table of Contents	i
List of Figures	iv
List of Tables	vii
List of Symbols	ix
Glossary	xi
Chapter 1 – Introduction	1
1.1 Background	1
1.2 Generalized Alpha Plane	4
1.2.1 GAP from Miller <i>et al.</i> (2010)	5
1.3 Motivation	7
1.4 Problem statement and Proposed Solution	7
1.5 Objective	8
1.6 Thesis Organization	8
Chapter 2 – Generalized Alpha Plane Formulation	10
2.1 Proposed Formulation	10
2.2 Setting η_1 and η_2	11
2.3 GAP Analysis	14
2.4 Study of variation of Γ_f and k_Δ	15
2.5 Silva & Bainy (2016) GAP versus new formulation	16
2.6 Summary	17
Chapter 3 – Application 1: Two-Terminal Transmission Line	18
3.1 Overview	18
3.2 Application Details	20
3.3 Transient Analysis	22

3.4	Massive Data Analysis	24
3.5	Summary	27
Chapter 4 – Application 2: Three-Terminals Transmission Line		29
4.1	Overview	29
4.2	Application Details	31
4.3	Transient Analysis	32
4.4	Massive Data Analysis	34
4.5	Summary	36
Chapter 5 – Application 3: Busbar Arrangement		38
5.1	Overview	38
5.2	Application Details	41
5.3	Transient Analysis	42
5.4	Massive Data Analysis	43
5.5	Summary	44
Chapter 6 – Application 4 - Power Transformer		46
6.1	Overview	46
6.2	Application Details	47
6.3	Transient Analysis	48
6.4	Massive Data Analysis	49
6.5	Summary	51
Chapter 7 – Conclusions and Future Work		52
7.1	Future Work	53
7.2	Publications during PhD	54
Bibliography		55
Appendix A – Differential Protection Basics		61
A.1	Differential Protection Fundamentals	62
A.2	Representation Planes	65
A.3	Enhanced Restraining Characteristic	67
Appendix B – Miller <i>et al.</i> (2010a) GAP Deduction		70

Appendix C – Silva <i>et al.</i> (2016) GAP Deduction	74
C.1 Mathematical Formulation	74
Appendix D – Short-circuit Contributions	77
D.1 Three-Phase Short-Circuit	80
D.2 Single-Phase Short-Circuit: AG	81
D.3 Phase-to-Phase Short-Circuit: BC	81
D.4 Phase-to-Phase-to-Ground Short-Circuit: BCT	82

LIST OF FIGURES

1.1	Planned power generation capacity increase - 2017 to 2022 (ONS, 2017a). (a) 2017; (b) 2022.	2
1.2	The GAP principle: (a) multi-terminal system; (b) two-terminal equivalent system.	4
2.1	Flowchart diagram of the protection scheme adapted from (BENMOUYAL, 2005)	12
2.2	Circle defined by Γ_f and k_Δ	13
2.3	Study of Γ_f and k_Δ variation.	15
3.1	Simulated Power System - 500 kV two-terminal Transmission Line	18
3.2	Simplified Representation of Transmission line Capacitive Current.	20
3.3	System 1 - 500 kV two-terminal Transmission Line.	21
3.4	Case 1.1 - BG (a) GAP <i>I</i> ; (b) GAP <i>II</i>	23
3.5	Case 1.2 - ABC (a) GAP <i>I</i> ; (b) GAP <i>II</i>	23
3.6	Case 1.3 - BG (a) GAP <i>I</i> ; (b) GAP <i>II</i>	24
3.7	Case 1.4 - BCG (a) GAP <i>I</i> ; (b) GAP <i>II</i>	24
3.8	Case 1.5 - ABC (a) GAP <i>I</i> ; (b) GAP <i>II</i>	25
3.9	Case 1.6 - AG (a) GAP <i>I</i> ; (b) GAP <i>II</i>	25
3.10	Case 1.7 - BG (a) GAP <i>I</i> ; (b) GAP <i>II</i>	26
3.11	Case 1.8 - BC (a) GAP <i>I</i> ; (b) GAP <i>II</i>	27
3.12	Case 1.9 - BC (a) GAP <i>I</i> ; (b) GAP <i>II</i>	27
4.1	Transmission line tapped by a generator and a substation.	29

4.2	Transmission line tapped by generator twice.	30
4.3	Example of 87L in a multi-terminal application.	31
4.4	System 2 - 500 kV three-terminal Transmission Line	32
4.5	Case 2.1 - ABC (a) GAP <i>I</i> ; (b) GAP <i>II</i>	33
4.6	Case 2.2 - BG (a) GAP <i>I</i> ; (b) GAP <i>II</i>	34
4.7	Case 2.3 - ABC (a) GAP <i>I</i> ; (b) GAP <i>II</i>	34
4.8	Case 2.4 - ABC (a) GAP <i>I</i> ; (b) GAP <i>II</i>	35
4.9	Case 2.5 - AG (a) GAP <i>I</i> ; (b) GAP <i>II</i>	36
4.10	Case 2.6 (a) GAP <i>I</i> ; (b) GAP <i>II</i>	36
5.1	Single Bus With Bus Sectionalizer (Tie Breaker)	38
5.2	Double Bus and Transfer Bus With Bus Coupler (Tie Breaker) and Outboard CTs.	39
5.3	System 3: Busbar Arrangement - 230 kV with six terminals.	41
5.4	Case 3.1 - ABC (a) GAP <i>I</i> ; (b) GAP <i>II</i>	42
5.5	Case 3.2 - AG (a) GAP <i>I</i> ; (b) GAP <i>II</i> (c)	43
5.6	Case 3.3 (a) GAP <i>I</i> ; (b) GAP <i>II</i>	44
5.7	Case 3.4 (a) GAP <i>I</i> ; (b) GAP <i>II</i>	44
6.1	System 4: power transformer Wye-Delta (230:69kV).	48
6.2	Case 4.1 - ABC (a) GAP <i>I</i> ; (b) GAP <i>II</i>	49
6.3	Case 4.2 - ABC (a) GAP <i>I</i> ; (b) GAP <i>II</i>	49
6.4	Case 4.3 - turn-to-turn (a) GAP <i>I</i> ; (b) GAP <i>II</i>	50
6.5	Case 4.4 - turn-to-earth (a) GAP <i>I</i> ; (b) GAP <i>II</i>	50
A.1	(a) Protected Zone. (b) Percentage Differential Relay. N_R e N_{OP} represent the number of turn of operating and restraining coils respectively.	62
A.2	Transient Path. (a) Operational Plane. (b) Alfa Plane.	65

A.3	Representation Planes: (a) Operational plane. (b) Alpha Plane.	66
A.4	Representation Planes Comparison (a) Operational Plane. (b) Alpha Plane. . .	67
A.5	Alpha Plane Areas. (a) Simple. (b) Rotation caused by channel time-delay compensation errors and the system impedance nonhomogeneity.	68
A.6	(a) Enhanced restraining characteristic. (b) Equal tolerance to Outfeed. (c) Equal tolerance to Channel time-delay.	69
B.1	GAP philosophy (MILLER <i>et al.</i> , 2010).	70
C.1	Multi-terminal equipment.	75
D.1	Unifiliars diagrams. (a) Short line model. (b) Zero sequence diagram. (c) Positive sequence diagram. (d) Negative sequence diagram.	78
D.2	Thévenin equivalentents. (a) Zero sequence. (b) Positive sequence. (c) Negative sequence.	79
D.3	Sequence circuits during a fault. (a) Zero sequence. (b) Positive sequence. (c) Negative sequence.	79

LIST OF TABLES

1.1	Partial shutdowns in Brazilian electrical system 2016 (ONS, 2013)	2
2.1	Comparison of 2016 and current formulation.	16
3.1	Application 1: Case Summary for Transient Analysis.	22
3.2	Criteria for Transient Analysis.	22
3.3	GAP identification names.	22
3.4	Application 1: Case Summary for Massive Data Analysis.	26
3.5	Criteria for Massive Data Analysis.	26
3.6	Application 1: Summary of Results	27
3.7	Application 1: Summary of Results	28
4.1	Application 2: Case Summary for Transient Analysis.	33
4.2	Variables interval of study for System 2	34
4.3	Application 2: Case Summary for Massive Data Analysis.	35
4.4	Application 2: Summary of Results	37
5.1	Application 3: Case Summary for Transient Analysis.	42
5.2	Range of Variable Values for Application 3	43
5.3	Application 3: Summary of Results	45
6.1	Application 4: Case Summary for Transient Analysis.	48
6.2	Application 4: Case Summary for Massive Data Analysis.	50

6.3	Application 4: Summary of Results	51
7.1	Summary of Results	53
D.1	Three-phase short-circuit Currents.	80
D.2	Single-phase short-circuit Currents.	81
D.3	phase-to-phase short-circuit Currents.	82
D.4	Biphasic-earth short current	83

LIST OF SYMBOLS

87	ANSI Code of Differential Protective Relay Protection
21G	ANSI Code of Ground Distance Protection
67N	ANSI Code of Neutral Directional Overcurrent Protection
87B	ANSI Code of Bus Differential Protection
87L	ANSI Code of Segregated Line Current Differential Protection
87LG	ANSI Code of Ground Line Current Differential Protection
87LQ	ANSI Code of Negative-sequence Line Current Differential Protection
87T	ANSI Transformer Differential Protection
a	Operator $1\angle 120^\circ$.
f	Fundamental Frequency.
Γ	Relation between currents M and N
\bar{I}_{dif}	Differential Current
I_{op}	Operation Current
I_{res}	Restraining Current
\bar{I}_L	Local Terminal Current
\bar{I}_M	Terminal M Current
\bar{I}_N	Terminal N Current
\bar{I}_R	Remote Terminal Current
im	imaginary part of a complex number

re	real part of a complex number
Γ_F	Γ Settlement adjustment of proposed GAP
k_Δ	Radius adjustment of proposed GAP
Ψ	Sequence network (i.e. 0, 1, or 2)
k_h	multiplying factor for harmonics
$\bar{I}_{dif,h}$	magnitude of the h -th differential harmonic current

GLOSSARY

ANSI	<i>American National Standards Institute</i>
CT	Current Transformer
CCVT	Coupling Capacitor Voltage Transformer
<i>EFD</i>	flag whose value is set based upon the external fault detection logic output
ATP	<i>Alternative Transients Program</i>
DC	<i>Direct Current</i>
FDA	External Fault Detection
IEEE	<i>Institute of Electrical and Electronics Engineers</i>
PAG	Plano Alfa Generalizado
GAP	Generalized Alpha Plane
SIN	Sistema Interligado Nacional
SIR	Source Impedance Ratio
CB	Circuit Breaker
TL	Transmission Line

1.1 BACKGROUND

Electrical power systems have become progressively interconnected, with new delivery paths inserted throughout these systems. Transmission lines play a major role in providing bulk power transmission from huge power plants to load centers; Substations tend to create complex busbar arrangements aimed at providing flexible ways to operate the system. Additionally, power transformers are still extremely important but susceptible to catastrophic internal faults. Nevertheless, disturbances caused in one or more mechanisms can instantly propagate throughout the system, and require for protection schemes that are capable of quickly and selectively clearing faults in order to avoid widespread blackouts (ZIEGLER, 2012).

Notwithstanding, the economic recession that Brazil has undergone since 2015, the Brazilian Transmission System Operator (TSO or *Operador Nacional do Sistema Elétrico - ONS* in Portuguese) planned to increase power generation capacity by 12% from 2017 to 2022, representing a growth of 19 GW (ONS, 2017a). Furthermore the diversity of primary sources is also planned to be changed as shown in Figure 1.1, and will require new transmission lines and substations (ONS, 2017b). Nearly 35.000 km of AC transmission lines (230 to 750 kV) and about 10.000 km of DC lines (800 kV) are planned to be added to the Brazilian Electrical System by 2023.

Table 1.1 lists the partial shutdowns in the Brazilian electrical system due to faults that have occurred in different type of devices. As expected, transmission lines had the highest percentage of faults. This could be anticipated because their lengthy dimensions result in more susceptibility to climate and unpredictable environmental conditions. However, even with a considerably lower percentage of occurrences, faults in essential electrical apparatuses such as transformers and busbars are extremely hazardous to a power system and can cause widespread blackouts.

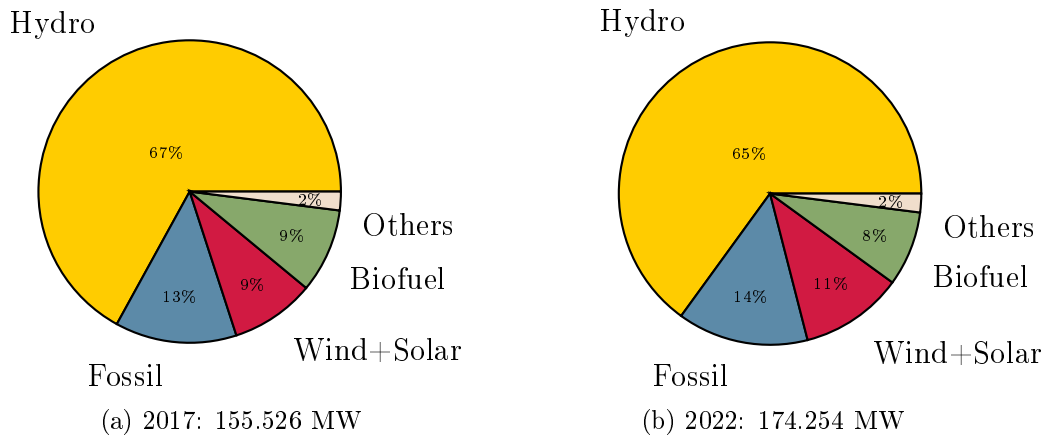


Figure 1.1. Planned power generation capacity increase - 2017 to 2022 (ONS, 2017a). (a) 2017; (b) 2022.

Table 1.1. Partial shutdowns in Brazilian electrical system 2016 (ONS, 2013)

Device	Shutdowns	Percentage (%)
Transmission Lines	2982	47.6
Transformers	767	12.3
Generators	1947	31.1
Busbars	114	1.8
Reactors	70	1.1
Capacitor Bank	83	1.3
Synchronous Compensator	109	1.7
Static Compensator	187	3.0
Total	6529	100.0

As a result, modern protection systems will be required to allow for the safe and steady operation of the Brazilian power grid. Unit protection schemes are designed to protect a specific device or an area of the system (i.e., transmission lines, busbar, transformer, etc.). ONS (2016) established that transmission electrical equipment must isolate short-circuits in less than 100 ms. In addition, graded protection schemes (i.e., distance/impedance, and current-based), provide backup protection due to the failure of unit schemes.

Among all unit protection schemes, the differential function scheme stands out because of its well-proven safety and selectivity (ZIEGLER, 2012). It therefore represents a great option for protecting transmission lines, transformers, and busbars (ELMORE, 2003). Differential schemes became a viable option for transmission lines because in recent years both new and old installations dispose easy access to an optical fiber communication channel (ALTUVE; SCHWEITZER, 2010).

Another interesting aspect about differential schemes is its allowance for a wide range of customization to better suit the desired application, like the use of direct samples in time, external fault modes, and adjustable zones of protection (ALTUVE; SCHWEITZER, 2010). The Institute of Electrical and Electronics Engineers (IEEE) affirms that the percentage differential function has been widely used as primary protection for transformers because it provides a reliable way to protect the devices and guarantees the selectivity (IEEE, 2008a). Improvements in power transformer differential protection now take advantages of new approaches to signal processing techniques and the use of artificial intelligence. These, therefore increase the protection scheme's ability to single out internal faults from other disturbances (BARBOSA *et al.*, 2011; BEHRENDT *et al.*, 2011; VAZQUEZ *et al.*, 2008; GUZMAN *et al.*, 2001a; MEDEIROS; COSTA, 2018). Over the last few years, technological breakthroughs, along with the installation of optical fiber composite overhead ground wires, have made new solutions possible for transmission line differential protection (TZIOUVARAS *et al.*, 2002; BENMOUYAL; MOONEY, 2006; DAMBHARE *et al.*, 2010; KASZTENNY *et al.*, 2011; XUE *et al.*, 2013; DENG *et al.*, 2015; SILVA; BAINY, 2016; ALMEIDA; SILVA, 2017; TANG *et al.*, 2017; SARANGI; PRADHAN, 2017; HOSSAIN *et al.*, 2018). Similarly, busbar differential protection combined with busbar replica strategies have provided valuable improvements, increasing security and reducing fault clearing times (QIN *et al.*, 2000; GUZMAN *et al.*, 2005; KANG *et al.*, 2005; KANG *et al.*, 2008; BAINY; SILVA, 2017; JENA; BHALJA, 2018).

Differential protection can selectively protect a specified zone and has several advantages when compared with other functions, such as overcome the challenges related to adjust the distance element (ALTUVE; SCHWEITZER, 2010; ANDERSON, 1999). Also, differential protection can be combined with alpha plane, see appendix A, to take advantage of its main remarks such as defining different unique restraining shapes, as well as the enhanced rainbow restraining characteristic proposed by Tziouvaras *et al.* (2002).

As originally proposed by Warrington (1962), the alpha plane represents the ratio of two measured currents, so that its application is limited to two-terminal apparatuses only. To overcome this drawback, Miller *et al.* (2010) proposed an innovative metamathematical formulation called a generalized alpha plane (GAP), which converts a set of currents measured in a multi-terminal transmission line into two equivalent ones, thus preserving the benefits of

the alpha-plane-based differential schemes reported by Tziouvaras *et al.* (2002). Even though it was originally proposed for line differential protection, this GAP can be straightforwardly used in other protection applications as Jena & Bhalja (2018) that reports the use of this GAP for busbar protection. Silva & Bainy (2016) reported on alternative GAP for multi-terminal transmission lines' differential protection applications that provides a more simple formulation by comparison with the one proposed by Miller *et al.* (2010); additionally it improves the sensitivity for internal faults during outfeed conditions. The proposal of a new and improved GAP represents a valuable step forward for multi-terminal devices differential protection.

1.2 GENERALIZED ALPHA PLANE

Previously the alpha plane was considered as exclusively for two-terminal elements. However multi-terminals' applications are possible by using a generalized alpha plane (GAP) strategy. Currently, there are two main options available in the literature on the subject, those reported by Miller *et al.* (2010) and Silva & Bainy (2016). In this section only the first one is discussed but a through description of both formulations are described in Appendices B and C. The GAP reported by Silva & Bainy (2016) is part of the proposed formulation, as discussed in this thesis.

The GAP enables alpha plane representation for a device with multi-terminals, by creating a virtual two-terminal element. For instance, a GAP enables the L terminals shown in Figure 1.2a to be mapped into the two-terminal system in Figure 1.2b.

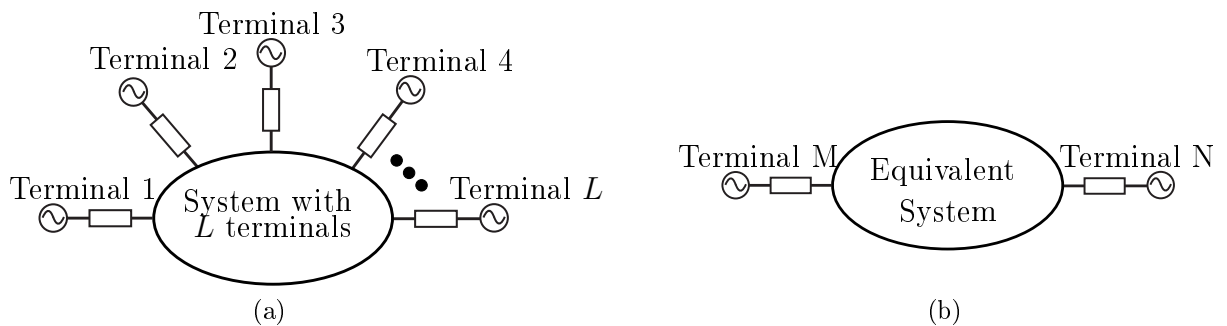


Figure 1.2. The GAP principle: (a) multi-terminal system; (b) two-terminal equivalent system.

1.2.1 GAP from Miller *et al.* (2010)

When considering the general L -terminal differential zone of protection, as exhibited in Figure 1.2a, Miller *et al.* (2010) derived differential $\bar{I}_{dif(L)}$ and restraining $I_{res(L)}$ currents through Equations (1.1) and (1.2), respectively. Both are obtained using the L measured currents and are phase segregated. The virtual equivalent consists of two terminals called M and N . The currents \bar{I}_M and \bar{I}_N result in differential $\bar{I}_{dif(2)}$ and restraining $I_{res(2)}$ currents, as one can observe in Equations (1.3) and (1.4), respectively.

$$\bar{I}_{dif(L)} = \sum_{i=1}^L \bar{I}_i, \quad (1.1)$$

$$I_{res(L)} = \sum_{i=1}^L |\bar{I}_i|, \quad (1.2)$$

$$\bar{I}_{dif(2)} = \bar{I}_M + \bar{I}_N, \quad (1.3)$$

$$I_{res(2)} = |\bar{I}_M + \bar{I}_N|, \quad (1.4)$$

where the math accent "–" represents a phasor quantity; L is the number of terminals.

The key assumption regarding the GAP strategy is to consider the differential and restraining currents identical in both systems (i.e. L and two terminals.), as shown below.

$$\bar{I}_{dif(L)} = \bar{I}_{dif(2)} \quad (1.5)$$

$$I_{res(L)} = I_{res(2)} \quad (1.6)$$

The currents \bar{I}_M and \bar{I}_N are complex numbers, and therefore a total of four variables are sought, namely two real and two imaginary portions, which result in a total of four degrees of freedom. However, Equations (1.5) and (1.6) establish only three boundary equations (i.e., real and imaginary parts of the differential current, and the magnitude of the restraining current). However, a last boundary equation is required in order to enable the GAP. Miller *et al.* (2010) states that one of the equivalent currents has the same angle as a reference current (\bar{I}_P) of the L -terminal element. The current with the largest projection on the differential current phasor is selected as the reference current (\bar{I}_P).

Miller *et al.* (2010) made this choice for two main reasons: First, during external faults with current transformer (CT) saturation, the spurious differential signal will be roughly located along the fault current phasor. Secondly, the solution helps to identify the external fault current.

In order to select the reference current, an auxiliary variable R_i is calculated for each current as follows:

$$R_i = Re\left(\bar{I}_i \cdot \bar{I}_{dif(N)}^*\right) \quad (1.7)$$

where $i = 1 \dots L$; * is conjugate of a complex number.

The reference current is the one with the highest value of R_i , and its angle is called β :

$$\beta = \angle \bar{I}_P \quad (1.8)$$

Aiming to simplify the formulation, the differential current $\bar{I}_{dif(N)}$ is shifted by β . Therefore, the following expressions are obtained for the equivalent currents:

$$\bar{I}_X = \bar{I}_{dif(L)} \cdot 1\angle(-\beta) \quad (1.9)$$

$$\bar{I}_M = \left(\frac{Im(\bar{I}_X)^2 - [I_{res(L)} - Re(\bar{I}_X)]^2}{2(I_{res(L)} - Re(\bar{I}_X))} + j \cdot Im(\bar{I}_X) \right) \cdot 1\angle\beta \quad (1.10)$$

$$\bar{I}_N = (I_{res(L)} - |\bar{I}_M|) \cdot 1\angle\beta \quad (1.11)$$

Then, the alpha plane is executed by computing the complex ratio Γ of the virtual currents \bar{I}_M and \bar{I}_N as follows:

$$\Gamma = \frac{\bar{I}_M}{\bar{I}_N} = \Gamma_{re} + j\Gamma_{im} \quad (1.12)$$

This GAP can be applied not only to phase currents, but also to negative and zero sequence currents (KASZTENNY *et al.*, 2011). The method also permits application where the restraint term ($I_{res(L)}$) is intentionally increased (i.e., harmonic restraint). A higher restraint value means that Γ is near the blocking position $(-1, 0)$. A balanced differential current (e.g. no fault) also results to the identical blocking position ($1\angle 180^\circ$). The Appendix B presents details of the GAP from Miller *et al.* (2010) formulation.

Special countermeasures are usually applied to provide security for external faults with CT saturation, such as the use of external fault detection logics. Harmonic restraining can thereby be performed by adding to I_{res} harmonics that may arise in the differential signal, so that (1.2) can be rewritten as (KASZTENNY *et al.*, 2011):

$$I_{res} = k \sum_{l=1}^L |\bar{I}_l| + EFD \cdot k_h |\bar{I}_{dif,h}|, \quad (1.13)$$

where the External Fault Detector (EFD) is a flag whose value is set based upon the external fault detection logic output (KASZTENNY *et al.*, 2011), k_h is a multiplying factor, and $|\bar{I}_{dif,h}|$ is the magnitude of the h -th differential harmonic current.

1.3 MOTIVATION

The proposal of a new generalized alpha plane formulation is of utmost importance for providing new ways to improve and customize differential protection schemes. It is generally understood to arise from mathematically transforming a multi-terminal system into a two-terminal one, thus allowing the use of the alpha plane (TZIOUVARAS *et al.*, 2002; MILLER *et al.*, 2010; SILVA; BAINY, 2016). However, Miller *et al.* (2010) presents limitations that may jeopardize its performance. For instance, Bainy & Silva (2017) discuss some reliability limitations when combined with busbar differential protection. Up to now, there has been no GAP formulation that creates a smooth transient path (from pre-fault to fault condition), combined with an adjustable settlement point in the right-side of the alpha plane in the steady state of a fault.

1.4 PROBLEM STATEMENT AND PROPOSED SOLUTION

Miller *et al.* (2010) has presented the main state-of-the-art strategy for the generalized alpha plane. It is highly desirable to use an alpha plane with its customizable bi-dimensional restraining shapes to thoroughly protect multi-terminal power apparatuses (TZIOUVARAS *et al.*, 2002). Equally important is a smooth and secure transient path, which allows adjustments by the protection engineer so that choose the settlement point can be chosen on the right side of the alpha plane in a fault steady state.

Miller *et al.* (2010) present a non-conventional way to calculate the equivalent two-terminal system, which may compromise the transient path and, in some conditions, may result in null value for a fault steady-state. Notwithstanding the importance and value of this strategy for power system protection, it might not provide a complete and convenient solution, depending upon the application. Motivated by that, we introduced a new GAP with advantages in comparison with the one reported by Miller *et al.* (2010), such as a more well-behaved response in the alpha plane, despite having a rather simpler formulation and requiring less computational burden (SILVA; BAINY, 2016). On the other hand, the proposed formulation still lacks as a complete solution due no control over settlement values of the fault steady state, and method to adjust the setting k based on trial and error. That is the why we decided to improve the solution proposed in 2016 aiming to create a new formulation capable of perform a smooth transient path, provide ways adjust the fault steady state settlement values in the alpha plane, and overcome the limitations imposed by the setting k . In fact the new GAP formulation encompass the one reported by Silva & Bainy (2016) in such way that it can be understood as its generalization.

1.5 OBJECTIVE

The main objective of this thesis is to propose a new GAP formulation that has been conceived to perform a smooth transient path during faults, and able to control the fault steady state settlement values in the alpha plane using straightforward adjustments. As a minor objective the performance of this new formulation is tested by computational simulations using Alternative Transients Program (ATP) for four different protection applications are discussed: Two-terminal and a three-terminal transmission lines; a transformer; and a busbar arrangement.

1.6 THESIS ORGANIZATION

This thesis presents the mathematical deduction, the simulation, and the analysis of a new generalized alpha plane, called Proposed GAP; it allows different values for Γ_f and k_Δ to fine control the settlement point in the right side of the alpha plane in fault steady state. Mathematical deduction, analytical and brief numerical analysis are shown in Chapter 2.

The simulated performance of the proposed formulation is investigated in four different applications in chapters 3, 4, 5, and 6. Moreover, to further test the proposed GAP each system is simulated extensively to enable a massive data analysis, which includes a wide range of systems' conditions, types of faults, fault resistance, etc. Finally four different appendices are presented, the first one consists of a brief discussion about differential protection fundamental. Appendices B and C present a detailed deduction regarding GAP formulations proposed by Miller *et al.* (2010) and Silva & Bairy (2016), respectively. The appendix D presents the formulation to calculate short-circuits contributions for a two-terminal transmission line.

GENERALIZED ALPHA PLANE FORMULATION

2.1 PROPOSED FORMULATION

When considering the multi-terminal device illustrated in Figure 1.2a, the differential current ($\bar{I}_{dif(L)}$) and restraining current ($I_{res(L)}$) for each phase can be defined as:

$$\bar{I}_{dif(L)} = \sum_{i=1}^L \bar{I}_i = I_{dif(L),re} + jI_{dif(L),im}, \quad (2.1)$$

$$I_{res(L)} = \sum_{i=1}^L |\bar{I}_i|, \quad (2.2)$$

where the math accent "–" represents a phasor quantity; the subscripts *re* and *im* represent its real and imaginary parts; and L is the device's number of terminals.

The differential protection element can be combined with alpha plane representation; however, for multi-terminal devices the use of a generalized alpha plane is mandatory. The main idea is to map the L terminals into only two. The two currents (\bar{I}_M and \bar{I}_N) compound an equivalent system. In order to do so, it is required to establish the differential ($\bar{I}_{dif(2)}$) and restraint ($\bar{I}_{res(2)}$) currents related to the equivalent system shown as follows:

$$\bar{I}_{dif(2)} = \bar{I}_M + \bar{I}_N \quad (2.3)$$

$$\bar{I}_{res(2)} = \eta_1 \bar{I}_M - \eta_2 \bar{I}_N \quad (2.4)$$

where η_1 and η_2 are multiplying factors to adjust the differential function.

Two main assumptions are defined: 1) the differential currents $\bar{I}_{dif(2)}$ and $\bar{I}_{dif(L)}$ are equal; 2) The restraining currents, $\bar{I}_{res(2)}$ and $I_{res(L)}$ are equal. Thereby, it is possible to achieve the equivalence between the original and the equivalent systems. Thus, a linear system can be obtained from Equations (2.1)-(2.4).

$$\begin{bmatrix} 1 & 0 & 1 & 0 \\ 0 & 1 & 0 & 1 \\ \eta_1 & 0 & -\eta_2 & 0 \\ 0 & \eta_1 & 0 & -\eta_2 \end{bmatrix} \cdot \begin{bmatrix} I_{M,re} \\ I_{M,im} \\ I_{N,re} \\ I_{N,im} \end{bmatrix} = \begin{bmatrix} I_{dif(L),re} \\ I_{dif(L),im} \\ I_{res(L)} \\ 0 \end{bmatrix} \quad (2.5)$$

The determined and consistent linear system of Equations (2.5) allows its solution to be obtained straightforwardly. It can be solved and therefore determine the deterministic expressions for \bar{I}_M and \bar{I}_N , shown below (See appendix C):

$$\bar{I}_M = \frac{1}{\eta_1 + \eta_2} (\eta_2 \bar{I}_{dif(L)} + I_{res(L)}) \quad (2.6)$$

$$\bar{I}_N = \frac{1}{\eta_1 + \eta_2} (\eta_1 \bar{I}_{dif(L)} - I_{res(L)}) \quad (2.7)$$

One last step is to calculate Γ , which is simply the relation between currents \bar{I}_M and \bar{I}_N as follows:

$$\Gamma = \frac{\bar{I}_M}{\bar{I}_N} = \Gamma_{re} + j\Gamma_{im} \quad (2.8)$$

Likewise, external faults with CT saturation requires the use of external fault detection logics. In this way, the harmonic restraint can be performed by adding to $I_{res(L)}$ harmonics, which may arise in the differential signal, so that (2.2) can be rewritten as:

$$I_{res(L)} = \sum_{i=1}^L |\bar{I}_i| + EFD \cdot \eta_h \left(\sum_{i=1}^L |\bar{I}_{i,h}| \right) \quad (2.9)$$

where the External Fault Detector EFD is a flag whose value is set based upon the external fault detection logic output (KASZTENNY *et al.*, 2011); η_h is a multiplying factor; and $(\bar{I}_{i,h})$ is the h -th harmonic current phasor of i -th terminal.

The protection scheme using the GAP for a multi-terminal device with L terminals is shown in Figure 2.1, and it is assumed that all measured currents are aligned in time. The GAP stage calculates \bar{I}_M and \bar{I}_N . The last step obtains Γ for each phase and compares them to the chosen restraining characteristic. In the diagram it is shown the shape proposed by Tziouvaras *et al.* (2002). Finally, the protection scheme can be decided for trip based on other user settings.

2.2 SETTING η_1 AND η_2

The proposed GAP has two settings: η_1 and η_2 . However, their values depend upon where on the alpha plane it is desired the settlement area of Γ to be. In order to set η_1 and η_2 , two new

coefficients are beforehand defined: Γ_f and k_Δ . The first one is the desirable fault steady-state value of Γ_{re} , and k_Δ is relative deviation from the center ($\Gamma_f, 0$).

It is noteworthy that Γ_f combined with k_Δ create a circular shape. The circle corresponds to the value of Γ on fault steady-state. Mathematically, the center and radius of the circle can be defined as:

$$\text{Center} = (\Gamma_f, 0) \quad (2.10)$$

$$\text{radius} = k_\Delta \quad (2.11)$$

One can observe that Γ_f controls the center position of the circle, whereas k_Δ adjusts its radius. The results are graphically presented in Figure 2.2. The circumference corresponds to the desired values of Γ calculated using GAP during a fault steady state.

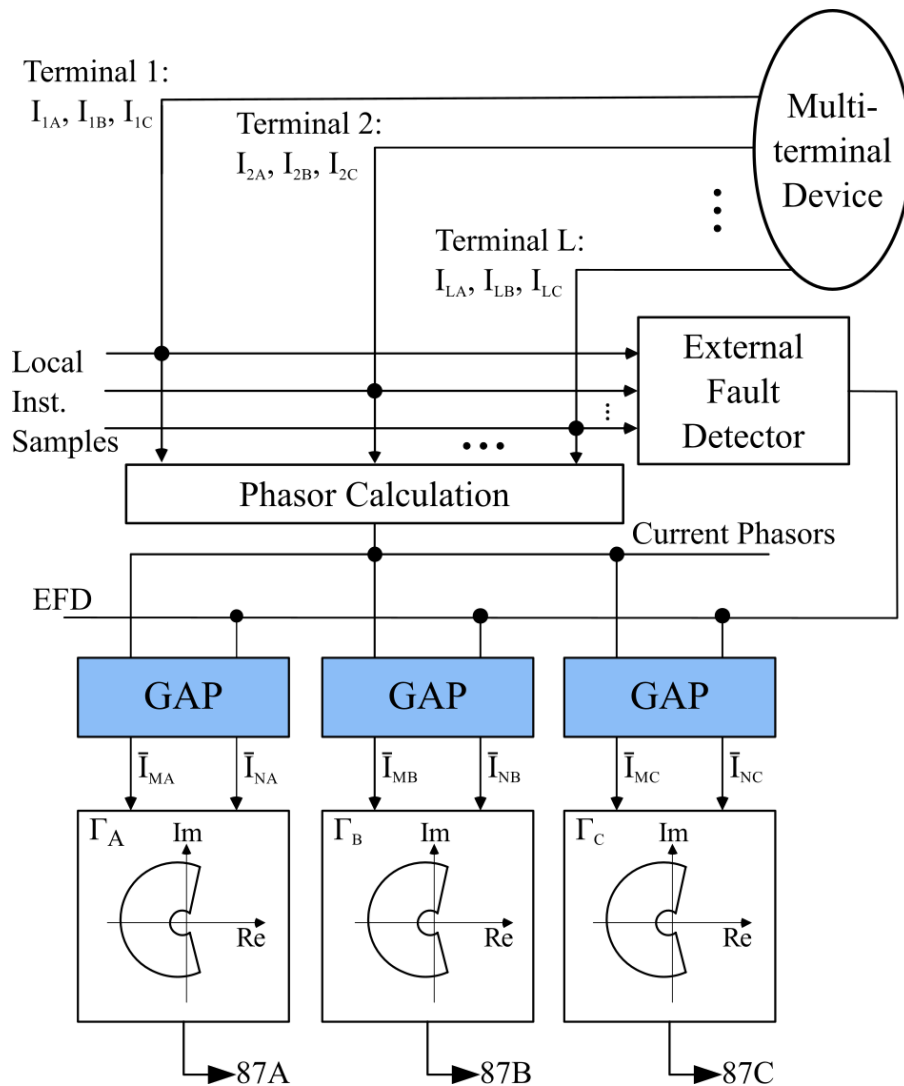


Figure 2.1. Flowchart diagram of the protection scheme adapted from (BENMOUYAL, 2005)

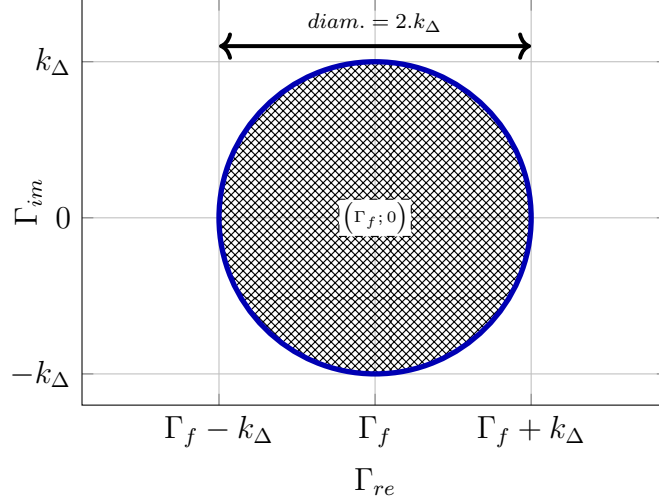


Figure 2.2. Circle defined by Γ_f and k_Δ .

The adjustment of η_1 and η_2 depends upon the chosen values of Γ_f and k_Δ ; η_1 and η_2 are defined as a function of Γ_f and k_Δ . The Equations (2.6)-(2.8) are combined to obtain:

$$\Gamma = \frac{\eta_2}{\eta_1} \left(\frac{I_{dif(L),re} + \frac{1}{\eta_2} I_{res(L)} + j I_{dif(L),im}}{I_{dif(L),re} - \frac{1}{\eta_1} I_{res(L)} + j I_{dif(L),im}} \right) \quad (2.12)$$

The Equation (2.12) can be split in real and imaginary parts, as follows:

$$\Gamma_{re} = M_{re} \left(\frac{|\bar{I}_{dif(L)}|^2 + I_{res(L)} f(\eta_1, \eta_2)}{|I_{dif(L)}|^2 + I_{res(L)} f(-\eta_2, \eta_2)} \right) \quad (2.13)$$

$$\Gamma_{im} = M_{im} \left(\frac{\bar{I}_{res(L)} I_{dif(L)}}{|I_{dif(L)}|^2 + I_{res(L)} f(-\eta_2, \eta_2)} \right) \quad (2.14)$$

where M_{re} , M_{im} , $f(\eta_1, \eta_2)$, and $f(-\eta_2, \eta_2)$ are defined as follows:

$$M_{re} = \frac{\eta_2}{\eta_1} \quad (2.15)$$

$$M_{im} = \eta_2 + \frac{\eta_2^2}{\eta_1} \quad (2.16)$$

$$f(\eta_1, \eta_2) = -\eta_1 \eta_2 I_{res(L)} + (\eta_1 - \eta_2) I_{dif(L),re} \quad (2.17)$$

$$f(-\eta_2, \eta_2) = \eta_2^2 I_{res(L)} - 2\eta_2 I_{dif(L),re} \quad (2.18)$$

When considering $\Gamma_f = M_{re}$ and $k_\Delta = M_{im} M_{re}$, Equations (2.15) and (2.16) form a linear system of Equations. The solution leads to:

$$\eta_1 = \frac{1}{k_\Delta} (1 + \Gamma_f) \quad (2.19)$$

$$\eta_2 = \frac{1}{k_\Delta} (\Gamma_f + \Gamma_f^2) \quad (2.20)$$

The values for Γ_f and k_Δ can be chosen provided that some boundaries are fulfilled: 1) to maintain good security level, Γ_f has to be greater than one ($\Gamma_f > 1$); and, 2) k_Δ has to be less than 10 % of Γ_f . The latter condition is important in order to guarantee a small circular area around the central point $(\Gamma_f, 0)$, thus resulting in closer values for Γ in all three phases.

2.3 GAP ANALYSIS

This analysis of the GAP clarifies its behavior during faults. A generic multi-terminal device was considered for this study. In order to do so, Equation (2.8) is thoroughly explored, with the focus on fault steady-state. When Equations (2.6)-(2.8) are combined with Equations (2.19) and (2.20) yields:

$$\Gamma = \frac{\Gamma_f(1 + \Gamma_f)I_{dif} + k_\Delta I_{res}}{(1 + \Gamma_f)I_{dif} - k_\Delta I_{res}} \quad (2.21)$$

Equation (2.21) is evaluated considering a single-phase fault (AG). One can assume that \bar{I}_{dif} for phase A is approximately equal to the fault current \bar{I}_F . This assumption leads to:

$$\Gamma = \frac{\Gamma_f(\alpha\bar{I}_F)^2 + \alpha^2\omega\bar{I}_F + \omega^2}{(\alpha\bar{I}_F)^2 - \omega^2} \quad (2.22)$$

where α is defined by $(1 + \Gamma_f)$; and ω is equal to $(k_\Delta I_{res})$. In order to control the settlement point in right side of alpha plane, k_Δ is set to values less than 10% of Γ_f , enabling the assumption that $(\alpha\bar{I}_F)^2 \gg \omega^2$, resulting in:

$$\Gamma \approx \Gamma_f + \frac{\omega}{\bar{I}_F} + \frac{\omega^2}{(\alpha\bar{I}_F)^2} = \Gamma_f + \frac{k_\Delta I_{res}}{\bar{I}_F} \quad (2.23)$$

From Equation (2.23), $\frac{k_\Delta I_{res}}{\bar{I}_F} \rightarrow 0$ and can be ignored due to the fact that \bar{I}_F is many times greater than $k_\Delta \bar{I}_{res}$. Since k_Δ is set to a value less than or equal to 0.1, each phase Γ results in approximately Γ_f for a symmetrical fault (e.g., three-phase fault).

When considering an external fault condition or normal operation, the current \bar{I}_{dif} is next to zero, and can be disregarded. This assumption results in:

$$\Gamma = \frac{I_{res}}{-I_{res}} = -1 \quad (2.24)$$

Indeed the Γ value for this conditions is approximately -1 : Other types of short-circuits (e.g., phase-to-phase) will lead to equivalent results, and the conclusions above mentioned

are valid for them too. Therefore, P1:($\Gamma_f, 0$) and P2:($-1, 0$) deserve comment: The first one indicates the center of a circumference where ideally Γ settles during an internal fault, while the second one represented the point where Γ stays during normal condition. One can conclude that the restraint characteristic has to be defined around P2, and never surpass P1 at risk of compromise reliability.

2.4 STUDY OF VARIATION OF Γ_f AND k_Δ

The adjustments Γ_f and k_Δ should be further analyzed. Both are explored numerically by simulating four different types of faults in a generic multi-terminal system: three-phase, phase-to-phase, double-phase-to-ground, and single-phase faults. Figure 2.3 presents eight pairs of variations, where k_Δ varied from 0.1 to 0.4, and Γ_f is equal to 5 and 10. For each pair of values, a combination of η_1 and η_2 , using Equations 2.19 and 2.20, respectively, was calculated.

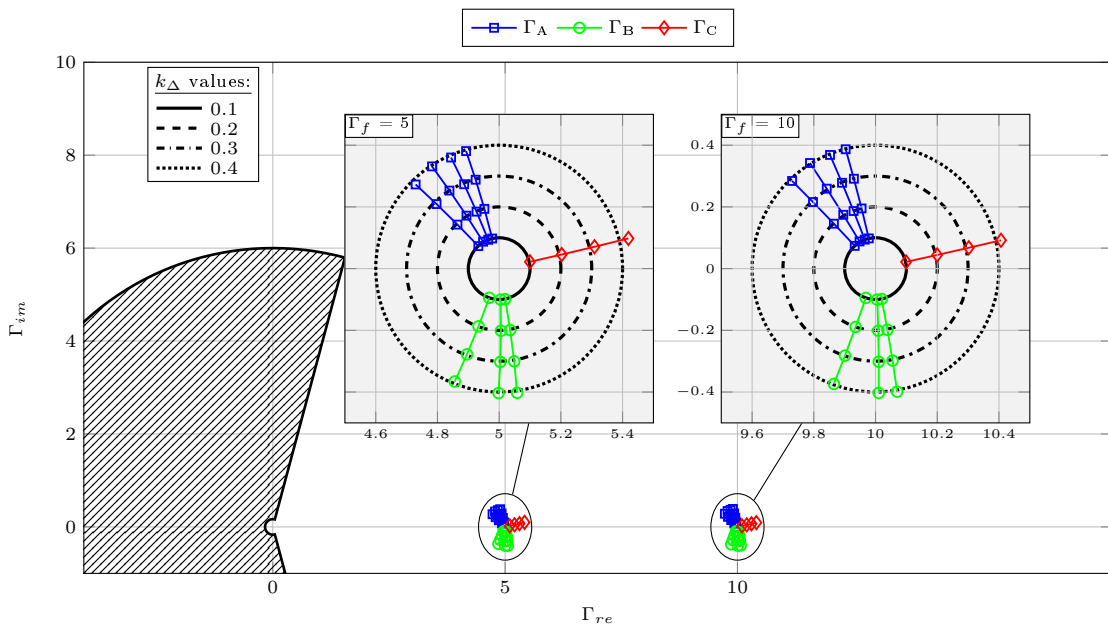


Figure 2.3. Study of Γ_f and k_Δ variation.

The results shown in Figure 2.3 confirm the conclusions expressed by Equation (2.23). In addition, the circle shown in Figure 2.2 and defined by Equations (2.10) and (2.11) were also confirmed by the numerical analysis. The rainbow restraining area from Tziouvaras *et al.* (2002) was used purely as an example; however, any other restraining characteristic can be chosen.

2.5 SILVA & BAINY (2016) GAP VERSUS NEW FORMULATION

In this section a brief comparison between the proposed formulation and the one reported in Silva & Bairy (2016). In order to do so, the Table 2.1 shows the equivalent currents \bar{I}_M and \bar{I}_N for both formulations.

Table 2.1. Comparison of 2016 and current formulation.

GAP	Silva & Bairy (2016)	Proposed Formulation
\bar{I}_M	$\frac{1}{2} (\bar{I}_{dif(L)} + kI_{res(L)})$	$\frac{\eta_2}{\eta_1 + \eta_2} \left(\bar{I}_{dif(L)} + \frac{1}{\eta_2} I_{res(L)} \right)$
\bar{I}_N	$\frac{1}{2} (\bar{I}_{dif(L)} - kI_{res(L)})$	$\frac{\eta_1}{\eta_1 + \eta_2} \left(\bar{I}_{dif(L)} - \frac{1}{\eta_1} I_{res(L)} \right)$

As can be seen the equations shown in Table 2.1 are quite similar. Accordingly, it is possible to obtain the following relations:

$$\frac{\eta_2}{\eta_1 + \eta_2} = \frac{1}{2} \quad (2.25)$$

$$k = \frac{1}{\eta_2} \quad (2.26)$$

$$k = \frac{1}{\eta_1} \quad (2.27)$$

The linear system formed by (2.25)-(2.27) is easily solved, therefore the possible solution requires η_1 and η_2 to be equal. Nonetheless, this conclusion defeats the adjustments Γ_f and k_Δ for the 2016 formulation, since by considering Equations (2.19) and (2.20) for $\Gamma_f > 0$ and $\eta_1 = \eta_2$ the only possible solution is $\Gamma_f = 1$ and $k_\Delta = k$. Additionally, Silva & Bairy (2016) defined the value for k as 0.09, which is in accordance with the limit defined in this chapter (i.e. $k_\Delta \leq 0.1\Gamma_f$).

Based on the observations listed above, the formulation proposed by Silva & Bairy (2016) only allows the adjustment of k_Δ which is a limitation when compared to the one presented in this chapter. Hence the proposed formulation can be understood as a generalization of the GAP reported by Silva & Bairy (2016), due its capacity to allow different values for Γ_f rather than only $\Gamma_f = 1$; besides a graphical and straightforward interpretation of Γ_f and k_Δ . These two adjustment enable the control of the settlement point in alpha plane which is beneficial for two main reasons: 1) Move away Γ from the pre-fault point $(-1, 0)$; 2) Allow more flexibility when defining a restraining characteristic.

2.6 SUMMARY

In this chapter the proposed GAP formulation was presented and discussed. Additionally, the problem stated in Chapter 1 is solved by means of Γ_f and k_Δ . In order to guarantee the settlement circumference during fault steady state, a maximum relation of 10 % between the two adjustments has to be followed, as shown in Equation 2.28.

This relation is important to allow the simplification of Equation 2.22 and guarantee the circular region to be defined.

$$k_\Delta = \Psi\Gamma_f \quad (2.28)$$

where Ψ can assume any value between 0.01 and 0.1, or 1 to 10 % of Γ_f . The smaller the more sensitive to faults the new GAP becomes. Electric systems that often run through communication problems, severe CT saturation, and frequent spurious differential current should maximize Ψ .

Equation 2.28 reduces the two settings into a single one: Γ_f . Considering a conservative approach ($\Psi = 0.1$) the Equations (2.19) and (2.20) can be simplified to:

$$\eta_1 = 10 \left(\frac{1}{\Gamma_f} + 1 \right) \quad (2.29)$$

$$\eta_2 = \Gamma_f \eta_1 \quad (2.30)$$

APPLICATION 1: TWO-TERMINAL TRANSMISSION LINE

Although the alpha plane can be directly used in a two-terminal transmission line without a GAP strategy, in this chapter it is highlighted the benefits and limitations provided by two different GAPs. The main goal is to discuss the results aiming on the improvements enabled by the use of the proposed GAP even in a two-terminal line.

3.1 OVERVIEW

Some remarkable issues arose when using differential protection on two-terminal transmission lines applications (BENMOUYAL; MOONEY, 2006). CT error and saturation are some problems that can lead the protection scheme to fail. However, further issues must be addressed regarding transmission line differential protection. In Figure 3.1 a common two-terminal transmission line is presented.

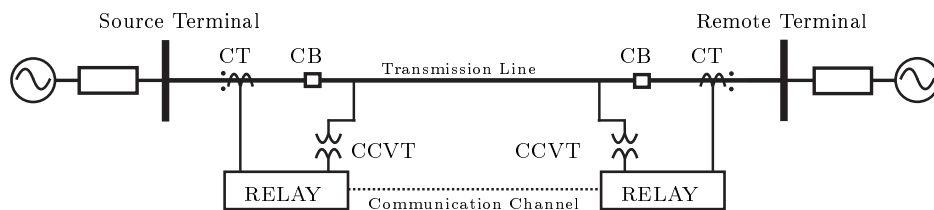


Figure 3.1. Simulated Power System - 500 kV two-terminal Transmission Line

Each end of the transmission line has a relay connected to maintain data communication with each other. Since transmission lines are usually tens or hundreds of kilometers in length, the communication channel becomes one of the main sources of protection failure. In addition, channel latency can be occasionally expected and means that the protection relay has to be set up to overcome this problem (KASZTENNY *et al.*, 2011; ALTUVE; SCHWEITZER, 2010). A spurious differential current caused by transmission line capacitance is an even greater problem.

Estimation followed by compensation is required in order to avoid unwanted protection scheme operation. Transmission lines are more likely to suffer from outfeed¹ current (BENMOUYAL; MOONEY, 2006).

Internal faults that are followed by subsequent outfeed currents can lead to an unexpected behavior of the Γ in the alpha plane, and commonly result in negative values for the Γ . This phenomenon depends mainly on the strength of each terminal, the value of the load currents, the fault resistance, and location as well (ALMEIDA; SILVA, 2017). During outfeed conditions the current phasor of one terminal is usually near null value, and thus in the alpha plane the Γ is near the origin $(0, 0)$ or close to infinity.

Transmission lines with series compensation occasionally suffer from the effects of sub-synchronous oscillations. The cause is mainly due to the electric resonance between the series compensators and the transmission line's own inductance and capacitance. At first glance a filter seems a viable option to overcome the problem; however, it is a remarkable challenge to estimate the oscillations frequency factor (BENMOUYAL, 2005). In the alpha plane this problem leads to an oscillation around the steady-state settlement point $(-1, 0)$. The load current greatly influences the magnitude of these frequency oscillations, and can reach a point where operation fails, gets slower, or there is a drastic reduction of overall protection system reliability.

As discussed above, communication latency is intrinsically present in transmission line differential protection. High latency can cause data misalignment. Spurious differential current is the direct side effect of misaligned phasors, even which may lead operation to fail. Data synchronization strategies are deeply important and mandatory for guaranteeing transmission line differential protection reliability (KASZTENNY *et al.*, 2011; ALTUVE; SCHWEITZER, 2010). The ping-pong method is a fairly possible mean for achieving data synchronization; another option is to obtain external time references provided by the Global Positioning System (GPS) (MILLS, 1991). The former has a downside because it requires symmetrical communication channels (i.e., a transceiver and receiver, called TX and RX, respectively). This means that the path, length, material, converters, etc. have to be nearly identical in both RX and TX

¹Outfeed is a phenomenon that occurs due a combination of a pre-fault condition during an internal fault. It is mainly identified when one of the terminals has a current leaving it instead of entering. It usually happens due to the combination of heavy load and low fault contribution.

channels. The latter relies on GPS to time-stamp the phasors; however, GPS service outages directly affect the correct operation of the protection scheme. Synchronization errors result on the rotation of points around the origin in the alpha plane (TZIOUVARAS *et al.*, 2002).

Any overhead transmission line has capacitance between the conductors and ground throughout its entire length. The capacitance is uniformly distributed over the length of the line. The current drawn by this capacitance is known as charging current, and it has to be compensated in order to prevent a spurious differential current. Figure 3.2 shows a simplified transmission line where both ends provide a charging current \bar{I}_C . The charging current directly affects the value of the Γ , as shown in Equation (3.1). The higher the charging current is, the closer to point (1,0) the Γ will be. Transmission line differential protection requires special algorithms that estimate and compensate the charging current mainly using the measured voltage (MILLER *et al.*, 2010). When energizing a transmission line, the charging current achieves a higher value than during the steady state. And therefore requires special pick-up settings to avoid undesirable operation (ALTUVE; SCHWEITZER, 2010).

$$\Gamma = \frac{\bar{I}_L}{\bar{I}_R} = \frac{-\bar{I}_{LD} + \bar{I}_C}{\bar{I}_{LD} + \bar{I}_C}, \quad (3.1)$$

where \bar{I}_{LD} is the load current.

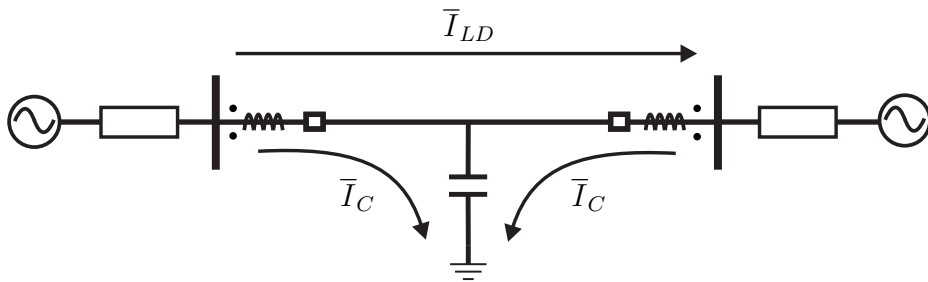


Figure 3.2. Simplified Representation of Transmission line Capacitive Current.

3.2 APPLICATION DETAILS

The first system consists of a 500 kV 200 km long two-terminal transmission line shown in Figure 3.3. Local and remote terminals are called Source 1 and 2, respectively. Their Thévenin equivalent impedance are defined based on the system-to-line impedance ratio (SIR), which represents the ratio between the Thévenin equivalent impedance of the source and the

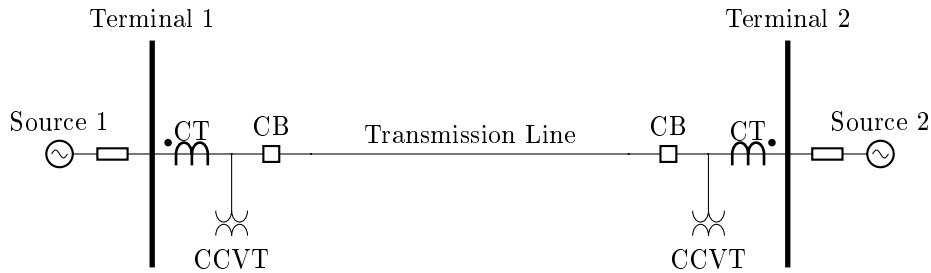


Figure 3.3. System 1 - 500 kV two-terminal Transmission Line.

series impedance of the transmission line (THOMPSON; SOMANI, 2015). In this way, the so called source strength can be addressed. Regarding charging current compensation, the current drawn by transmission line capacitance can be estimated by following the procedure performed by Kasztenny *et al.* (2011). Additionally, both the local and remote SIRs are equal to 0.1 (i.e., $SIR_L = SIR_R = 0.1$). The CT was specified and modeled as ANSI C800 2000-5A, as proposed by the IEEE Power System Relaying Committee in (IEEE POWER SYSTEM RELAYING COMMITTEE, 2004). The Coupling Capacitor Voltage Transformer (CCVT) is identical to the one presented by Pajuelo *et al.* (2008).

The parameters Γ_f and k_Δ attributed to the proposed GAP were tuned to 10.0 and 0.2, respectively. Another essential aspect to be considered is the restraint characteristic to be defined in the alpha plane. Accordingly, in all four power systems the enhanced rainbow characteristic reported in Tziouvaras *et al.* (2002) was used.

The results were accomplished in ATP by using a time-step of 1 micro-second ($1 \mu s$). The required current and voltage measurements are processed using an anti-aliasing low-pass third-order Butterwoth filter, with the cutoff frequency at 180 Hz (HART *et al.*, 2000). Afterwards, the signals are sampled into 16 samples per cycle ($\approx 1ms$ time step). The phasors of voltages and currents are estimated using the discrete signal and a full-cycle cosine filter. The base frequency of all systems is 60 Hz.

A total of nine cases (from 1.1 to 1.9) are discussed regarding System 1. The first four cases are transient response performance evaluations, while the latter five consist of massive data analyses. The proposed formulation is thoroughly compared with GAP strategy reported by Miller *et al.* (2010).

3.3 TRANSIENT ANALYSIS

In this analysis the transient response of two different GAP strategies are demonstrated. In order to do so, four different cases, listed in Table 3.1, are presented. It is important to highlight three criterion chosen to analyze the transient response of each GAP (i.e., speed, reliability, and evenness). Speed is measured by the number of samples required for operation after a fault occurrence. Reliability is obtained if the GAP operates when expected. Evenness is measured by visual inspection where a good quality path is therefore achieved when no ricochets occur (reentries in the trip area), there is small settlement time (e.g., few samples to steady state), and, there is a soft trajectory to the rest area (e.g., a straight line). The defined criteria is listed in Table 3.2. In order to better organize the upcoming results, the GAP found on literature and the proposed formulation will be called in accordance with Table 3.3.

Figures 3.4 and 3.5 show the transient response of two different GAPs for cases 1.1 and 1.2. A comparison among them allows to point out the smoothness of results obtained thorough the GAPs *II*. Moreover the settings Γ_f and k_Δ successfully adjusted Γ around the point (10,0).

Table 3.1. Application 1: Case Summary for Transient Analysis.

Case	Fault	d	$R_f(\Omega)$	SIR_L	SIR_R	δ
1.1	BG	50%	0	1,0	1,0	-5°
1.2	ABC	50%	0	1,0	1,0	-5°
1.3	BG	50%	100	1,0	1,0	-30°
1.4	BCG	external	0	1,0	1,0	-5°

Table 3.2. Criteria for Transient Analysis.

Criteria	Description
Speed	Number of samples required for operation.
Reliability	GAP operates only when expected.
Evenness	Soft trajectory to the rest area.

Table 3.3. GAP identification names.

Identification	Name
GAP <i>I</i>	reported by Miller <i>et al.</i> (2010)
GAP <i>II</i>	Proposed Formulation

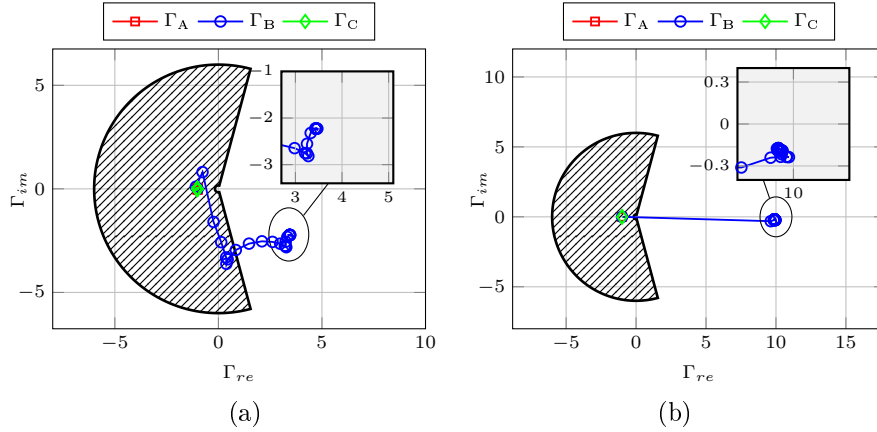


Figure 3.4. Case 1.1 - BG (a) GAP *I*; (b) GAP *II*

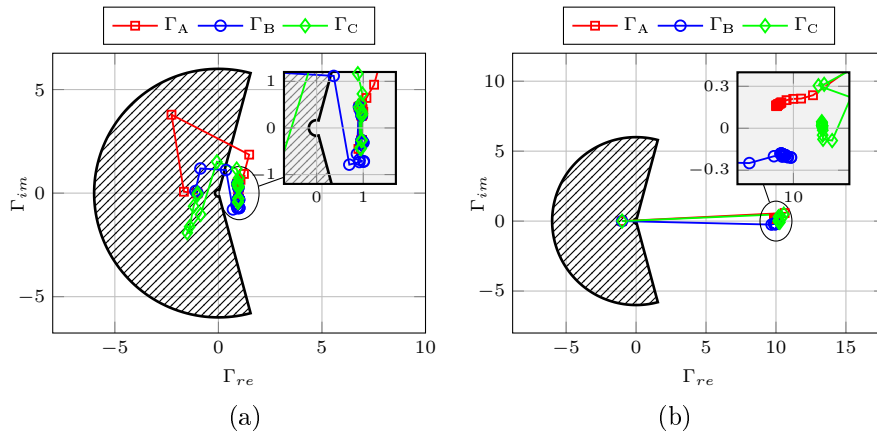


Figure 3.5. Case 1.2 - ABC (a) GAP *I*; (b) GAP *II*

Concerning speed, on both cases the slowest among all was GAP *I* with about 2-3 samples. Reliability was fulfilled flawlessly for both. Regarding evenness, the extend settlement time and tortuous trajectory of GAP *I* makes it the less qualified for this category, while GAPs *II* presented flat response and fast settlement time.

A better evaluation of the improvement in reliability provided by the proposed formulation can be seen in Figure 3.6. Case 1.3 presents an outfeed current, thus a challenge for transmission-line differential protection. GAP *I* failed to operate while GAPs *II* successfully tripped, proven the reliability achieved by the formulation. In respect with speed and evenness both had equivalent results as shown in Figure 3.6a and 3.6b. GAPs *II* presented slower settlement time and complicated trajectory due the extreme outfeed current. The proposed formulation settled around (8.7, 0.3), thus considerable away from the desired point (10, 0) proven this case to be a challenge for differential protection.

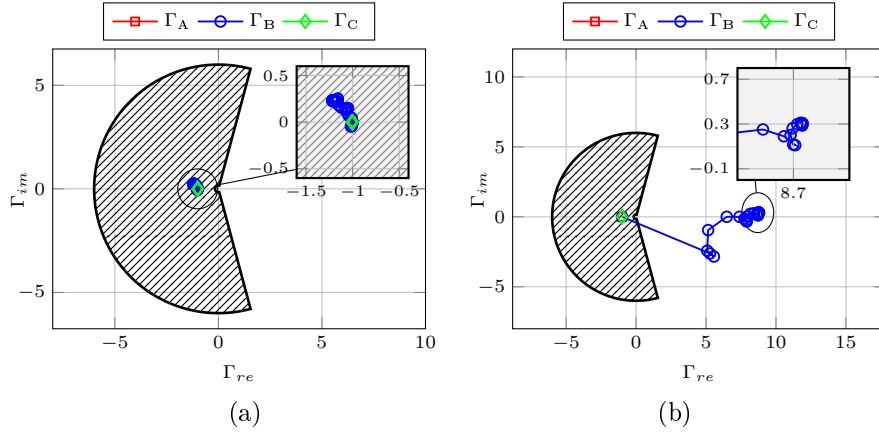


Figure 3.6. Case 1.3 - BG (a) GAP I; (b) GAP II

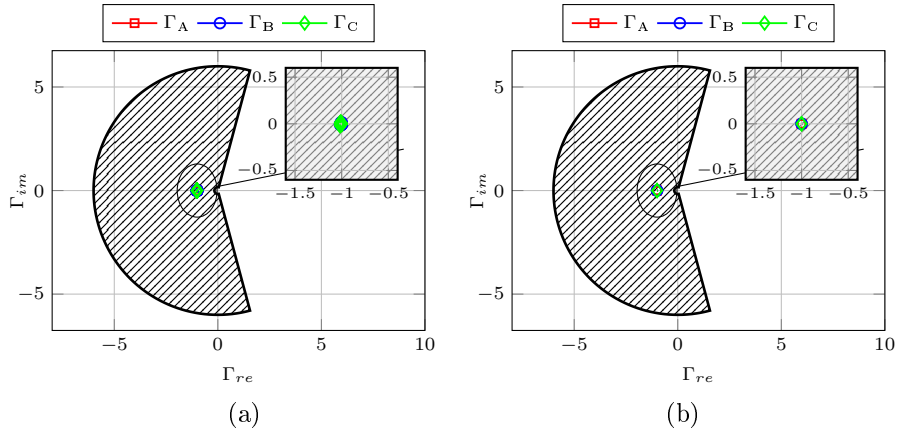


Figure 3.7. Case 1.4 - BCG (a) GAP I; (b) GAP II

Last case is shown in Figure 3.7 and presents an external fault with heavy CT saturation. The harmonic restraining performs an important task by avoiding miss-operation for all GAPs. However, one can observe that between the them, GAP II was the one most affected by the CT saturation. This is confirmed due the undeniable oscillations around point $(-1,0)$ in Figure 3.7b.

3.4 MASSIVE DATA ANALYSIS

The massive data analysis consists of five cases, in each one a wide variety of pre-fault conditions are simulated. The fault steady-state values of Γ are plotted for each condition. In this analysis two criterion are defined to analyze the results of each GAP, i.e. reliability and trajectory length. Reliability is obtained if the GAP operates only when expected to. The second one is measured by how affected the GAP is due the variation of pre-fault conditions,

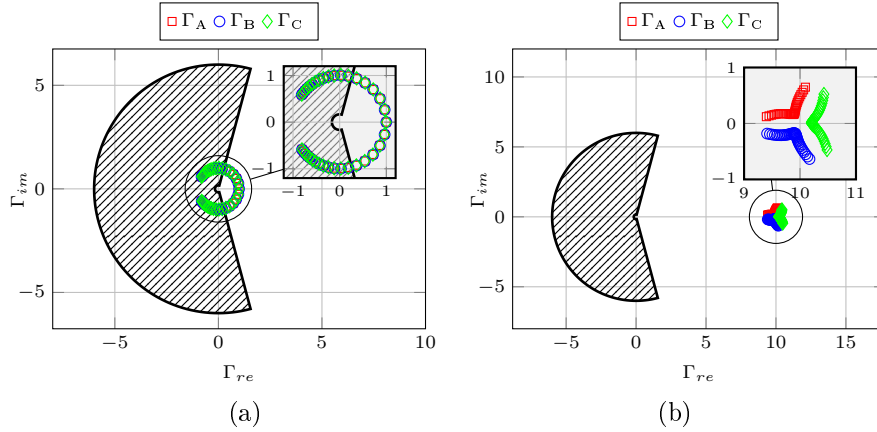


Figure 3.8. Case 1.5 - ABC (a) GAP *I*; (b) GAP *II*

therefore a good quality trajectory is achieved if the plotted points are concentrated in a small region, where the smaller the area better the results are. The criteria for classify the massive data analysis results is listed in Table 3.5

The list of cases is shown in Table 3.4. To highlight the advantages of the proposed formulation even for a two-terminal line, Figures 3.8 and 3.9 show the trajectories of two different GAP for cases 1.5 and 1.6. GAP *I* was unable to successfully operate for all the imposed conditions, while GAP *II* worked as desired. Therefore they are more reliable than formulation *I*. It is worthwhile to point out that the settings Γ_f and k_Δ successfully adjusted Γ around the point (10,0) for GAP *II*. In accordance with the second criterion, the two GAPs performed similarly. Formulation *II* presented slightly better results, due smaller deviation from settlement point (10,0).

Cases 1.7 and 1.8 results are shown in Figure 3.10 and 3.11, respectively. The two GAPs were capable to operate successfully for all simulated conditions, therefore first criterion is fulfilled

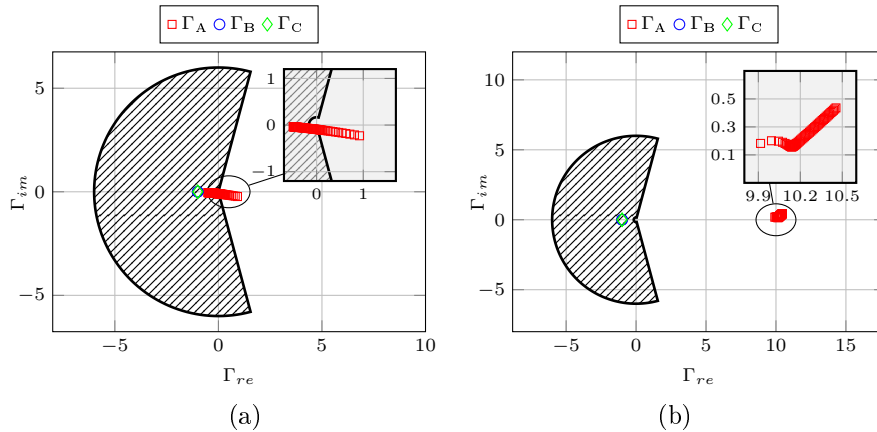


Figure 3.9. Case 1.6 - AG (a) GAP *I*; (b) GAP *II*

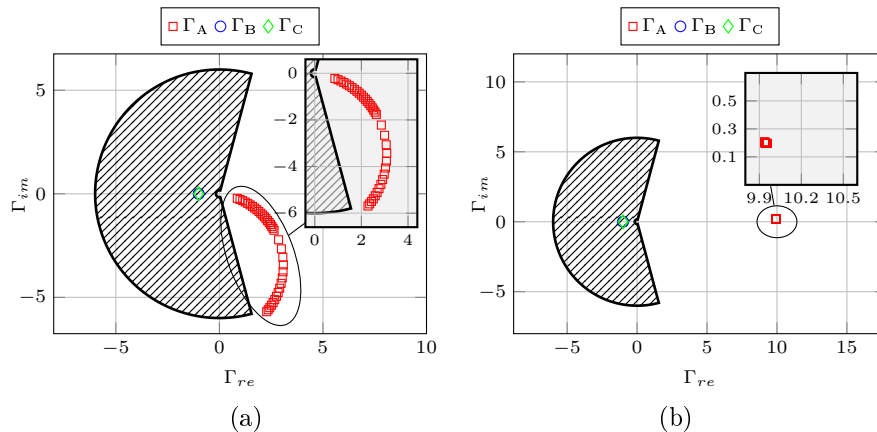
Table 3.4. Application 1: Case Summary for Massive Data Analysis.

Case	Type	d	$R_f(\Omega)$	SIR_L	δ
1.5	ABC	50%	0	0,1	-90° to -90°
1.6	AG	50%	0 to 1k	0,1	-5°
1.7	BG	50%	0	0,1 to 10	-5°
1.8	BC	1 to 99%	10	0,1	-5°
1.9	BC	external	0 to 1k	0,1	-5°

Table 3.5. Criteria for Massive Data Analysis.

Criteria	Description
Reliability	GAP operates only when expected.
Trajectory length	how critically affected the GAP is due the variation of pre-fault conditions

for all of them. On the other hand, regarding to second criterion formulation *II* presented flawless results when compared to GAP *I*. This is undeniably proved by the approximate equal steady-state value for all conditions, therefore truly supports the benefits enabled by GAP *II*. In addition, the settings Γ_f and k_Δ were capable to set Γ around the point (10,0) for GAP *II*. Aiming to further investigate the reliability of the GAPs during CT saturation, in Figure 3.12 the results for case 1.9 are displayed. Indeed, all GAPs correctly not operate for all conditions, whereas GAP *II* remarkable oscillation resulted in smaller reliability. It reveals that the proposed formulation and the GAP *I* accommodates inaccuracies due CT saturation errors better than the GAP *II* approach.

**Figure 3.10.** Case 1.7 - BG (a) GAP *I*; (b) GAP *II*

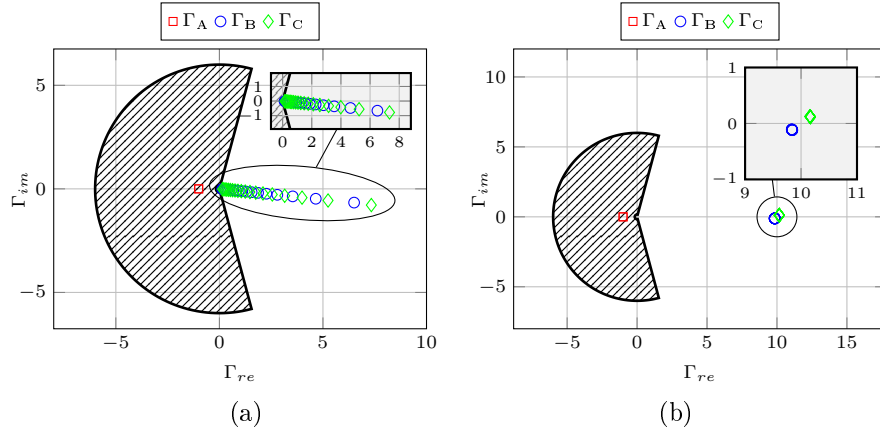


Figure 3.11. Case 1.8 - BC (a) GAP I; (b) GAP II

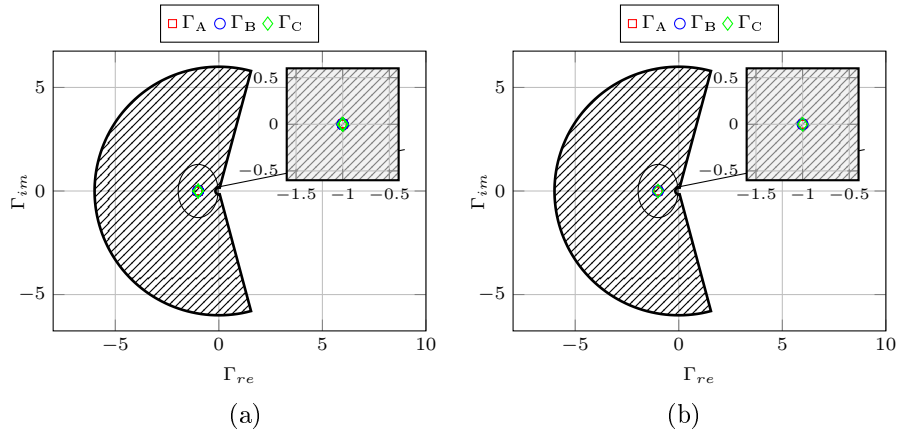


Figure 3.12. Case 1.9 - BC (a) GAP I; (b) GAP II

3.5 SUMMARY

In order to provide an overall comparison among the two GAPs, in Table 3.7 is listed a summary of all results obtained through each simulated case. Aiming to scale the performance of each GAP, three grades are created and their meaning is listed in Table 3.6. Afterwards the GAPs are graded, a mean value can be obtained by considering the values listed in same Table. In short, GAPs *I* and *II* will get a grade from zero to ten, where the greater the grade

Table 3.6. Application 1: Summary of Results

Grade	Meaning	Value
A	Criteria is fulfilled flawlessly.	10
B	Criteria is fulfilled, but the overall quality is inferior than other GAP	5
F	One or more criterion is not fulfilled, thus the GAP failed	0

The overall performance was measured using three different scores²: **A**, **B**, and **F**. All GAPs are scored in accordance with previously defined criteria. Indeed all formulations presented acceptable results, the proposed one obtained the best final score (8.8). While GAP *I* presented the worst performance, achieving 4.4. When compared to GAP *I*, the proposed formulation was 2 times better.

GAP *II* can be interpreted as a current mapping strategy (CMS), since currents \bar{I}_M and \bar{I}_N are different from the original one. Moreover GAP *I* results in same currents from the original system, as confirmed by Kaszteny *et al.* (2011).

Table 3.7. Application 1: Summary of Results

Case	GAP <i>I</i>	GAP <i>II</i>
1.1	B	A
1.2	B	A
1.3	F	A
1.4	A	A
1.5	F	B
1.6	F	B
1.7	B	A
1.8	B	A
1.9	A	A
score:	4.4	8.8

Finally, the proposed formulation is capable of improve the overall performance for a two-terminal line, even-thought a GAP strategy is not necessarily required for a two-terminal device. The fault conditions evaluated in this section are:

- Internal and external faults.
- Fault type, resistance and location alongside the transmission line.
- Load.
- Outfeed condition and CT saturation.

²The score was calculated by considering: **A** = 10; **B** = 5; **F** = 0.

APPLICATION 2: THREE-TERMINALS TRANSMISSION LINE

4.1 OVERVIEW

Power system expansion sometimes asks for modify a straightforward two-terminal transmission line into a tapped one, resulting in a multi-terminal apparatus. Indeed operation, control and protection are a main concern, but economical and geographical requirements are usually more strict. A transmission line can be tapped in any point of its extension aiming to follow those requirements. Therefore, protection challenges arise as main concern for power companies.

In Figure 4.1 an example of a tapped transmission line is shown. The first tap is to connect a substation and the second one a generator. In fact, one can expect a wide variety and quantity of taps, although operational requirements may limit that. Commonly wind farms and solar plants are connected to the power system through taps, since this approach usually represents smaller and cheaper substations (PERERA; KASZTENNY, 2014).

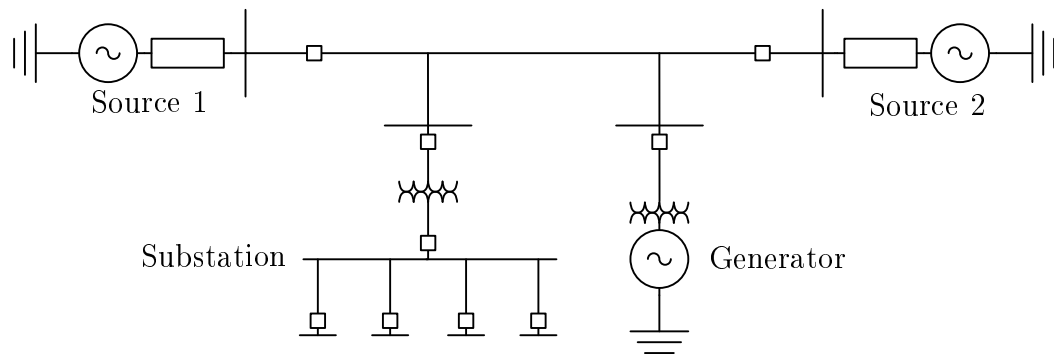


Figure 4.1. Transmission line tapped by a generator and a substation.

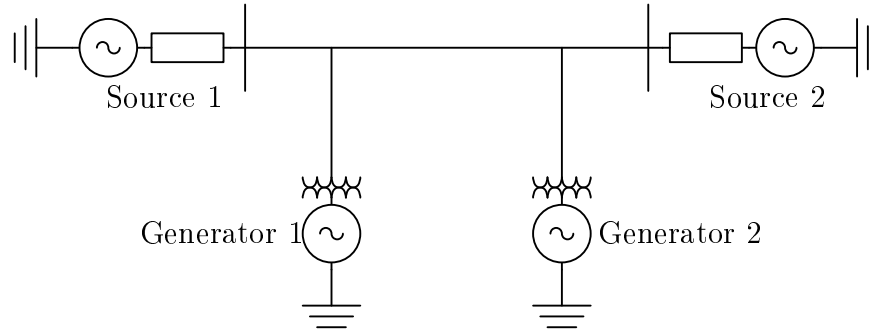


Figure 4.2. Transmission line tapped by generator twice.

Among several possibilities reported in literature, the configuration displayed in Figure 4.2 has some unique aspects that may affect the protection system design. Each tap consists of a transmission line, a transformer, and a generator.

In Figure 4.2 the challenge arises at first sight if grounded-star transformer are inside the transmission line protection zone. The existence of such devices can emulate an infeed current due the ground path. Therefore protection functions that use zero-sequence or neutral current may reduce their sensibility greatly, i.e. directional 67N, distance 21N, and differential 87G (PERERA; KASZTENNY, 2014). Indeed the biggest challenge occurs when the transformer is energized, due the presence of high magnetization currents called inrush currents. Therefore special strategies or separated protection functions may be required in order to guarantee acceptable safety during such maneuvers.

Aiming to overcome this challenge, a dual protection systems arises as an interesting option, i.e. use of two different function. Among several options, the combination of differential and directional functions are indeed attractive (PERERA; KASZTENNY, 2014). On the other hand, special countermeasures have to be accounted regarding performance, starting by adjust sensibility during inrush currents and avoid the use of zero sequence units. Besides that, another option is to use the overreach enabled by the second zone of a distance function as a supervision signal (PERERA; KASZTENNY, 2014).

Whenever a differential scheme is chosen to protect a multi-terminal transmission line, the protection engineer has to decide whether all currents are included or not. Although this undeniably reduces the overall sensibility and reliability of the scheme. Perera & Kasztenny (2014) affirms that only a single tap may be neglected, nevertheless its current magnitude has

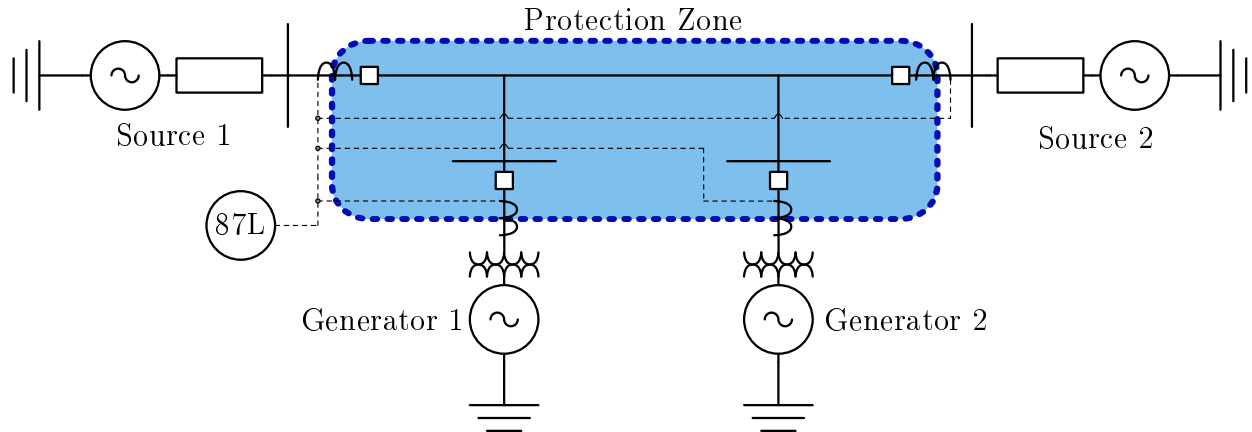


Figure 4.3. Example of 87L in a multi-terminal application.

to be small otherwise the protection sensibility can be drastically reduced. The optimal way to implement differential protection into a multi terminal transmission line is shown in Figure 4.3. The highlighted protection zone that bounds only the transmission line, while transformers and other devices requires their own protection system, also called in-line transformers. Perera & Kasztenny (2014) discuss important considerations regarding protecting a transmission line terminated on a transformer whenever it is required a single protection zone that includes both the line and the transformer.

4.2 APPLICATION DETAILS

Figure 4.4 shows the single line diagram for the 500 kV three-terminal transmission line evaluated in this chapter. The terminals are called Source 1, 2, and 3. They are represented by an ideal source and a impedance. Their Thévenin equivalent impedance is defined based on the SIR of each terminal. The segments between midpoint and the terminals are 100 km long each. Similarly to application 1, the charging current compensation is estimated following the procedure presented by (KASZTENNY *et al.*, 2011). The transmission line was modeled and simulated using ATP, more specific the Bergeron model which is a single frequency model. The SIR in each terminal was adjusted to 0.1, i.e. $SIR_1 = SIR_2 = SIR_3 = 0.1$. The CT was specified and modeled as ANSI C800 2000-5A, following guidelines from IEEE Power System Relaying Committee in (IEEE POWER SYSTEM RELAYING COMMITTEE, 2004). The CCVT is identical to the one presented by Pajuelo *et al.* (2008).

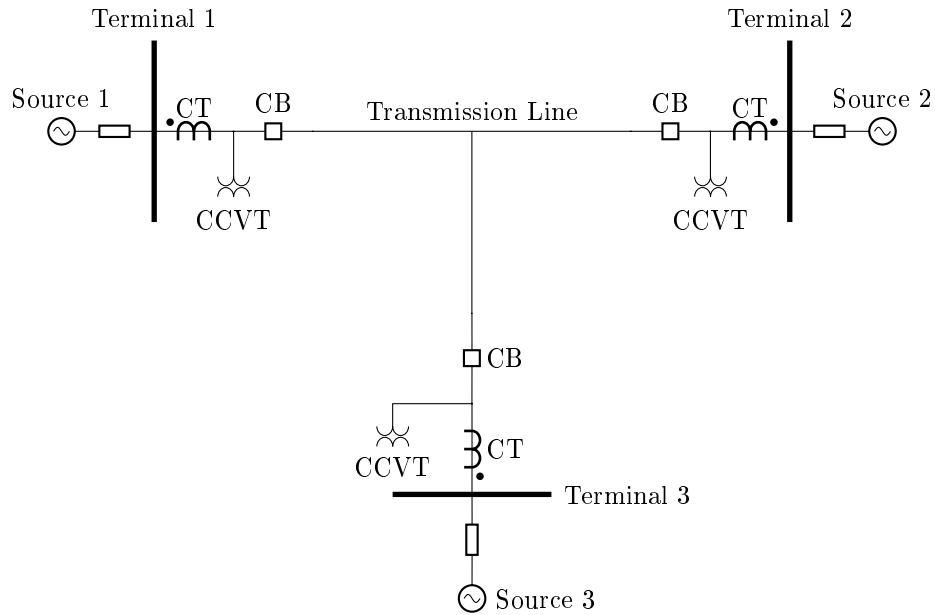


Figure 4.4. System 2 - 500 kV three-terminal Transmission Line

The ATP simulation was performed using a time-step of 1 micro-second ($1 \mu\text{s}$). The required current and voltages measurements are processed using an anti-aliasing low-pass third-order Butterworth filter, with cutoff frequency at 180 Hz. The base frequency of all systems is 60 Hz. Finally the signals are sampled into 16 samples per cycle ($\approx 1 \text{ ms}$). The phasors of voltages and currents are estimated using the discrete signal and a full-cycle cosine filter (HART *et al.*, 2000).

In order to analyze application 2, a total of six cases (2.1 to 2.6) will be presented. The first three cases are a transient response performance evaluation, while the other three consists in a massive data analysis. The proposed formulation is compared with GAP strategy presented by Miller *et al.* (2010). The results are shown separated for each GAP, consequently the same identification shown in Table 3.3 is applied.

4.3 TRANSIENT ANALYSIS

The proposed formulation is compared with GAP strategy reported by Miller *et al.* (2010), regarding transient response due to a fault in a three-terminal transmission line. Three different cases listed in Table 4.1 are presented. The analysis follows same three criterion from previous application, i.e. speed, reliability, and evenness. The number of required samples to cross the

trip area represents the speed. While reliability stands for operation only when expected to. Evenness is measured in accordance with how simple and consistent the transient response is.

In Figure 4.5 the results for case 2.1 are shown. Regarding speed of operation, GAPs *II* presented fast response while GAP *I* was the slowest. Following to second criterion, both GAPs successfully operated, and thus can be considered reliable. When measuring evenness GAP *I* undeniably results in the most tortuous path among all. On the other hand, GAP *II* presented equivalent results in regards third criterion. Case 2.2 presents 100Ω of fault resistance in the midpoint of the power system and thus a challenge to differential protection. Figure 4.6 shown the results. One can observe the slow response presented by GAP *I*, it took about 9 samples ($\approx \frac{1}{2} \times \text{cycle}$) to finally leave the restraint area. Differently, formulation *II* operated at same speed, but two times faster in relation to GAP *I*. Additionally, in regards to speed and evenness, both GAPs were more or less equivalent.

Case 2.3 is shown in Figure 4.7. The external fault followed by heavy CT saturation may lead to unexpected operation, and thus unnecessary power outages. Both GAPs endured the extreme fault condition, and can therefore be considered reliable. On the other hand, GAP *II* was less effected for CT saturation, since it presents in fewer oscillations when compared to the other GAP, this is enabled the adjustment $k_{\Delta} = 0.2$ or $\Psi = 2\%$.

Table 4.1. Application 2: Case Summary for Transient Analysis.

ATC	Fault	d	$R_f(\Omega)$	Observation
2.1	ABC	midpoint	0	Internal fault
2.2	BG	midpoint	100	Small Differential Current
2.3	ABC	external	0	Heavy CT saturation

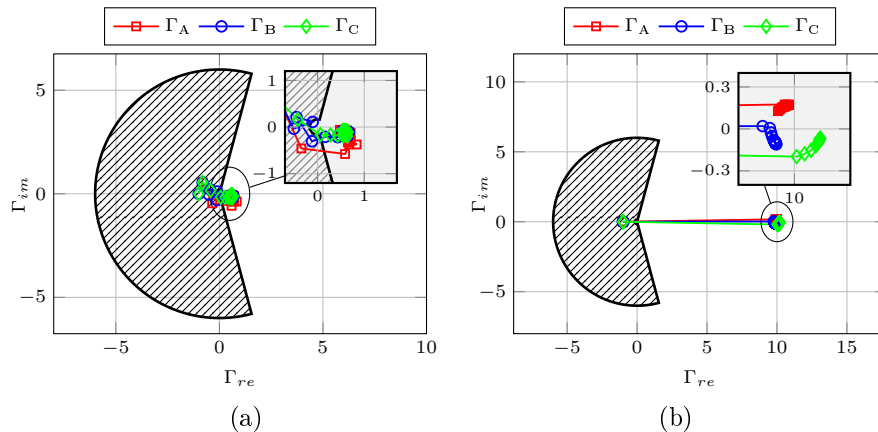


Figure 4.5. Case 2.1 - ABC (a) GAP *I*; (b) GAP *II*

4.4 MASSIVE DATA ANALYSIS

The performance of the proposed formulation was further evaluated through a massive data analysis. Same criteria from last application are used (i.e., reliability and trajectory length). The massive data is obtained by the variation of two previously chosen variables (i.e., Fault resistance and location). The interval of variation is listed in Table 4.2. The list of cases is shown in Table 4.3.

Table 4.2. Variables interval of study for System 2

Variable	Values
Fault Resistance (R_f)	phase-to-phase: 0, 5,...,195, 200. (Ω)
	phase-to-ground: 0, 10,...,90, 1000. (Ω)
Fault Location (p)	5, 10,...,90, 95. (% of each line segment)

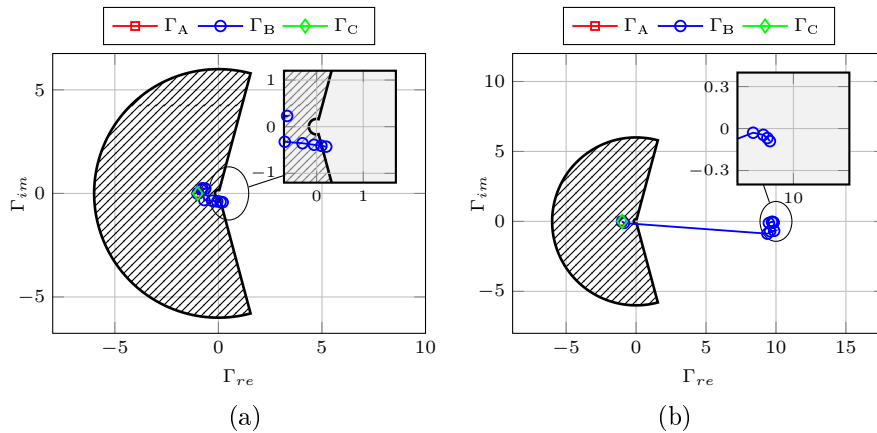


Figure 4.6. Case 2.2 - BG (a) GAP I; (b) GAP II

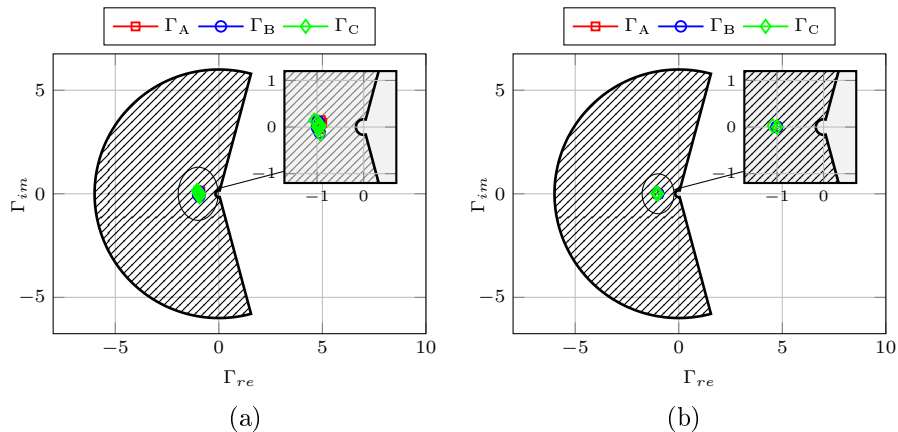


Figure 4.7. Case 2.3 - ABC (a) GAP I; (b) GAP II

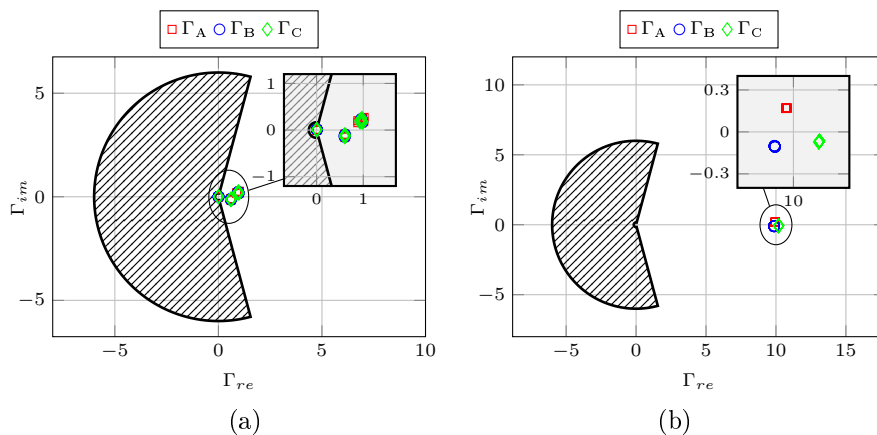
Table 4.3. Application 2: Case Summary for Massive Data Analysis.

Case	Type	p	$R_f(\Omega)$
2.4	ABC	5 to 95% of each line segment	0
2.5	AG	midpoint	0 to 1k
2.6	All	5 to 95% of each line	0 to 1k

Four different cases are listed in Table 4.3. Case 2.6 deserves special attention, it encompasses all different type of faults considering every phase combination possible (i.e., phase-to-ground, phase-to-phase, and three-phase).

In Figure 4.8 the obtained results for Case 2.4 are shown. The two GAPs successfully operated for the whole analysis interval, and can be considered reliable for this case. In regards of trajectory length, the plotted data allows to conclude that the trajectory were minimum, and therefore similar for the two studied formulations. Finally, fault location was not enough to cause trouble to any of the GAPs.

Next case is shown in Figure 4.9. The GAP *I* failed in first criterion, as one can observe in Figure 4.9a and can therefore be considered unreliable for some values of R_f . On the other hand, GAP *II* operated flawlessly. Concerning to trajectory length, GAP *I* presented the longest one, while formulation *II* resulted in equivalent dimension.

**Figure 4.8.** Case 2.4 - ABC (a) GAP *I*; (b) GAP *II*

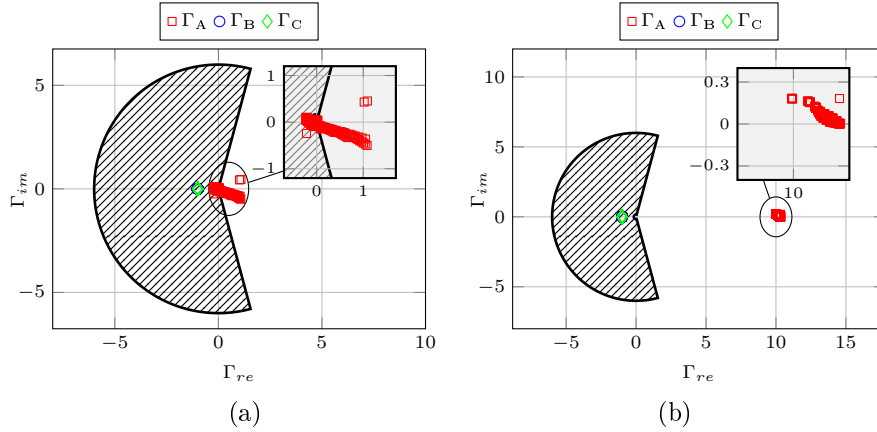


Figure 4.9. Case 2.5 - AG (a) GAP *I*; (b) GAP *II*

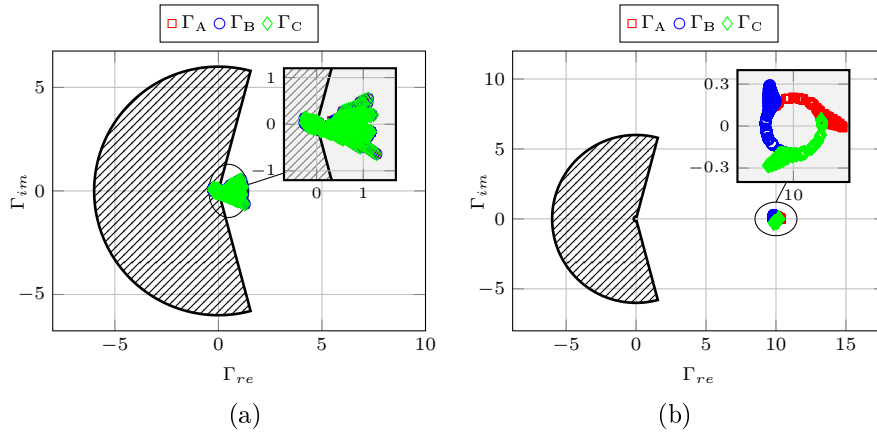


Figure 4.10. Case 2.6 (a) GAP *I*; (b) GAP *II*

A total of 5130 faults were simulated in Case 2.6 and are shown in Figure 4.10. The GAP *I* was the one most affected by the fault parameters, its performance is diminished in presence of outfeed currents. On the other hand, GAP *II* were capable to operate as expected, and can therefore be considered more reliable than formulation *I*. It is noteworthy that Miller *et al.* (2010) suggest the use of sequence elements in order to complement the unit protection of the multi-terminal transmission line. Additionally, the settings Γ_f and k_Δ enabled to GAP *II* a well-defined region in the right half-plane.

4.5 SUMMARY

Indeed both GAP strategies performed well in previous analyses, it is necessary to obtain a final and direct comparison among all. In Table 4.4 is listed scores (i.e., **A**, **B**, and **F**).

for each GAP in regards all six cases. The proposed one obtained the perfect final score¹. On the other hand, GAP *I* performed the worst, reaching 4.2. Finally, the GAP *II* was 2.3 times better than GAP *I*.

Table 4.4. Application 2: Summary of Results

Case	GAP <i>I</i>	GAP <i>II</i>
2.1	B	A
2.2	B	A
2.3	B	A
2.4	A	A
2.5	F	A
2.6	F	A
score:	4.2	10

¹The score was calculated by considering: A = 10; B = 5; F = 0.

APPLICATION 3: BUSBAR ARRANGEMENT

5.1 OVERVIEW

Busbar arrangements vary in size, complexity, and number of devices. To ensure an effective protection scheme, valuable guidelines are presented in (IEEE C37.234TM, 2009), whereas details regarding a wide variety of bus arrangements, possible protection schemes, and special applications are presented. Also, it is thoroughly discussed how to adjust dynamically protection bus zones, in accordance with the disconnect switches (DS) electrical position (opened or closed). For instance, the busbar arrangement shown in Figure 5.1 does not require dynamic zone selection. On the other hand, some busbar arrangements (e.g. double-bus-single-breaker) present flexible bus configuration, in which a network element can be connected to two or even more buses through disconnect switches. In Figure 5.2 an example of such system is shown. Besides that, protection schemes for a non-static busbar arrangement demands breaker failure protection (BFP) and dead zone tie breaker requirements as a byproduct (IEEE C37.234TM, 2009; IEEE C37.119TM, 2016).

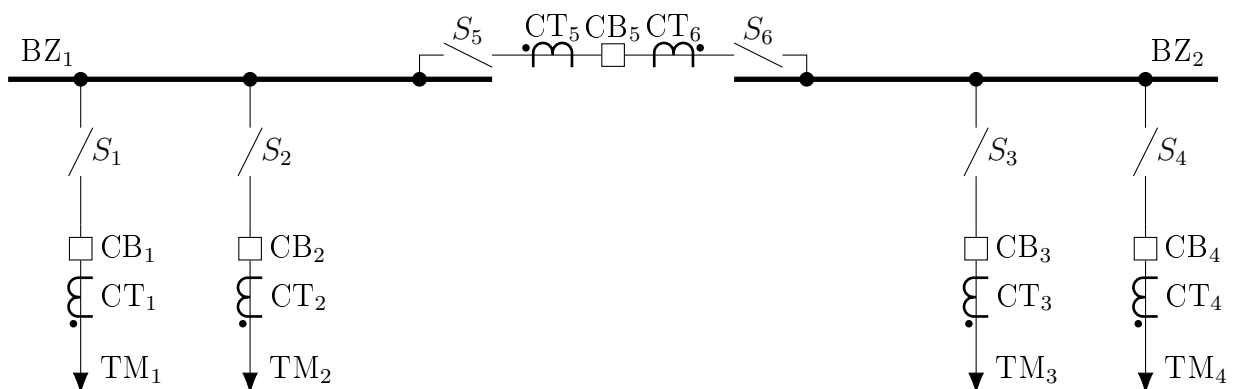


Figure 5.1. Single Bus With Bus Sectionalizer (Tie Breaker)

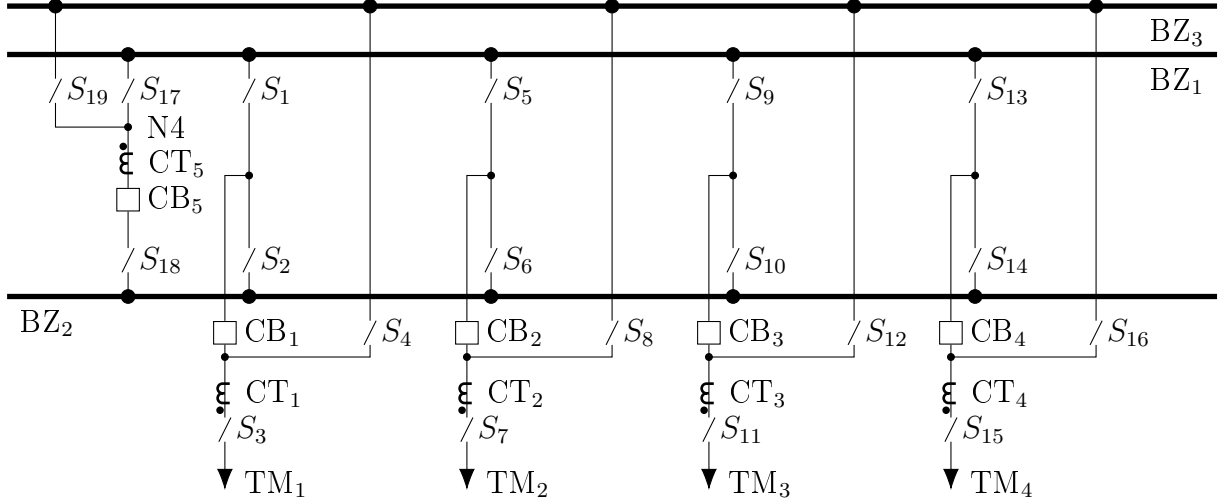


Figure 5.2. Double Bus and Transfer Bus With Bus Coupler (Tie Breaker) and Outboard CTs.

Busbars are divided into protection zones, in order to reduce the disturbances footprint. The busbar protection zones are bounded by position and polarity of CTs. Therefore, considering the flexible arrangement shown in Figure 5.2, the scheme has to adjust and select protection zones dynamically, in accordance with the instantaneous electrical configuration of the busbar (GUZMAN *et al.*, 2005; STEENKAMP K. BEHRENDT, 2007). Thereby, each bus has its own protection zone (ZIEGLER, 2012). Consequently, enabling flags have to be considered when calculating operational and restraining currents, I_{op} and I_{res} , respectively. Aiming to exemplify that:

$$I_{op}^{Z_\phi} = \left| \sum_{k=1}^n f_k^Z \cdot \bar{I}_k^\phi \right|, \quad (5.1)$$

$$I_{res}^{Z_\phi} = \sum_{k=1}^n f_k^Z \cdot \left| \bar{I}_k^\phi \right|, \quad (5.2)$$

where $I_{op}^{Z_\phi}$ and $I_{res}^{Z_\phi}$ corresponds to operational and restraining current of each phase ϕ , on the zone Z ; \bar{I}_k^ϕ is the current phasor on phase ϕ of the k -th circuit; and f_k^Z is the flag that enables the current to that zone.

A previous effort to improve protection zone selection used a method based on graph theory (Bai-Lin Qin *et al.*, 2000; QIN; GUZMAN-CASILLAS, 2002; SU *et al.*, 2005). Bai-Lin Qin *et al.* (2000) described their method as a graphical representation of bus arrangements where predefined branches (e.g breaker, CT, breaker-CT, DS) are represented as edges and the other components are vertexes. Three different graph operations (e.g.contraction, ring sum and removal) are executed or combined depending on the position and the logical status of disconnect

switches, therefore the central unit relay has the duty to update in real time the zone selection whenever a switch is operated. Logic control equations regarding protection zone supervision and check zone are enabled by the method, besides the ability to handle faults occurring in an “end zone” between a breaker and a series connected CT. Nevertheless selectivity and reliability are also stickily provided based on IEEE C37.234TM (2009). However, the representation using a single incident matrix can lead to a high order sparse matrix, either compromising the speed and reliability of zone selection, or demanding extensive computer burden from the microprocessor-based bus relay. Other important limitation lies on the requirement that logic equations for supervision and check zone have to be calculated manually, which can achieve high degree of complexity for mixed bus configurations.

Guzman *et al.* (2004) presented thoroughly a reliable protection system that includes busbar protection and advanced zone selection based on Bai-Lin Qin *et al.* (2000) and Qin & Guzman-Casillas (2002). This work considered protection zone (PZ) as an protection area formed by at least one bus-zone (BZ), nevertheless a protection zone can include more than one bus-zone, if there is a solid connection among them. Whenever two or more bus-zones are merged, a single protection zone arises including all adjacency connections. Two main programmable equations IqBZp (Terminal-to-Bus-zone) and BZpBZp determine terminals and BZ to be included in each PZ, likewise terminals to trip in accordance to differential protection operation in each PZ.

In regards of protection algorithms, most of the schemes use directional and differential functions (ALTUVE; SCHWEITZER, 2010). Nonetheless, each function allows several variants (QIN *et al.*, 2000; GUZMAN *et al.*, 2005; KANG *et al.*, 2005; KANG *et al.*, 2008). Likewise Bainy & Silva (2017) and Jena & Bhalja (2018) present the benefits and remarks due the adoption of a GAP strategy with differential busbar protection. Wavelet transform based algorithms have been reported as an option to reduce the protection operating time (EISSA, 2004; GAFOOR; RAO, 2011; EISSA, 2014; SILVA *et al.*, 2018).

5.2 APPLICATION DETAILS

The next system is the busbar arrangement shown in Figure 5.3. The configuration is a double bus with one breaker and five switches, with rated voltage of 230 kV and base frequency of 60 Hz. The diagram comprises a substation with six feeders, in which four 180 km long transmission lines (TL1, TL2, TL3 e TL4) and two power transformers (TF1 and TF2) are connected. During normal operating conditions, TL1, TL3 and TF1 are connected to Bus 1, whereas TL2, TL4 and TF2 are connected to Bus 2, and Buses 1 and 2 are connected through the bus coupler circuit breaker (CB). The transmission lines were modeled as perfectly transposed with distributed and frequency dependent parameters (Bergeron model), whereas power transformers were modeled using the saturable transformer model. For this analysis, only the zone 1 was studied, also three out of six circuits are connected to bus 1. The dynamic zone selection was implemented following the guidelines from (IEEE C37.234TM, 2009).

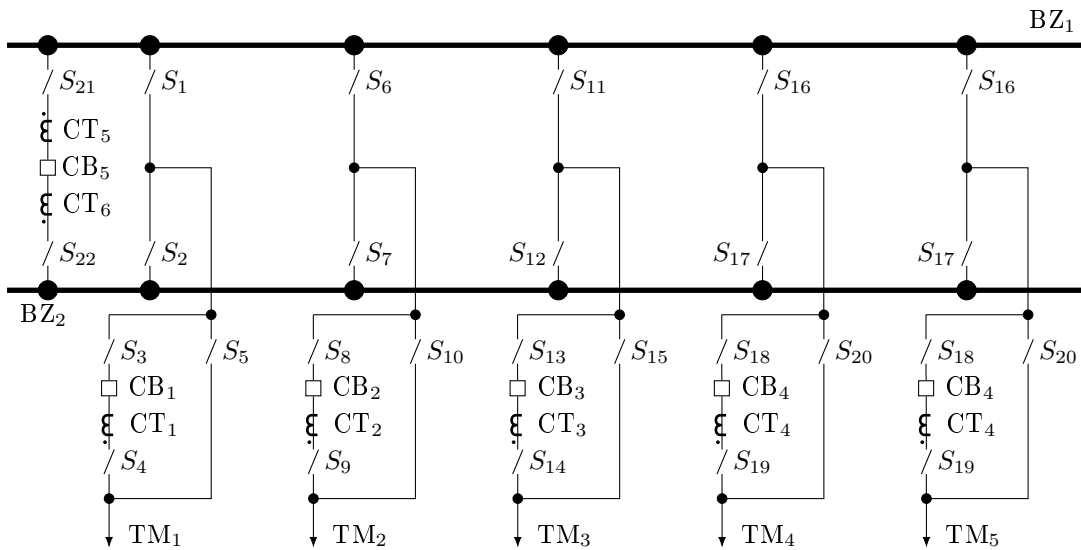


Figure 5.3. System 3: Busbar Arrangement - 230 kV with six terminals.

This busbar was simulated in the ATP software and using a time-step of 1 micro-second ($1 \mu\text{s}$). The required current are processed using an anti-aliasing low-pass third-order Butterwoth filter, with cutoff frequency tuned to 180 Hz. Additionally, the signals are sampled into 16 samples per cycle, and therefore the phasors of currents are estimated using the discrete signal and a full-cycle cosine filter (HART *et al.*, 2000).

Four different cases are analyzed in this Section (3.1 to 3.4). The first two cases are a transient response performance evaluation, while from the rest consists in a massive data analysis. The proposed formulation is compared with GAP strategy presented by Miller *et al.* (2010). Finally the results are shown separated for each GAP, consequently the same identification shown in Table 3.3 is employed.

5.3 TRANSIENT ANALYSIS

The two transient analysis cases are detailed in Table 5.1. Identical three criterion from previous application are employed (i.e., speed, reliability, and evenness).

Table 5.1. Application 3: Case Summary for Transient Analysis.

Case	Fault	d	$R_f(\Omega)$	Fault Angle (Θ)	Observation:
3.1	ABC	internal	0	0°	Internal fault
3.2	AG	external	0	0°	Heavy CT saturation

In Case 3.1 a solid three-phase internal fault occurs at bus 1, and the results are shown in Figure 5.4. the GAP *II* is faster in about 3 samples when compared to GAP *I*, which represents around 3 ms. In regard of reliability both formulations operated without problems, and can therefore be considered reliable for the simulated conditions. Finally, the GAP *II* presented the transient path with best evenness.

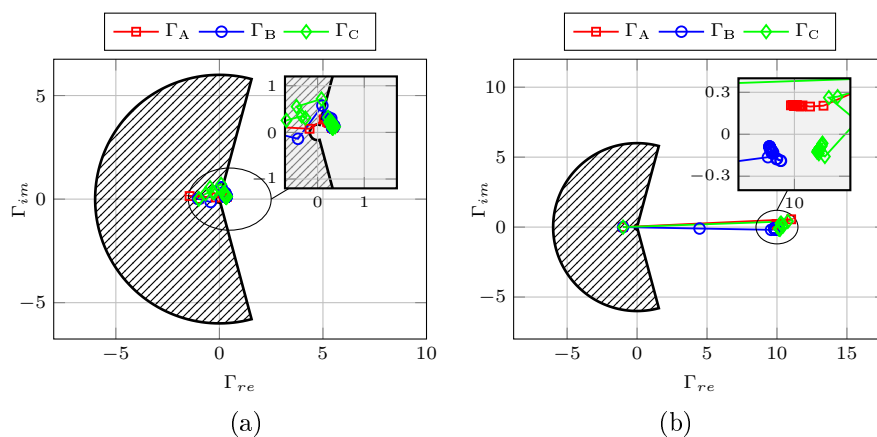


Figure 5.4. Case 3.1 - ABC (a) GAP *I*; (b) GAP *II*

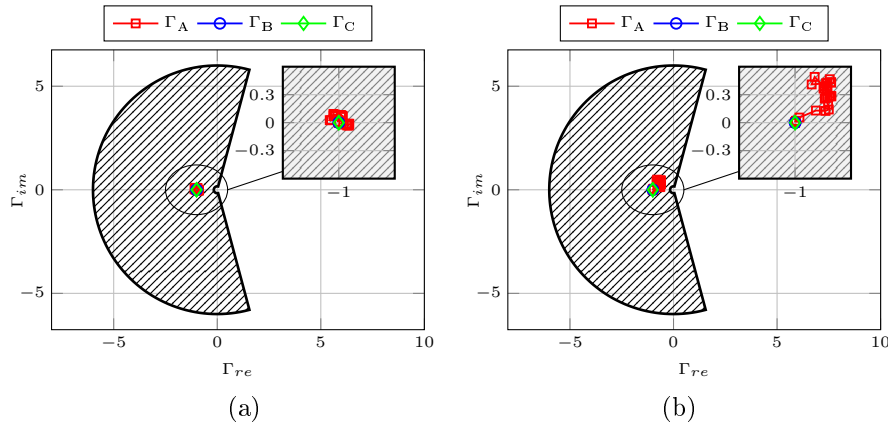


Figure 5.5. Case 3.2 - AG (a) GAP *I*; (b) GAP *II* (c)

Figure 5.5 presents the results for Case 3.2. It is noteworthy that the external fault causes severe CT saturation, thus a challenge for busbar differential protection. Both GAPS have not operated, and can therefore be considered reliable. GAP *II* presented more sensitivity to the external fault than formulation *I*. Situations the results in even higher CT saturation could possibly cause a miss-operation of the GAP *II*.

5.4 MASSIVE DATA ANALYSIS

The massive data analysis enables further evaluation about the proposed GAP. Two main cases are analyzed and the studied variables intervals are listed in Table 5.2. The internal fault conditions for Case 3.3 varies in accordance with Table 5.2, while the only difference of Case 3.4 is that it consists of an evolutive fault (i.e., external to internal). The criteria of analysis are identical to last application (i.e., reliability and trajectory length).

In Figure 5.6 the results for case 3.3 are shown. A total of 350 simulations were performed using ATP for this case. In regards of reliability, GAP *I* misoperated 21 times thus corre-

Table 5.2. Range of Variable Values for Application 3

Simulation Variables	Chosen Values
Fault Resistance	phase-to-phase (R_F): 0, 5, 10, 15, and 20 (Ω)
	phase-to-ground (R_G): 0, 25, 50, 75, and 100 (Ω)
Fault Angle (Θ)	0, 30, 60,...,150, and 180 ($^\circ$)
Fault type	AG,...,CG, AB,...,CA, ABG,...,CAG, and ABC

sponding to 6 % fail-rate. On the other hand, GAP *II* operated for all cases, moreover settings Γ_f and k_Δ settle Γ into well-defined region around the point $(\Gamma_f, 0)$ in the right-half-plane. Additionally, the trajectory length was similar for both GAPs.

Finally Case 3.4 is shown in Figure 5.7. Likewise last case, GAP *I* was incapable of operate for around 10 % of all cases. In addition, another problem is the critical close proximity between the values of Γ and the restraint characteristic. On the other hand, the proposed formulation successfully operated for all interval of study shown in Table 5.2 thanks to the proposed settings Γ_f and k_Δ . Indeed the settlement point control enabled by the proposed GAP has proven to be a valuable improvement of the formulation previously reported in Silva & Bainy (2016).

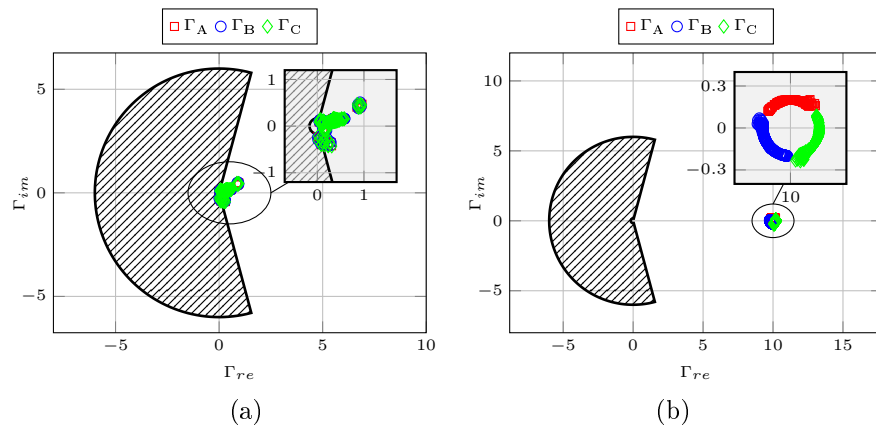


Figure 5.6. Case 3.3 (a) GAP *I*; (b) GAP *II*

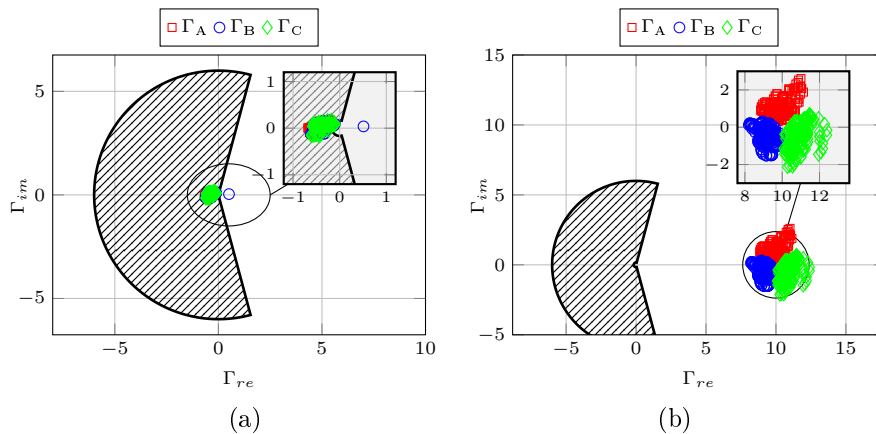


Figure 5.7. Case 3.4 (a) GAP *I*; (b) GAP *II*

5.5 SUMMARY

Both GAPs were pushed to their limits in this application, and until some degree are adequate to protect a busbar. In Table 5.3 is listed scores (i.e., **A**, **B**, and **F**.) for each GAP

in regards the four cases. The GAP *II* obtained the best final score¹ 8.7, and in second place is GAP *I*. The proposed formulation was 2.3 better than GAP *I*.

Table 5.3. Application 3: Summary of Results

Case	GAP <i>I</i>	GAP <i>II</i>
3.1	B	A
3.2	A	B
3.3	F	A
3.4	F	A
score:	3.7	8.7

It is noteworthy to mention that particularities regarding busbar protection were not investigated in this chapter, due the uncommon use of GAP based differential protection schemes to protect busbar applications. The fault conditions evaluated in this section are:

- Internal and external faults.
- Fault type.
- Fault resistance.
- Fault angle.
- CT saturation.

¹The score was calculated by considering: A = 10; B = 5; F = 0.

CHAPTER 6

APPLICATION 4 - POWER TRANSFORMER

6.1 OVERVIEW

Power transformers are more often protected by differential schemes (ALTUVE; SCHWEITZER, 2010). Protection against internal faults is achieved by measuring input/output currents for all three phases, and therefore defining a protection zone. Additionally, the transformer is protected by others unique functions that usually monitors intrinsic variables, such as oil pressure.

When protecting a transformer, some important aspects have to be considered beforehand in order to guarantee a valid protection scheme: ratio, phase-group, CT saturation, overexcitation, and sympathetic inrush current. The ratio is important in order to convert the measured to the per unit (pu) system (ALTUVE; SCHWEITZER, 2010). In addition, phase compensation can be required if the transformer has delta or zig-zag connections, since a spurious differential current may arise (IEEE, 2008b).

The magnetic core of CTs can saturate during certain conditions, and thus compromise differential protection optimum performance (ZIEGLER, 2012). Both external and internal faults are able to cause CT saturation, the first affects security in first place due the high chances of occur unnecessary operation. For internal faults, according to the relation of harmonics, the restraining can gets so high that the protection becomes either slow or unable to operate. Both compromises are extensively harmful to the transformer protection scheme. The magnetic flux insides CT's core is directly proportional to the input voltage, and inversely proportional to the power frequency. Therefore, over-voltages and under-frequencies can cause CT saturation. One can use the fifth harmonics current signals to detect overexcitation (BLACKBURN; DOMIN, 2014). Another challenge is due the inrush currents, it is unpredictable and may result in misoperation of the protection scheme (B5.07, 2011). They are mostly expected during transformer energization, and therefore require special settings in order to overcome false trips occurrence.

In regards of internal faults, some of them such as interturn faults taking few turns arise as a challenge for the protection to operate properly (KASZTENNY *et al.*, 2010). When aiming to overcome this drawback two options arise: negative sequence and restricted earth-fault (REF) elements (KASZTENNY *et al.*, 2010; GUZMAN *et al.*, 2009; KASZTENNY *et al.*, 2015). Other important strategies adopted to avoid relay misoperation are: the harmonic restraint and blocking strategies (GUZMAN *et al.*, 2009; HAMILTON, 2013). On the other hand, these strategies usually result in some degree of compromise regarding the protection scheme’s speed and reliability. One can expect operation delay, and even inhibit the operation for minor internal turn-to-turn faults (GUZMAN *et al.*, 2001b).

Methods based on symmetrical components applied to transformer protection are extremely popular and widely used (KASZTENNY *et al.*, 2010; RASOULPOOR; BANEJAD, 2013), their high sensitivity to operate due unbalanced faults can be really useful for the protection scheme. On the other hand, the symmetrical components usually have to be blocked during external faults and transformer energization maneuvers, since those are capable to cause misoperation. Similarly to chapter 3 the two-terminal transformer does not require a GAP formulation to use alpha plane. In this manner, the objective of this chapter is identify the benefits enabled by the proposed GAP in comparison with GAP *I* and *II* even when applied to transformers.

6.2 APPLICATION DETAILS

The System 4 consists of: two Thevenin equivalents represented by the voltage sources 1 and 2, their related impedances, connected to the primary and secondary windings of the power transformer, respectively. The system is shown in Figure 6.1. The power transformer has ratio of $V_p : V_s = 230 : 69$ kV, rated power of 100 MVA, and has the high voltage winding connected in star with grounded neutral terminal and the low voltage winding in delta (YNd1). Aiming to model its non-linear characteristics, the Hevia Hysteresis ATP routine was used to model the power transformer and the windings were partitioned for simulation of incipient internal faults. The CT installed on high voltage winding was specified as ANSI C400 400-5A, while the low voltage winding was modeled as ANSI C800 2000-5A (IEEE POWER SYSTEM RELAYING COMMITTEE, 2004).

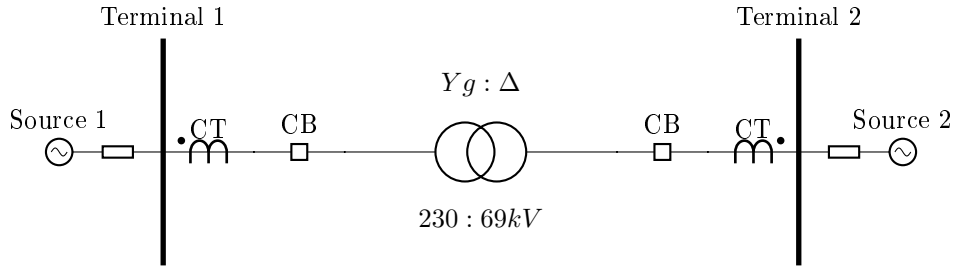


Figure 6.1. System 4: power transformer Wye-Delta (230:69kV).

The simulations were executed using the ATP, considering a time-step of 1 micro-second ($1 \mu\text{s}$). The in/out currents are processed using an anti-aliasing low-pass third-order Butterworth filter, with the cutoff frequency tuned to 180 Hz. The signals are sampled into 16 samples per cycle ($\approx 1\text{ms}$). Finally, the phasors of currents are estimated using the discrete signal and a full-cycle cosine filter (HART *et al.*, 2000). The base frequency of all systems is 60 Hz.

A total of four cases (4.1 to 4.4) are thoroughly analyzed using System 4. The transient response performance evaluation is performed in the two first cases. Additionally, the other two are the massive data analyses. The proposed formulation is extensively compared with GAP reported by Miller *et al.* (2010). Finally the results are shown separated for each GAP, consequently the same identification shown in Table 3.3 is carried out.

6.3 TRANSIENT ANALYSIS

Two cases are presented in this section. The details for cases 4.1 and 4.2 are summarized in Table 6.1. The three criterion from previous application are used to analyzed the transient path of each GAP (i.e., speed, reliability, and evenness).

Table 6.1. Application 4: Case Summary for Transient Analysis.

Case	Fault	Type	d	Side
4.1	ABC	turn-to-turn	50 %	Wye
4.2	ABC	turn-to-turn	20 %	Delta

In case 4.1 each winding (A, B, and C) undergo a turn-to-earth fault at 50% of each winding, high voltage side (grounded Wye). Figure 6.2 highlights that both GAPs operated as expected, although a faster detection can be identified in GAP *II* transient response by around 3 samples.

Following to the case 4.2 where its results is shown in Figure 6.3. The fault is a turn-turn in delta-side (low-voltage) in all three winding and 20% of each is shorten. The GAP *I* failed to operate, nonetheless GAP *II* operated correctly. In regards of evenness, GAP *II* performed better than GAP *I*.

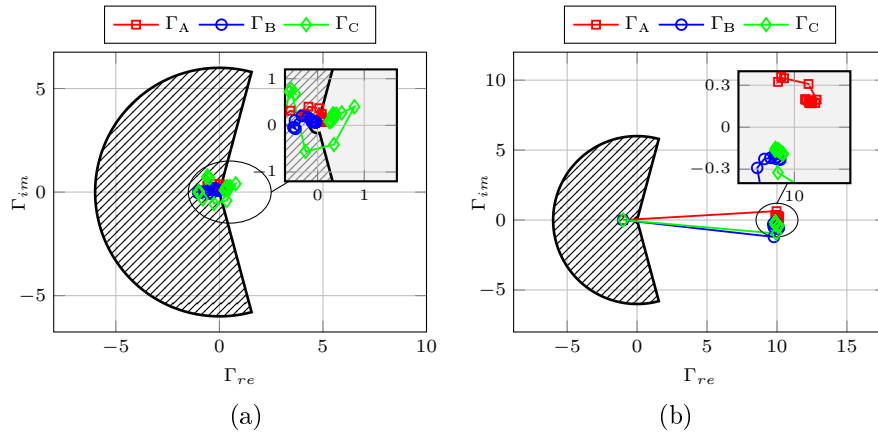


Figure 6.2. Case 4.1 - ABC (a) GAP *I*; (b) GAP *II*

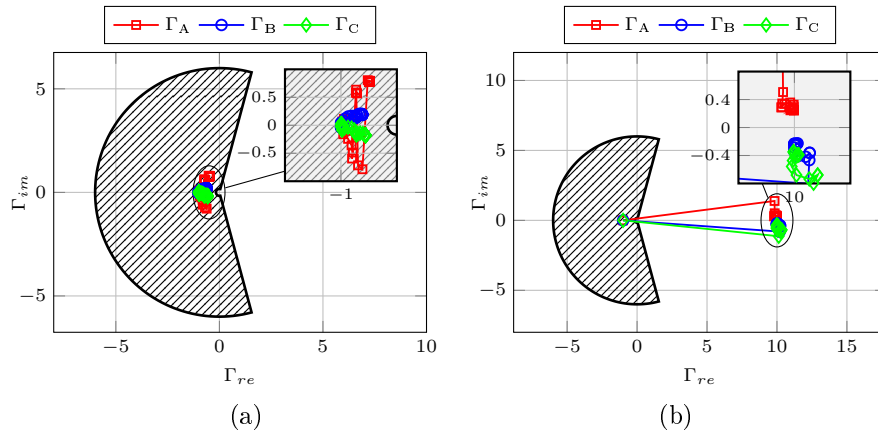


Figure 6.3. Case 4.2 - ABC (a) GAP *I*; (b) GAP *II*

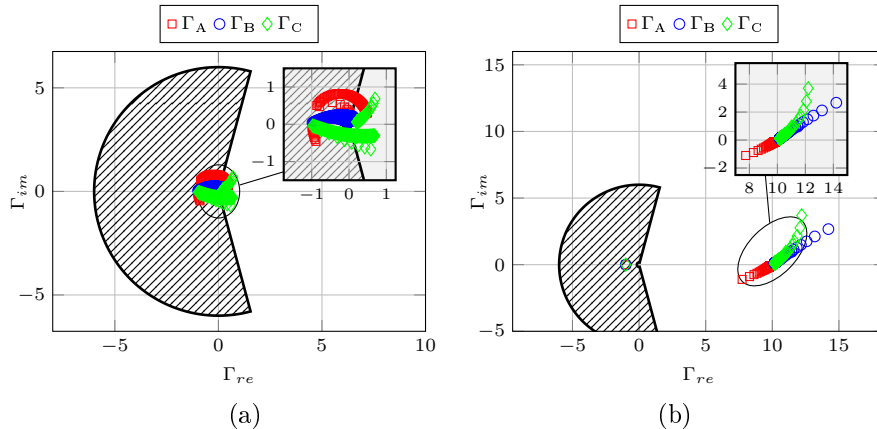
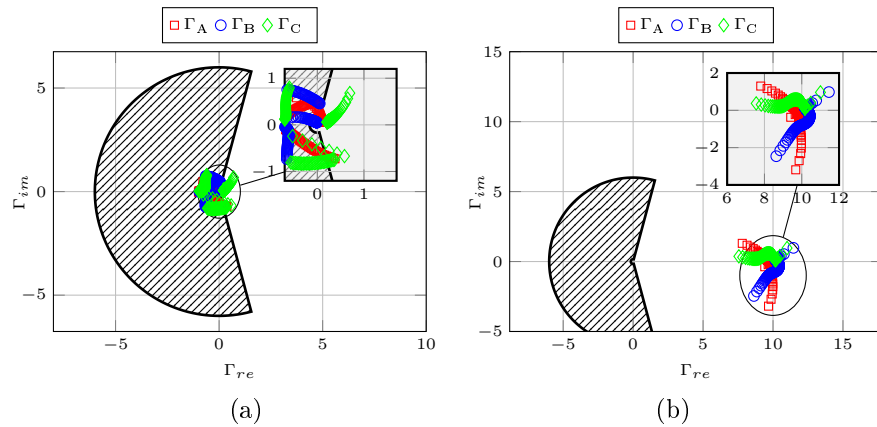
6.4 MASSIVE DATA ANALYSIS

The massive data analysis allows to identify limitations of any GAP regarding extreme conditions. Two cases are analyzed and the studied variables intervals are listed in Table 6.2. The criteria of analysis are identical to last application (i.e., reliability and trajectory length).

Table 6.2. Application 4: Case Summary for Massive Data Analysis.

Case	Phases	Type	d (%)	Side
4.3	ABC	turn-to-turn	1, 2,...,97, and 98	both
4.4	ABC	turn-to-earth	1, 2,...,97, and 98	both

The case 4.3 results are shown in Figure 6.4. A total of 196 simulations were performed and the GAP *I* failed to operate in about 25% of the simulations, while the GAP *II* failed for about 0.5%. Furthermore, GAP *I* had more difficult to detect small winding percentages (below 45%) and faults in Delta side. On the other hand, the GAP *II* failed only in one case: 2% in Delta-side. Finally, the last case for system 4 is shown in Figure 6.5. A set of 196 simulations were presented in this case. The GAP had a lot of trouble to operate properly. It did no operate for 91 simulations, that is around 45% of fail rate. The GAP *II* has proven its reliability and speed for a wide variety os faults, and an acceptable trajectory length.

**Figure 6.4.** Case 4.3 - turn-to-turn (a) GAP *I*; (b) GAP *II***Figure 6.5.** Case 4.4 - turn-to-earth (a) GAP *I*; (b) GAP *II*

6.5 SUMMARY

In the last application both GAPs were thoroughly analyzed and their limits tested. In Table 6.3 is listed scores (i.e., **A**, **B**, and **F**.) for each GAP in regards the four cases. The GAP *I* was the one with lowest score¹ 1.3 due a high degree of misoperations detected. Finally the proposed formulation was the best with score of 7.5. The GAP *II* was 6 timer more effective than GAP *I*, therefore proven its quality for transformer protection applications.

Table 6.3. Application 4: Summary of Results

Case	GAP <i>I</i>	GAP <i>II</i>
4.1	B	A
4.2	F	A
4.3	F	F
4.4	F	A
score:	1.3	7.5

It is noteworthy to mention that particularities such as transformer energization (inrush currents) were not investigated in this chapter. In order to do so, a more refined GAP based differential protection scheme has to be developed and tested. The GAP allows special customization in order to overcome problems related to the inrush current, however such solutions were not explored in this thesis and are expected to be investigated in future works. The fault conditions evaluated in this section are:

- Internal and external faults.
- Fault location alongside the transformer coils
- Fault type.

¹The score was calculated by considering: **A** = 10; **B** = 5; **F** = 0.

CONCLUSIONS AND FUTURE WORK

The main topics and remarks of a differential protection scheme for alpha plane applications in multi-terminal power system apparatuses has been presented. A new generalized alpha plane strategy has been proposed for multi-terminal differential protection devices. The formulation is based on Silva & Bainty (2016), but allows two settings, called Γ_f and k_Δ , to adjust the settlement point during fault steady state. An analytical analysis is performed to preliminary the proposed GAP response in alpha plane and the main remarks have been described.

The proposed GAP was conceived to perform a smooth transient path during faults, and adjust the fault steady state settlement values in the alpha plane. Afterwards, it was shown that Γ_f and k_Δ define a circumference in right-half alpha plane, which Γ will settle under fault conditions during steady-state.

In order to test the proposed GAP, four different applications were simulated using ATP (i.e., two and three terminals transmission lines, busbar, and transformer). In addition the proposed GAP was compared with GAP reported by (MILLER *et al.*, 2010). The simulations were divided into two different types: transients and massive data analysis. Each GAP was scored into with the shown results, and the final score is listed in Table 7.1.

The transient response and trajectories obtained by using the proposed GAP were presented and discussed. The advantage of proposed formulation over GAP (MILLER *et al.*, 2010) has been shown. The smooth and direct transient path during faults was present in every application. The main advantage of this GAP is high reliability and speed. It can mitigate wide conditions for each application efficiently.

One important conclusion that can be inferred is that the proposed formulation consists of a generalization of the GAP in (SILVA; BAINY, 2016), presenting great improvements due the proposition of adjustments Γ_f and k_Δ . Additionally, the parameter k which had no straightforward procedure to be adjusted, now is substituted by Γ_f and k_Δ .

Table 7.1. Summary of Results

Application	GAP <i>I</i>	GAP <i>II</i>
1	4.4	8.8
2	4.2	10
3	3.7	8.7
4	1.3	7.5
final score:	3.4	8.8

In respect to computational burden requirements, the GAP *I* requires 19 float-point operations (FLOPs), whereas the GAP *II* and the proposed one requires 11 FLOPs only, attesting its better computational efficiency.

7.1 FUTURE WORK

The future work should include more detailed analysis of the proposed GAP for different applications and for more extreme conditions. In addition, a comparison of its performance combined with real-life relays in a laboratory interfaced to an Real Time Digital Simulator (RTDS).

The GAP developed in this thesis could be used as a starting point to investigate the following:

- Define a new and improved restraint characteristic based in the enhanced one proposed by Tziouvaras *et al.* (2002) . Moreover, specify it specially for busbar, multi-terminal transmission lines, and transformers.
- Investigate possible advantages of using adaptive settings (i.e., Γ_f , k_Δ and Ψ).
- Implement refined protection scheme that use the proposed GAP to protect different equipment considering their particularities.
- Test the method in series compensated transmission lines.
- Study an alternative restraining characteristic, such as an operational characteristic.

7.2 PUBLICATIONS DURING PHD

A list of all publications related to this thesis are listed below:

- BAINY, R. G.; SILVA, K. M. Proteção Diferencial de Barramentos Baseada no Plano Alfa Generalizado. In: *2016 Simpósio Brasileiro de Sistemas Elétricos (SBSE)*. Brasília, Brasil: Natal-RN.
- SILVA, K. M.; BAINY, R. G. Generalized Alpha Plane for Numerical Differential Protection Applications. *IEEE Transactions on Power Delivery*, v. 31, n. 6, p. 2565–2566, dec 2016. ISSN 0885-8977.
- BAINY, R. G.; SILVA, K. M. Generalized Alpha Plane for Numerical Differential Protection Applications. In: *2017 Power and Energy Society General Meeting (PESGM)*. Chicago, US: IEEE, 2017. p. 1–4.
- BAINY, R. G.; SILVA, K. M. Busbar differential protection based on generalized alpha plane. In: *2017 Workshop on Communication Networks and Power Systems (WCNPS)*. Brasilia, Brasil: IEEE, 2017. p. 1–4.

BIBLIOGRAPHY

- ALMEIDA, M. L. S.; SILVA, K. M. Transmission lines differential protection based on an alternative incremental complex power alpha plane. *IET Generation, Transmission Distribution*, v. 11, n. 1, p. 10–17, 2017. ISSN 1751-8687. Cited 4 times in pages 3, 19, 70, and 71.
- ALTUVE, H. J.; SCHWEITZER, E. O. *Modern Solutions for Protection, Control and Monitoring of Electric Power Systems*. 1st. ed. Pullman, USA: Quality Books, 2010. Cited 8 times in pages 2, 3, 18, 19, 20, 40, 46, and 62.
- ANDERSON, P. M. *Power System Protection*. Piscataway, New Jersey, USA: IEEE Press Series on Power Engineering, 1999. Cited 3 times in pages 3, 61, and 64.
- B5.07, W. *Modern Techniques for Protecting and Monitoring of Transmission Lines*. [S.l.], 2011. Cited in page 46.
- Bai-Lin Qin; GUZMAN-CASILLAS, A.; SCHWEITZER, E. A new method for protection zone selection in microprocessor-based bus relays. *IEEE Transactions on Power Delivery*, v. 15, n. 3, p. 876–887, jul 2000. Disponível em: <<http://ieeexplore.ieee.org/document/871347/>>. Cited 2 times in pages 39 and 40.
- BAINY, R. G.; SILVA, K. M. Busbar differential protection based on generalized alpha plane. In: *2017 Workshop on Communication Networks and Power Systems (WCNPS)*. Brasilia, Brasil: IEEE, 2017. p. 1–4. Cited 3 times in pages 3, 7, and 40.
- BARBOSA, D.; NETTO, U. C.; COURY, D. V.; OLESKOVICZ, M. Power transformer differential protection based on clarke's transform and fuzzy systems. *IEEE Transactions on Power Delivery*, v. 26, n. 2, p. 1212–1220, April 2011. ISSN 0885-8977. Cited in page 3.
- BEHRENDT, K.; FISCHER, N.; LABUSCHAGNE, C. Considerations for using harmonic blocking and harmonic restraint techniques on transformer differential relays. *Journal of Reliable Power*, v. 2, n. 3, p. 36–52, 2011. Cited in page 3.
- BENMOUYAL, G. The Trajectories of Line Current Differential Faults in the Alpha Plane. In: *32nd Annual Western Protective Relay Conference*. Spokane, Washington: WPRC, 2005. Cited 3 times in pages iv, 12, and 19.
- BENMOUYAL, G.; MOONEY, J. B. Advanced Sequence Elements for Line Current Differential Protection. In: *33rd Annual Western Protective Relay Conference*. Spokane, Washington: WPRC, 2006. Cited 3 times in pages 3, 18, and 19.
- BLACKBURN, J. L.; DOMIN, T. J. *Protective relaying : principles and applications*. CRC Press, 2014. 646 p. ISBN 9781439888117. Disponível em: <<https://www.crcpress.com/Protective-Relaying-Principles-and-Applications-Fourth-Edition/Blackburn-Domin/p/book/9781439888117>>. Cited in page 46.

- DAMBHARE, S.; SOMAN, S. A.; CHANDORKAR, M. C. Current differential protection of transmission line using the moving window averaging technique. *IEEE Transactions on Power Delivery*, v. 25, n. 2, p. 610–620, April 2010. ISSN 0885-8977. Cited in page 3.
- DENG, X.; YUAN, R.; LI, T.; LIU, W.; SHEN, Y.; XIAO, Z. Digital differential protection technique of transmission line using instantaneous active current: theory, simulation and experiment. *IET Generation, Transmission Distribution*, v. 9, n. 11, p. 996–1005, 2015. ISSN 1751-8687. Cited in page 3.
- EISSA, M. M. A novel wavelet approach to busbar protection during ct saturation and ratio-mismatch. *Electric Power Systems Research*, v. 72, p. 41–48, 2004. Cited in page 40.
- EISSA, M. M. New differential busbar characteristic based on high frequencies extracted from faulted signal during current transformer saturation. *IET Generation, Transmission & Distribution*, v. 8, p. 619–628, 2014. Cited in page 40.
- ELMORE, W. A. *Protective relaying: theory and applications*. USA: CRC press, 2003. v. 1. ISBN 0-8247-0972-1. Cited in page 2.
- GAFOOR, S. A.; RAO, P. V. R. A transient current based busbar protection scheme using wavelet transforms. *International Journal of Electrical Power & Energy Systems*, v. 33, p. 1049–1053, 2011. Cited in page 40.
- GUZMAN, A.; FISCHER, N.; LABUSCHAGNE, C. Improvements in transformer protection and control. In: *2009 62nd Annual Conference for Protective Relay Engineers*. Spokane, Washington: IEEE, 2009. p. 563–579. Cited in page 47.
- GUZMAN, A.; LABUSCHAGNE, C.; QIN, B.-L. Reliable Busbar and Breaker Failure Protection With Advanced Zone Selection. In: *31st Annual Western Protective Relay Conference*. Spokane, Washington: Schweitzer Engineering Laboratories, Inc., 2004. p. 1–51. Cited in page 40.
- GUZMAN, A.; QIN, B.-L.; LABUSCHAGNE, C. Reliable busbar protection with advanced zone selection. *IEEE Transactions on Power Delivery*, v. 20, n. 2, p. 625–629, Apr. 2005. Cited in page 39.
- GUZMAN, A.; ZOCHOLL, Z.; BENMOUYAL, G.; ALTUVE, H. J. A current-based solution for transformer differential protection. i. problem statement. *IEEE Transactions on Power Delivery*, v. 16, n. 4, p. 485–491, Oct 2001. ISSN 0885-8977. Cited in page 3.
- GUZMAN, A.; ZOCHOLL, Z.; BENMOUYAL, G.; ALTUVE, H. J. A current-based solution for transformer differential protection. i. problem statement. *IEEE Transactions on Power Delivery*, v. 16, n. 4, p. 485–491, Oct 2001. ISSN 0885-8977. Cited in page 47.
- GUZMAN, B.-L. Q. A.; GUZMAN-CASILLAS, A.; LABUSCHAGNE, C. Realible busbar protection with advanced zone selection. *IEEE Transactions on Power Delivery*, v. 20, n. 2, p. 876–887, Apr 2005. ISSN 625-629. Cited 2 times in pages 3 and 40.
- HAMILTON, R. Analysis of transformer inrush current and comparison of harmonic restraint methods in transformer protection. *IEEE Transactions on Industry Applications*, v. 49, n. 4, p. 1890–1899, July 2013. ISSN 0093-9994. Cited in page 47.

- HART, D. G.; NOVOSEL, D.; SMITH, R. A. *Modified cosine filters*. 2000. US Patent 6,154,687. Cited 4 times in pages 21, 32, 41, and 48.
- HOROWITZ, S. H.; PHADKE, A. G.; NIEMIRA, J. K. *Power System Relaying*. 2nd. ed. West Sussex, England: John Wiley & Sons, 2014. Cited in page 64.
- HOSSAIN, M.; LEEVONGWAT, I.; RASTGOUFARD, P. Revisions on alpha plane for enhanced sensitivity of line differential protection. *IEEE Transactions on Power Delivery*, 2018. ISSN 0885-8977. Early Access. Cited in page 3.
- IEEE. Ieee guide for protecting power transformers. *IEEE Std C37.91-2008 (Revision of IEEE Std C37.91-2000)*, p. 1–139, May 2008. Cited in page 3.
- IEEE. Ieee guide for protecting power transformers. *IEEE Std C37.91-2008 (Revision of IEEE Std C37.91-2000)*, p. 1–139, May 2008. Cited in page 46.
- IEEE C37.119™. *IEEE Guide for Breaker Failure Protection of Power Circuit Breakers*. 2016. Disponível em: <<http://ieeexplore.ieee.org/document/7509575/>>. Cited in page 38.
- IEEE C37.234™. *IEEE Guide for protective Relay Applications to Power System Buses*. 2009. Cited 3 times in pages 38, 40, and 41.
- IEEE POWER SYSTEM RELAYING COMMITTEE. *EMTP Reference Models for Transmission Line Relay Testing*. USA, 2004. Disponível em: <<http://www.pes-psrc.org/>>. Cited 3 times in pages 21, 31, and 47.
- JENA, S.; BHALJA, B. R. Numerical busbar differential protection using generalised alpha plane. *IET Generation, Transmission Distribution*, v. 12, n. 1, p. 227–234, 2018. ISSN 1751-8687. Cited 3 times in pages 3, 4, and 40.
- KANG, Y.; LIM, U.; KANG, S.; CROSSLEY, P. A Busbar Differential Protection Relay Suitable for Use With Measurement Type Current Transformers. *IEEE Transactions on Power Delivery*, IEEE, v. 20, n. 2, p. 1291–1298, apr 2005. Cited 2 times in pages 3 and 40.
- KANG, Y.; YUN, J.; LEE, B.; KANG, S.; JANG, S.; KIM, Y. Busbar differential protection in conjunction with a current transformer compensating algorithm. *IET Generation, Transmission & Distribution*, v. 2, n. 1, p. 100, 2008. ISSN 17518687. Cited 2 times in pages 3 and 40.
- KASZTENNY, B.; FISCHER, N.; ALTUVE, H. J. Negative-sequence differential protection - principles, sensitivity, and security. In: *2015 69th Annual Georgia Tech Protective Relaying Conference*. Atlanta, Georgia: Schweitzer Engineering Laboratories, Inc., 2015. p. 364–378. Cited in page 47.
- KASZTENNY, B.; THOMPSON, M.; FISCHER, N. Fundamentals of short-circuit protection for transformers. In: *2010 63rd Annual Conference for Protective Relay Engineers*. College Station, Texas: Schweitzer Engineering Laboratories, Inc., 2010. p. 1–13. Cited in page 47.
- KASZTENNY, B. Z.; BENMOUYAL, G.; ALTUVE, H. J.; FISCHER, N. Tutorial on Operating Characteristics of Microprocessor-Based Multiterminal Line Current Differential Relays. In: *38th Annual Western Protective Relay Conference*. Spokane,

- Washington: Schweitzer Engineering Laboratories, Inc., 2011. p. 1–30. Cited 10 times in pages 3, 6, 7, 11, 18, 19, 21, 28, 31, and 76.
- MASON, C. R. *The Art and Science of Protective Relaying*. New York, USA: John Wiley & Sons Inc., 1956. Cited 2 times in pages 62 and 63.
- MEDEIROS, R. P.; COSTA, F. B. A wavelet-based transformer differential protection with differential current transformer saturation and cross-country fault detection. *IEEE Transactions on Power Delivery*, v. 33, n. 2, p. 789–799, April 2018. ISSN 0885-8977. Cited in page 3.
- MILLER, H.; BURGER, J.; FISCHER, N.; KASZTENNY, B. Modern line current differential protection solutions. In: *2010 63rd Annual Conference for Protective Relay Engineers*. Spokane, Washington: Schweitzer Engineering Laboratories, Inc., 2010. ISBN 978-1-4244-6073-1. Cited 21 times in pages i, vi, 3, 4, 5, 6, 7, 8, 9, 20, 21, 22, 32, 36, 42, 48, 52, 70, 71, 74, and 75.
- MILLS, D. L. Internet time synchronization: The network time protocol. *IEEE Transactions on Communications*, v. 39, n. 10, p. 1482–1493, oct. 1991. Cited in page 19.
- NAVARRO, E. C.; ORDACGI, J. M.; COURY, D. V.; MENEZES, R. Proteção diferencial de linhas de transmissão análise no plano alpha. In: VII SEMINÁRIO TÉCNICO DE PROTEÇÃO E CONTROLE. Rio de Janeiro, RJ, 2003. Cited in page 63.
- ONS. *"In Portuguese" Análise Estatística dos Desligamentos Forçados de Componentes do Sistema Elétrico Brasileiro Referente ao Ano de 2012 - RE 3/076/2013*. Rio de Janeiro Brasil: Operador Nacional do Sistema Elétrico, 2013. Cited 2 times in pages vii and 2.
- ONS. *"In Portuguese" Plano da Operação Energética 2017/2021 - PEN 2017*. Rio de Janeiro, 2017. 41 p. Disponível em: <<http://www.ons.org.br/AcervoDigitalDocumentosEPublicacoes/RE-3-0108-2017/PEN2017/SumarioExecutivo.pdf>>. Cited 3 times in pages iv, 1, and 2.
- ONS. *"In Portuguese" PAR 2017-2019 Plano de Ampliações e Reforços nas Instalações de Transmissão do SIN*. Brasília, Distrito Federal, 2017. Disponível em: <<http://ons.org.br/Paginas/Noticias/PAR-2017-2019/05072017.aspx>>. Cited in page 1.
- OPERADOR NACIONAL DO SISTEMA ELÉTRICO. *"In Portuguese" Procedimentos de Rede - Submódulo 2.6: Requisitos mínimos para os sistemas de proteção e de telecomunicações*. Brasília, 2016. Disponível em: <<http://www.ons.org.br/procedimentos/index.aspx>>. Cited in page 2.
- PAITHANKAR, Y. G.; BHIDE, S. R. *Fundamentals of Power System Protection*. New Delhi, India: Prentice-Hall, 2007. Cited 2 times in pages 63 and 64.
- PAJUELO, E.; RAMAKRISHNA, G.; SACHDEV, M. S. Phasor estimation technique to reduce the impact of coupling capacitor voltage transformer transients. *IET Generation, Transmission & Distribution*, v. 2, 2008. Cited 2 times in pages 21 and 31.
- PERERA, R.; KASZTENNY, B. Application considerations when protecting lines with tapped and in-line transformers. In: *2014 67th Annual Conference for Protective Relay Engineers, CPRE 2014*. IEEE, 2014. p. 84–94. ISBN 9781479947393. Disponível em: <<http://ieeexplore.ieee.org/document/6798996/>>. Cited 3 times in pages 29, 30, and 31.

- QIN, B.-L.; GUZMAN-CASILLAS, A. *System for protection zone selection in microprocessor-based relays in an electric power system*. 2002. Disponível em: <<https://patents.google.com/patent/US6411865B1/en>>. Cited 2 times in pages 39 and 40.
- QIN, B.-L.; GUZMAN-CASILLAS, A.; SCHWEITZER, E. O. A new method for protection zone selection in microprocessor-based bus relays. *IEEE Transactions on Power Delivery*, v. 15, n. 3, p. 876–887, July 2000. ISSN 0885-8977. Cited 2 times in pages 3 and 40.
- RASOULPOOR, M.; BANEJAD, M. A correlation based method for discrimination between inrush and short circuit currents in differential protection of power transformer using Discrete Wavelet Transform: Theory, simulation and experimental validation. *International Journal of Electrical Power & Energy Systems*, Elsevier, v. 51, p. 168–177, oct 2013. ISSN 0142-0615. Disponível em: <<https://www.sciencedirect.com/science/article/pii/S014206151300094X>>. Cited in page 47.
- SARANGI, S.; PRADHAN, A. K. Adaptive α -plane line differential protection. *IET Generation, Transmission Distribution*, v. 11, n. 10, p. 2468–2477, 2017. ISSN 1751-8687. Cited in page 3.
- SILVA, K. M.; BAINY, R. G. Generalized Alpha Plane for Numerical Differential Protection Applications. *IEEE Transactions on Power Delivery*, v. 31, n. 6, p. 2565–2566, dec 2016. ISSN 0885-8977. Cited 8 times in pages 3, 4, 7, 8, 9, 16, 44, and 52.
- SILVA, K. M.; ESCUDERO, A. M. P.; LOPES, F. V.; COSTA, F. B. A Wavelet-Based Busbar Differential Protection. *IEEE Transactions on Power Delivery*, v. 33, n. 3, p. 1194–1204, 2018. ISSN 08858977. Cited in page 40.
- STEENKAMP K. BEHRENDT, E. S. L. *Tutorial: Complex Busbar Protection Application*. Schweitzer Engineering Laboratories, Inc., an, Washington USA, 2007. Cited in page 39.
- SU, S.; LIU, J.; XIAO, H.; JIANG, D. Expert System for Wide Area Protection Zone Selection. In: *2005 IEEE/PES Transmission and Distribution Conference and Exposition: Asia and Pacific*. Dalian, China: IEEE, 2005. ISBN 0-7803-9114-4. ISSN 2160-8644. Disponível em: <<http://ieeexplore.ieee.org/document/1547054/>>. Cited in page 39.
- TANG, L.; DONG, X.; LUO, S.; SHI, S.; WANG, B. A new differential protection of transmission line based on equivalent travelling wave. *IEEE Transactions on Power Delivery*, v. 32, n. 3, p. 1359–1369, June 2017. ISSN 0885-8977. Cited in page 3.
- THOMPSON, M.; SOMANI, A. A tutorial on calculating source impedance ratios for determining line length. In: *2015 68th Annual Conference for Protective Relay Engineers*. College Station, Texas: IEEE, 2015. p. 833–841. Cited in page 21.
- TZIOUVARAS, D.; ALTUVE, H.; BENMOUYAL, G.; ROBERTS, J. *The Effect of Multiprinciple Line Protection on Dependability and Security*. Schweitzer Engineering Laboratories Inc., Pullman, WA, 2001. Cited in page 64.
- TZIOUVARAS, D. A.; ALTUVE, H.; BENMOUYAL, G.; ROBERTS, J. Line differential protection with an enhanced characteristic. In: *3rd Mediterranean Conference and Exhibition on Power Generation, Transmission, Distribution and Energy Conversion*. Amsterdam, Netherlands: IEEE, 2002. Cited 12 times in pages 3, 4, 7, 11, 15, 20, 21, 53, 65, 67, 68, and 74.

- VAZQUEZ, E.; MIJARES, I. I.; CHACON, O. L.; CONDE, A. Transformer differential protection using principal component analysis. *IEEE Transactions on Power Delivery*, v. 23, n. 1, p. 67–72, Jan 2008. ISSN 0885-8977. Cited in page 3.
- WARRINGTON, A. R. C. *Protective Relays: Their Theory and Practice, Volume one*. 1. ed. London: Chapman & Hall, 1962. Cited 2 times in pages 3 and 65.
- XUE, Y.; KASZTENNY, B.; TAYLOR, D.; XIA, Y. Series compensation, power swings, and inverter-based sources and their impact on line current differential protection. In: *2013 66th Annual Conference for Protective Relay Engineers*. College Station, Texas: IEEE, 2013. p. 80–91. Cited in page 3.
- ZIEGLER, G. *Numerical Differential Protection: Principles and Applications*. 2nd. ed. Berlin, Germany: Siemens, 2012. Cited 5 times in pages 1, 2, 39, 46, and 74.

APPENDIX A

DIFFERENTIAL PROTECTION BASICS

Power is generated and distributed over long distances in order to reach the consumers. As a result, any system transients have the strength to impact the entire system's integrity. Power system protection play a major role to guarantee safe and reliable energy. A defective or inappropriate protection system can lead to catastrophic fails, or result in a huge amount of consumers without service. Damaged devices due a protection system failure result in high financial loss and, in order to be fixed, may require expensive and long labor. Therefore, protection systems have to be carried with special attention so important aspects such speed of operation, selectivity, and security are optimized for each project. Below it is displayed a list of seven key-aspects to take in count when analyzing and projecting a protection system or function (ANDERSON, 1999):

- *Sensibility*: operate exclusively for faults it was designed for.
- *Reliability*: ability to operate when expected.
- *Security*: capacity to avoid miss-operation during unpredictable conditions, e.g. CT saturation.
- *Selectivity*: skill to disconnect the lowest possible amount of consumer in order to isolate the faulty device or area.
- *Coordination*: Appropriate settings that guarantee selectivity, but also allowing multiple relays to work together for a device or area.
- *Speed*: Capacity to operate as fast as possible to isolate the fault from power system.
- *Simplicity*: Use of minimum number of relays, measuring points, and circuits.

A.1 DIFFERENTIAL PROTECTION FUNDAMENTALS

Mason (1956) states that the differential relay can be defined as "one that operates when the vector difference of two or more similar electrical quantities exceeds a predetermined amount". Several type of relay can be made to operate as a differential relay, depending on the way they are connected. This is possible due fundamentally the differential function use of an overcurrent relay (ANSI 50/51) applied to a nodal sum of currents. The Kirchhoff's current law (KCL) is the basic concept for differential protection and can be applied anywhere from a single node, a device, or even an area provided that in and out currents are measured. The algebraic sum of all currents is ideally zero in normal operation. Differential protection can be used to protect transformers, busbar, and transmission lines, although either device presents their own challenges and strategies (ALTUVE; SCHWEITZER, 2010).

Figure A.1a illustrates the measuring zone delimited by the CTs. The basic differential relaying system has three elements; one for each phase. This makes the differential protection inherently phase segregated. Considering a two-terminal device (e.g. three phase transformer), each phase has a pair of CTs installed. An advantage of differential protection is the allowance of single phasing trip, allowing flexibility when the system can handle such condition. Usually the ANSI code can be combined with the phase identification, e.g. phase A of a transformer differential scheme is called 87TA.

First let's focus on conditions showed in Figure A.1a. The current flows through the primary circuit either to a load or to a short circuit, identified as an external fault in the Figure. If the two CTs have the same ratio, and are properly connected (e.g. correct CT polarity), their secondary currents will merely circulate between the two CTs ($\bar{I}_1 = \bar{I}_2$), and no current will

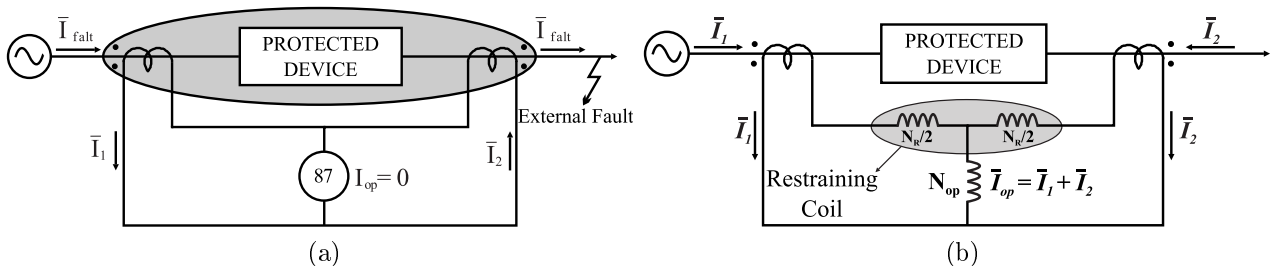


Figure A.1. (a) Protected Zone. (b) Percentage Differential Relay. N_R e N_{OP} represent the number of turn of operating and restraining coils respectively.

flow through the differential relay ($I_{op} = 0$). The secondary currents \bar{I}_1 and \bar{I}_2 phasors have same module, but opposite phase values. But, provided that a short circuit occurs anywhere between the two CTs, the operating current will not be zero. Upon the pickup setting (I_{pk}) the differential function should operate (NAVARRO *et al.*, 2003).

Although the approach showed in Figure A.1a works as intended, it presents critical limitations in real life applications. Such that, percentage differential relays are extensively used. The main idea is identical in both approaches, but the latter presents a differential circuit, as shown in Figure A.1b. One advantage is the adjustable differential current required to operate, owing to the number of turns of the restraining coil (N_r). In operating coil the differential current flows ($\bar{I}_1 + \bar{I}_2$), and the equivalent current in the restraining coil is proportional to $\frac{\bar{I}_1 + \bar{I}_2}{2}$, due the operating coil been connected to the midpoint of the restraining coil. Other main advantage of this relay is that when a short circuit occurs external to the protected zone, the relay chances to incorrectly operate are lower (MASON, 1956). It is worthwhile to mention that current transformers sometimes during fault condition, do not present identical secondary currents. Slight differences in magnetic properties or different amounts of residual magnetism cause that problem. The decaying DC offset commonly present in fault currents yields to even more distortion. Notwithstanding same CT models are used, one can expect minor errors that can cause missoperation. However, due to the rising pickup characteristic presented in percentage differential relays as the magnitude of current increases, the relay is restrained against operating improperly.

The relation shown in Equation (A.1) represents the operation threshold of a percentage differential electromechanical relay (PAITHANKAR; BHIDE, 2007):

$$|\bar{I}_1 + \bar{I}_2| = K \frac{|\bar{I}_1 - \bar{I}_2|}{2} + K_0, \quad (\text{A.1})$$

where $K = N_r/N_{op}$ e K_0 is the minimum torque adjusted by the restraining coil, analogous to the *pick-up* current.

The relay operating current (I_{op}) assumes the expression $|\bar{I}_1 + \bar{I}_2|$, K is a constant coefficient representing the slope of the relay characteristic. The restraining current (I_{res}) is defined by $\frac{|\bar{I}_1 - \bar{I}_2|}{2}$, while K_0 is equivalent to a pick-up current (I_{pk}). Therefore Equation (A.1) becomes (A.2).

Anderson (1999) announces that the relay operates upon I_{op} surpasses the minimum current value I_{pk} summed with the portion KI_{res} . Therefore, the restraining current represents a mechanics to avoid miss-operation of the differential function (PAITHANKAR; BHIDE, 2007). Another possible definition of the relay operation is by separating the condition (A.2) in two parts, as showed in Equation (A.3). This partition improves relay sensibility (HOROWITZ *et al.*, 2014).

$$I_{op} > KI_{res} + I_{pk} \quad (\text{A.2})$$

$$I_{op} > KI_{res} \text{ and } I_{op} > I_{pk} \quad (\text{A.3})$$

The conditions listed in Equation (A.3) are the basic definition of the differential relay operation and can be customized according to manufacturer. The protection relay equips the differential function with several different logics, i.e. dual-slope, external-fault modes, CT saturation detection, dynamic zone selection, capacitive current compensation, instantaneous samples combined to phasors, etc. The advent of numerical relays provides a wide-variety of mathematical definitions for the operating and restraining currents. Sometimes I_{op} is referred as differential current I_{dif} . The restraining current for instance, can be replaced by Equations (A.5) à (A.6) (TZIOUVARAS *et al.*, 2001):

$$I_{dif} = |\bar{I}_1 + \bar{I}_2| \quad (\text{A.4})$$

$$I_{res} = K |\bar{I}_1 - \bar{I}_2| \quad (\text{A.5})$$

$$I_{res} = K (|\bar{I}_1| + |\bar{I}_2|) \quad (\text{A.6})$$

$$I_{res} = \max(|\bar{I}_1|, |\bar{I}_2|) \quad (\text{A.7})$$

$$I_{res} = \sqrt{|\bar{I}_1| \cdot |\bar{I}_2| \cos \theta} \quad (\text{A.8})$$

where θ is the angle between \bar{I}_1 and \bar{I}_2 .

A.2 REPRESENTATION PLANES

Usually the percentage differential function is represented in a bi-dimensional plane, where the operating and restraining currents are the axes. It is called operational plane and relay operates in accordance with the chosen condition, such as Equation (A.3). Other popular way of representation is through alpha plane (WARRINGTON, 1962), where the plotted variable is called Γ and consists of the relation between currents in terminal 1 and 2 (e.g. primary and secondary for transformers). The condition of operation is defined by a restraining shape, such as the enhanced rainbow one proposed by Tziouvaras *et al.* (2002). If the value of Γ is outside the restraining area, the relay operates.

The transient path from pre-fault to internal fault steady-state is showed in Figure A.2a. Either planes presents an equivalent restraining characteristic which is called "no-trip". The relay operates when the path cross these limits and reach the operation area,.

Figure A.3a shows the operational plane. One can observe that y-axis is represented by I_{op} and x-axis by I_{res} . The conditions from Equation (A.3) are represented by the hatched area above the line defined by K and I_{pk} . The relay sensibility is increased when K is decreased. Aiming to reduce the sensibility during CT saturation, some manufacturers implement a dual-slope setting, as showed by the dashed line in Figure A.3a. The relay is capable to adjust the value of K upon CT saturation is detected (e.g. harmonic detection).

Warrington (1962) proposed the alpha plane. It consists of a complex Cartesian plane in which the relation $\frac{\bar{I}_2}{\bar{I}_1}$, called Γ , has its real and imaginary parts plotted. Currents \bar{I}_1 and \bar{I}_2

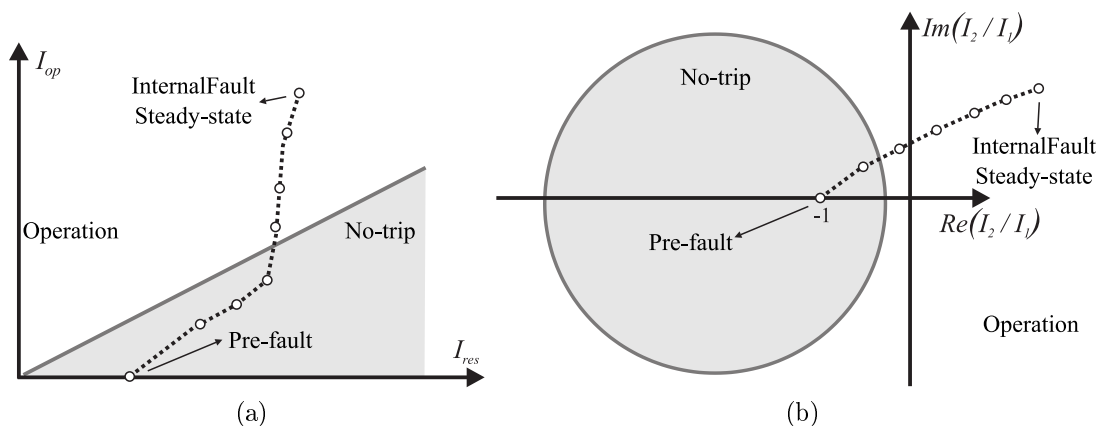


Figure A.2. Transient Path. (a) Operational Plane. (b) Alfa Plane.

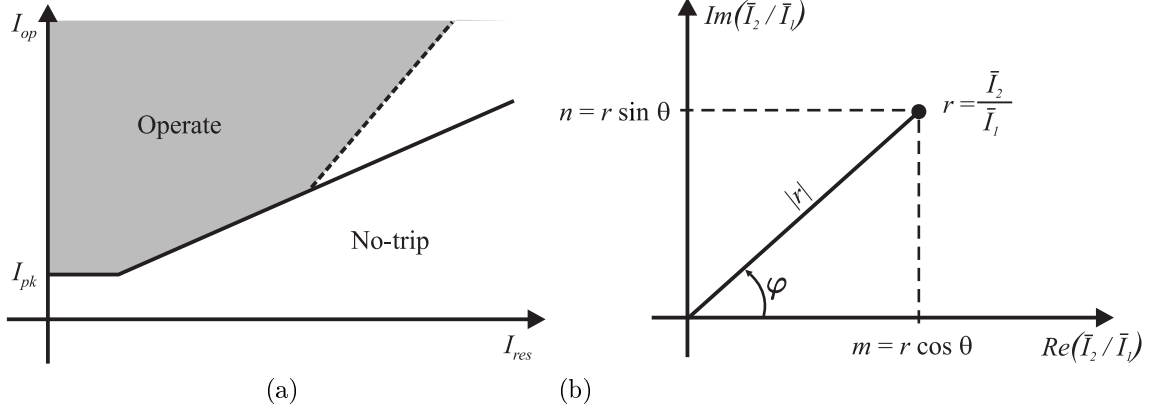


Figure A.3. Representation Planes: (a) Operational plane. (b) Alpha Plane.

refer to each terminal. It is worthwhile to highlight that the definition of Γ implies alpha plane as inherently for two-terminal elements. The alpha plane is defined by the Equations (A.9) to (A.11), and by the representation showed in Figure A.2.

$$\frac{\bar{I}_2}{\bar{I}_1} = m + jn = r = |r|e^{j\theta}, \quad (\text{A.9})$$

where:

$$|r| = \frac{|\bar{I}_2|}{|\bar{I}_1|} = \sqrt{m^2 + n^2}, \quad \theta = \arctan\left(\frac{n}{m}\right), \quad (\text{A.10})$$

$$m = |r| \cos \theta, \quad n = |r| \sin \theta. \quad (\text{A.11})$$

One way to define a restraining shape in alpha plane is by using the condition (A.3) created for operational plane. In order to so, the Equations (A.4), (A.5) and (A.9) are combined with Equation (A.3), leading to Equations A.12 and A.19 :

$$|\bar{I}_2 + \bar{I}_1| = K |\bar{I}_1 - \bar{I}_2| \quad (\text{A.12})$$

$$\left| \frac{\bar{I}_2}{\bar{I}_1} + 1 \right| = K \left| 1 - \frac{\bar{I}_2}{\bar{I}_1} \right| \quad (\text{A.13})$$

$$|m + jn + 1| = K |-m - jn + 1| \quad (\text{A.14})$$

$$\sqrt{(m+1)^2 + n^2} = K \sqrt{(1-m)^2 + n^2} \quad (\text{A.15})$$

$$m^2(1-K^2) + n^2(1-K^2) + 2m(1+K^2) + 1 - K^2 = 0 \quad (\text{A.16})$$

$$m^2 + n^2 + 2m \frac{(1+K^2)}{(1-K^2)} + 1 = 0, \quad (\text{A.17})$$

Solving quadratics by completing the square:

$$\left(m^2 + \frac{1+K^2}{1-K^2} \right)^2 + n^2 = \left(\frac{1+K^2}{1-K^2} \right)^2 - 1, \quad (\text{A.18})$$

which results in a circle defined by the following Equations:

$$center : \left(-\frac{1 + K^2}{1 - K^2}, 0 \right); \quad radius : \frac{2K}{1 - K^2}. \quad (A.19)$$

The circular shape represents the restraining limits of the relay, thus the no-trip area. On the other hand, the relay operates in the area outside. In Figure A.4 a comparative analysis between the planes is showed in respect with the variation of slope K . One can observe that the higher K value is, the smaller the restraining area will be. Furthermore increasing the relay sensibility.

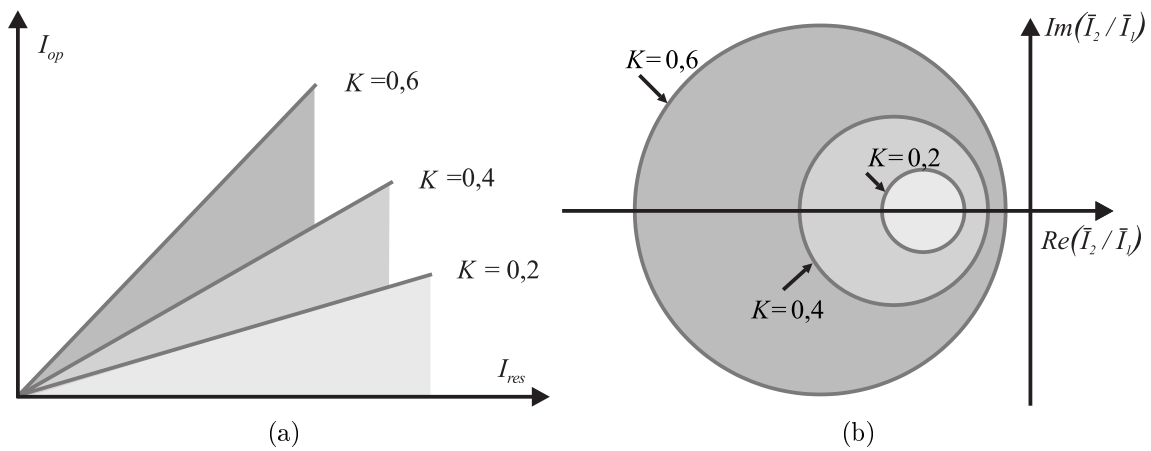


Figure A.4. Representation Planes Comparison (a) Operational Plane. (b) Alpha Plane.

A.3 ENHANCED RESTRAINING CHARACTERISTIC

The slope setting of a traditional percentage differential element defines the circular restraining characteristic. A downside is that security, dependability and sensitivity cannot be adjusted separately. The Enhanced Restraining Characteristic (ERC) designed by (TZIOUVARAS *et al.*, 2002) overcomes this limitation. The ERC was primarily defined with line differential applications in mind. To define the shape a total of four key factors were considered: channel time-delay compensation errors, power system impedance nonhomogeneity, CT saturation, and low frequency oscillations in series-compensated lines.

Tziouvaras *et al.* (2002) defined ERC based on alpha plane regions areas along the real axis. Figure A.5a shows the fault areas allowing ± 30 degrees for system power angle and impedance angle difference. Both the channel time-delay compensation errors and the system impedance

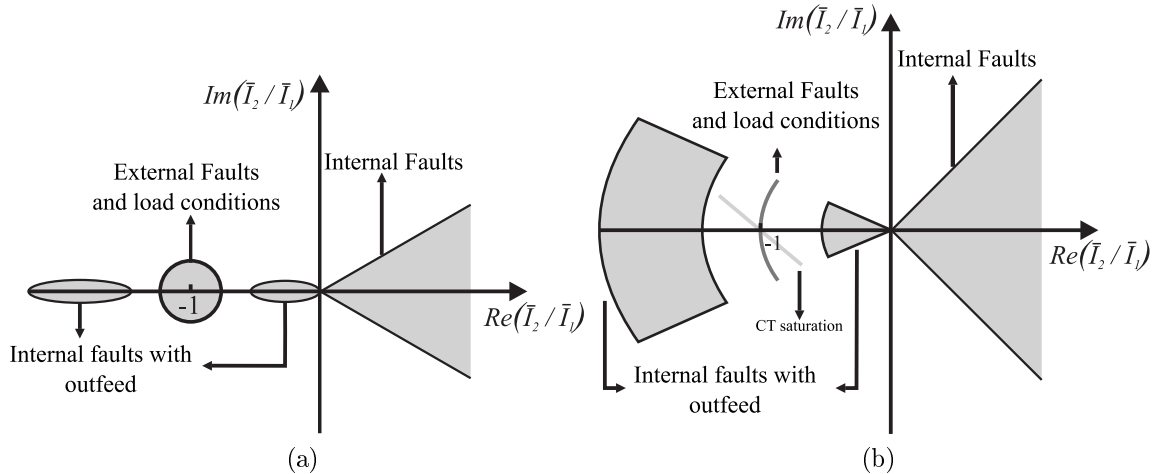


Figure A.5. Alpha Plane Areas. (a) Simple. (b) Rotation caused by channel time-delay compensation errors and the system impedance nonhomogeneity.

nonhomogeneity also produce a rotation of the ideal internal fault region in the alpha plane. Figure A.5b shows the effect of this rotation to alpha plane fault areas.

Two parameters define the shape of ERC, the angle a and the radius R . Their graphical effect is shown on Figure A.6a. The angle a allows the ERC to be adjust in order to compensate channel time-delay errors. Applications where measuring terminals are far from each other (e.g. transmission lines) can suffer from misaligned samples. Tziouvaras *et al.* (2002) states that such delays can vary between 3 to 5 ms and may occur rarely on lines longer than 160 km. Therefore, a can be adjusted between 180° e 210° to overcome channel time-delay errors. The second setting is R , adjusted to compensate CT saturation and frequency oscillations. Values between 8 and 10 are enough to provide safety during such conditions.

The ERC presents remarkable advantages when compared to the circular restraining characteristic (CRC). In short, ERC permits the benefits of two different CRC - i.e. two adjustments of value K - while avoiding their drawbacks. Figures A.6b and A.6c exemplify that. In first figure, both restraining characteristics are set for the same level of tolerance to outfeed. The hatched area highlights CRC lower tolerance to channel asymmetry when compared to ERC. An higher value of K - i.e. increase of CRC radius - compensates extreme channel asymmetry. But it causes sensitivity problems to detect internal faults with outfeed, as showed by the hatched area in Figure A.6c (TZIOUVARAS *et al.*, 2002).

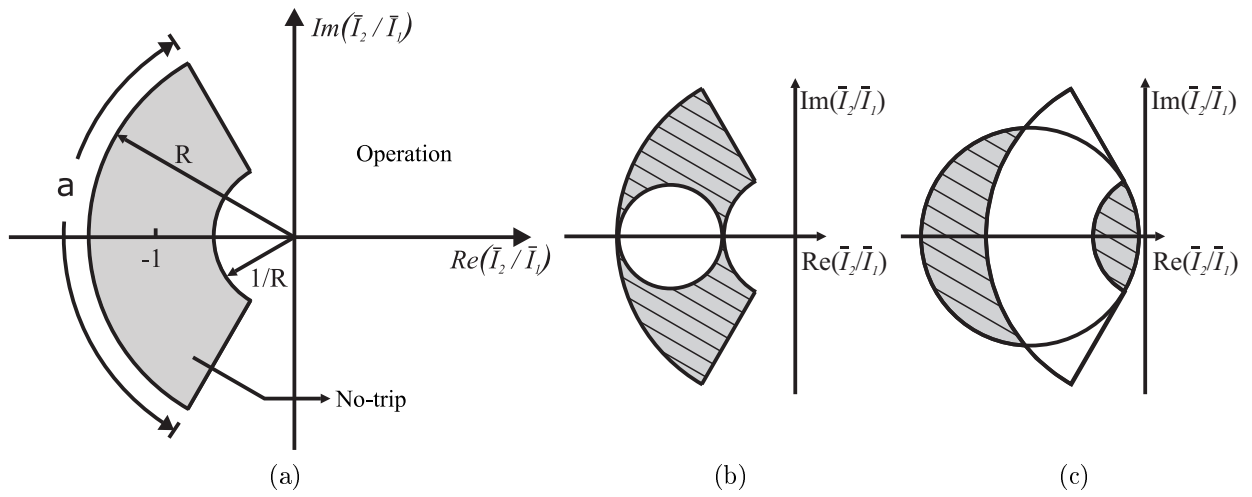


Figure A.6. (a) Enhanced restraining characteristic. (b) Equal tolerance to Outfeed. (c) Equal tolerance to Channel time-delay.

MILLER *ET AL.* (2010A) GAP DEDUCTION

The GAP proposed by Miller *et al.* (2010) consists in an implementation of fault detection using alpha plane employable in protection zones defined by any number n of currents. The principal characteristic of the GAP is to differentiate passing currents (i.e., Currents that enter and leaves the protection zone) from internal faults. Thus, in order to the equivalent currents truthfully represent the system's condition, they must indicate the direction of currents (i.e., entering or leaving the protection zone), see (ALMEIDA; SILVA, 2017). To employ the GAP, it needs to calculate the differential current \bar{I}_{dif} and restraining currents I_{res} in accordance to (B.1) and (B.2), adjusted to the n terminals bounding the protection zone.

$$\bar{I}_{dif} = \sum_{l=1}^n \bar{I}_l = I_{dif,re} + jI_{dif,im} \quad (\text{B.1})$$

$$I_{res} = \sum_{l=1}^n |\bar{I}_l| \quad (\text{B.2})$$

GAP's philosophy can be understood by the relationship shown in Figure (B.1). In (B.1) it can be observed that a system of n terminals will be equivalent to another system of only two-terminals, in which the restraining and differential currents are equal.

Both currents \bar{I}_L and \bar{I}_R of the equivalent system will be used to calculate the differential

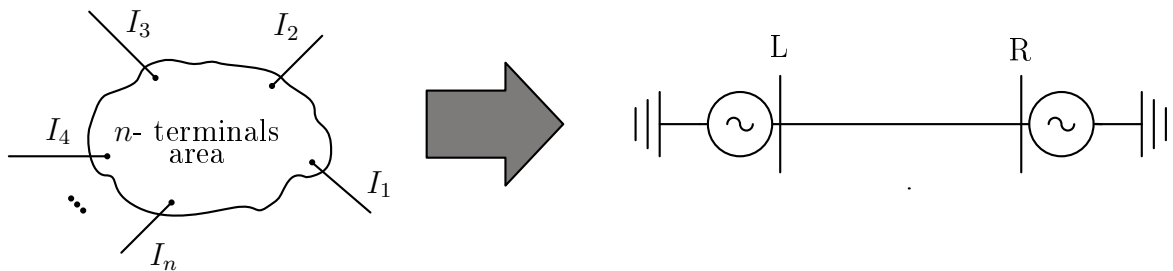


Figure B.1. GAP philosophy (MILLER *et al.*, 2010).

current and restriction current. Therefore, the equivalent system is written by equations (B.3) and (B.4).

$$\bar{I}_{dif,eq} = \bar{I}_L + \bar{I}_R \quad (\text{B.3})$$

$$I_{res,eq} = |\bar{I}_L| + |\bar{I}_R| \quad (\text{B.4})$$

where $\bar{I}_L = I_L \angle \theta_L$ and $\bar{I}_R = I_R \angle \theta_R$.

The requirement of equality for the differential and restraining currents, before and after the computation of equivalent currents, implies the system of linear equations (B.5).

$$\begin{cases} \bar{I}_{dif} = \bar{I}_{dif,eq} \\ I_{res} = I_{res,eq}, \end{cases} \quad (\text{B.5})$$

Miller *et al.* (2010), one must chose one of the currents that define the protected zone to be the angular reference for the following derivations. The appropriate choice is the one with largest projection over the differential current of system. During internal faults, all currents present approximately the same angle, hence with little influence in the final result (ALMEIDA; SILVA, 2017). However, in the most critical external faults in which there is saturation of one of the CT, this assumption is the one that best approximate the passing current. Indeed, this is the case since in this type of fault the differential current is constituted of the inserted error by the saturated TC, hence the current which better approximate the differential current (in phase) is at maximum 90° (extreme case of saturation) out of phase to the passing current.

To determine the angular reference \bar{I}_P we first determine with equation (B.6) n values for R_i , which represent the projection of each current of the protected zone to the differential current. The phase of the current with highest result is defined as β , as shown in equation (B.7).

$$R_i = Re\left(\bar{I}_i \cdot \bar{I}_{dif}^*\right) \quad (\text{B.6})$$

$$\beta = \angle \bar{I}_P \quad (\text{B.7})$$

where $i = \{1, \dots, n\}$.

According to Miller *et al.* (2010), this choice guarantees a higher sensibility for internal short-circuits and higher safety for external short-circuits with CTs saturation. Now we define auxiliary current \bar{I}_X , which consist of \bar{I}_{dif} out of phase by angle $-\beta$, according to equation (B.8):

$$\bar{I}_X = \bar{I}_{dif} \cdot 1 \angle (-\beta). \quad (\text{B.8})$$

To determine currents \bar{I}_L e \bar{I}_R , we employ equations (B.5) and (B.3) combined with a phase change of $-\beta$,

$$\bar{I}_{dif} \cdot 1\angle(-\beta) = (\bar{I}_L + \bar{I}_R) \cdot 1\angle(-\beta) \quad (\text{B.9})$$

By manipulating equation (B.9) it is possible to identify in equation (B.10) currents \bar{I}_X and \bar{I}_{LX} , the latter being current \bar{I}_L with a phase shift of $-\beta$. Furthermore, it is possible to identify virtual current \bar{I}_R , since it has angle β , has value equal to it's absolute value I_R .

$$\underbrace{\bar{I}_{dif} \cdot 1\angle(-\beta)}_{\bar{I}_X} = \underbrace{\bar{I}_L \cdot 1\angle(-\beta)}_{\bar{I}_{LX}} + I_R \quad (\text{B.10})$$

Equation (B.10) may be re-arranged in real and imaginary parts, as shown in equation (B.11):

$$\underbrace{\bar{I}_X}_{phasor} = \underbrace{(I_{LX,re} + I_R)}_{\text{real part}} + \underbrace{jI_{LX,im}}_{\text{imaginary part}} \quad (\text{B.11})$$

Equation (B.11) can be presented as the set of equations (B.12), it's important to remind that currents \bar{I}_{LX} has the same absolute value of current \bar{I}_L , as noted in equation (B.10).

$$\begin{cases} I_{X,re} &= I_L \cos(\theta_{LX}) + I_R \\ I_{X,im} &= I_L \sin(\theta_{LX}) \end{cases}, \quad (\text{B.12})$$

The trigonometric functions *sine* and *cosine* can be isolated and squared as shown in (B.13):

$$\begin{cases} \cos(\theta_{LX}) &= \frac{I_{X,re} - I_R}{I_L} \\ \sin(\theta_{LX}) &= \frac{I_{X,im}}{I_L} \end{cases} \xrightarrow{\text{Squared}} \begin{cases} \cos^2(\theta_{LX}) &= \left(\frac{I_{X,re} - I_R}{I_L} \right)^2 \\ \sin^2(\theta_{LX}) &= \left(\frac{I_{X,im}}{I_L} \right)^2 \end{cases}, \quad (\text{B.13})$$

The squared trigonometric functions shown in equation (B.13) can be related by the trigonometric identity $1 = \cos^2 \theta + \sin^2 \theta$ and reorganized as in equations (B.14) and (B.15).

$$1 = \left(\frac{I_{X,re} - I_R}{I_L} \right)^2 + \left(\frac{I_{X,im}}{I_L} \right)^2 \quad (\text{B.14})$$

$$I_L^2 = (I_{X,re} - I_R)^2 + I_{X,im}^2 \quad (\text{B.15})$$

From equation (B.4), it is possible to write the relation $I_L = I_{res} - I_R$, which, when employed in equation (B.15), allows the following relation:

$$(I_{res} - I_R)^2 = (I_{X,re} - I_R)^2 + I_{X,im}^2 \quad (\text{B.16})$$

$$I_{res}^2 - 2I_{res}I_R + I_R^2 = I_{X,re}^2 - 2I_{X,re}I_R + I_R^2 + I_{X,im}^2 \quad (\text{B.17})$$

Equation (B.17) may be utilized to isolate current I_R , as shown in equation (B.18).

$$I_R = \frac{I_{res}^2 - I_{X,re}^2 - I_{X,im}^2}{2(I_{res} - I_{x,re})} \quad (\text{B.18})$$

With the purpose to write an expression for current \bar{I}_{LX} , we use the set of equations B.12 and relation (B.18), generating equation (B.19)

$$\bar{I}_{LX} = \frac{I_{X,im}^2 - (I_{res} - I_{X,re})^2}{2(I_{res} - I_{X,re})} + jI_{X,im} \quad (\text{B.19})$$

Current \bar{I}_{LX} may be employed in addition to relation $\bar{I}_L = \bar{I}_{LX} \cdot 1\angle\beta$ to write equation (B.20). Moreover, given relation $I_L = I_{res} - I_R$ it is possible to write a relation from current \bar{I}_R in terms of $|I_L|$, as shown in equation (B.21).

$$\bar{I}_L = \left\{ \frac{Im(\bar{I}_X)^2 - [I_{res} - Re(\bar{I}_X)]^2}{2[I_{res} - Re(\bar{I}_X)]} + j \cdot Im(\bar{I}_X) \right\} \cdot 1\angle\beta, \quad (\text{B.20})$$

$$\bar{I}_R = (I_{res} - |\bar{I}_{Leq}|) \cdot 1\angle\beta. \quad (\text{B.21})$$

SILVA ET AL. (2016) GAP DEDUCTION

The differential protection function has often been used as a unitary protection of various devices in the electrical system (ZIEGLER, 2012). It is generally implemented through a percentage differential element in the operational plan. However, Tziouvaras *et al.* (2002) presents some particularities of the protection of transmission lines that are better solved through the plan- α . In addition, the modified restriction feature proposed by Tziouvaras *et al.* (2002) represents a valuable resource. The GAP proposal of Miller *et al.* (2010) enables a multiple terminal element to be represented by only two terminals, so that the benefits of the plan- α presented by Tziouvaras *et al.* (2002) are still valid in this case. Although this GAP is presented for transmission line protection applications, it can be applied to other devices.

This GAP approach consists of a clever way to calculate the equivalent currents \bar{I}_M and \bar{I}_N , which is simpler than the one presented by Miller *et al.* (2010). The proposed GAP replaces the 87LQ and 87LG sequence units and is able to calculate *trip* commands segregated by phase, as well as other benefits that are exposed throughout the chapter.

C.1 MATHEMATICAL FORMULATION

Consider the element shown in Figure C.1 as any n terminal device. The differential current (\bar{I}_{dif}) and the restraining current (I_{res}) can be defined as:

If we consider the newly shown element as any n terminal device, the differential current (\bar{I}_{dif}) and the restriction current (I_{res}) can be defined as:

$$\bar{I}_{dif} = \sum_{l=1}^n \bar{I}_l = I_{dif,re} + jI_{dif,im} \quad (\text{C.1})$$

$$I_{res} = k \sum_{l=1}^n |\bar{I}_l| \quad (\text{C.2})$$

where the superscript "–" indicates that the magnitude is a phasor; the subscripts *re* and *im* represent whether the real and imaginary parts of the phasor, respectively; and *k* is a multiplying factor.

In order to be able to use the plan- α in this *n* terminal device, it is necessary here to map the set of them on only two equivalent terminals, whose virtual chains are called \bar{I}_M and \bar{I}_N . Thus, the differential and restriction currents of the equivalent system can be defined as the Equations (C.3) and (C.4), respectively:

$$\bar{I}_{dif,eq} = \bar{I}_M + \bar{I}_N \quad (C.3)$$

$$\bar{I}_{res,eq} = \bar{I}_M - \bar{I}_N \quad (C.4)$$

The premise here is that the equivalence of the systems is guaranteed if the differential and constraint currents for both the *n* terminal system and the *n* terminal system are equal to only two. In addition, from the Equations (C.1)-(C.4), the following linear system of equations is obtained:

$$\begin{bmatrix} 1 & 0 & 1 & 0 \\ 0 & 1 & 0 & 1 \\ 1 & 0 & -1 & 0 \\ 0 & 1 & 0 & -1 \end{bmatrix} \cdot \begin{bmatrix} I_{M,re} \\ I_{M,im} \\ I_{N,re} \\ I_{N,im} \end{bmatrix} = \begin{bmatrix} I_{dif,re} \\ I_{dif,im} \\ I_{res} \\ 0 \end{bmatrix} \quad (C.5)$$

In the GAP proposed by Miller *et al.* (2010), the restriction current of the equivalent system is calculated through the sum of magnitudes of \bar{I}_M and \bar{I}_N (pure real number), resulting in a possible and indeterminate linear system of equations with one degree of freedom, being necessary to eliminate one of the variables by giving it an arbitrary value. On the other hand, the proposed GAP, due to the fact that $I_{res,eq}$ is a complex quantity calculated in Equation (C.4), the linear system of equations is possible and determined, greatly simplifying the formulation

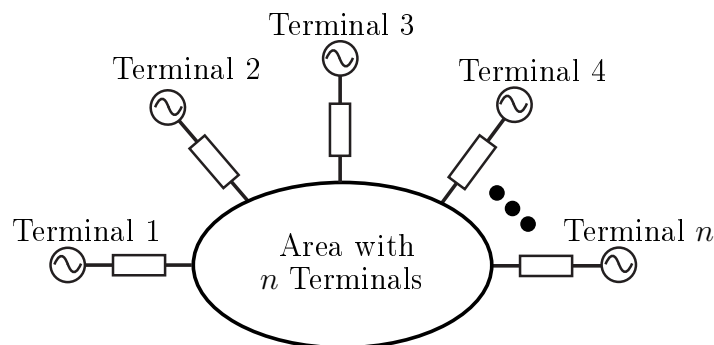


Figure C.1. Multi-terminal equipment.

of GAP. The solution of the linear system of equations (C.5) is presented below:

$$\bar{I}_M = 0.5 [(I_{dif,re} + I_{res}) + jI_{dif,im}] \quad (C.6)$$

$$\bar{I}_N = 0.5 [(I_{dif,re} - I_{res}) + jI_{dif,im}] \quad (C.7)$$

After that, the value drawn in the plan- α is calculated using the complex magnitude Γ , and the ratio between the chains \bar{I}_M and \bar{I}_N is as follows:

$$\Gamma = \frac{\bar{I}_M}{\bar{I}_N} = \Gamma_{re} + j\Gamma_{im} \quad (C.8)$$

It is important to note that some special measures are necessary in order to ensure the safest operation of the GAP during the eventual saturation of TCs for external short circuits. To this end, an external fault detection logic is essential. In addition, the harmonic components can be added to the restriction current I_{res} , making the algorithm more restricted in the presence of harmonics and external fault, so the Equation (C.2) can be rewritten as (KASZTENNY *et al.*, 2011):

$$I_{res} = k \sum_{l=1}^n |\bar{I}_l| + EFD \cdot k_h |\bar{I}_{dif,h}| \quad (C.9)$$

in which EFD is a *flag* whose value is obtained from the output of the external fault detection logic (KASZTENNY *et al.*, 2011); k_h is a multiplicative factor; and $|\bar{I}_{dif,h}|$ is the magnitude of the order h harmonic current.

APPENDIX D

SHORT-CIRCUIT CONTRIBUTIONS

This appendix presents the deduction of the short circuit contributions used in Chapter 2. The approach is developed for a short line, represented only by its serial impedance. The components that make up the system are: the voltage sources \bar{V}_S and \bar{V}_R , Thevenin equivalent impedances, Z_S and Z_R , and the line serial impedance, Z_L . The contributions \bar{I}_S e \bar{I}_R , provided by each of the sources during a shortage, have two parts: the load current and the contribution to the pure fault current. By the superposition theorem, if the load current is considered constant, it can be calculated, independently, by analysing the system on a permanent basis before and during the absence. The pre-fault sequence circuits are obtained as a function of the F point of fault application. These are illustrated in Figures D.1b to D.1d, in which the impedances of the sequence of sources and the impedance of the line, segmented into two parts at the location of the fault. The subscripts 0, 1 or 2 refer to the zero, positive and negative sequences respectively, and the parameter d indicates the percentage of the line in relation to bar S where the defect occurs. To simplify the analysis, denote the impedances shown in (D.1):

$$Z_{0M} = Z_{S0} + d \cdot Z_{L0} \qquad Z_{0N} = Z_{R0} + (1 - d) \cdot Z_{L0} \qquad (D.1a)$$

$$Z_{1M} = Z_{S1} + d \cdot Z_{L1} \qquad Z_{1N} = Z_{R1} + (1 - d) \cdot Z_{L1} \qquad (D.1b)$$

$$Z_{2M} = Z_{S2} + d \cdot Z_{L2} \qquad Z_{2N} = Z_{R2} + (1 - d) \cdot Z_{L2} \qquad (D.1c)$$

In steady state, only the positive sequence is present, so that the load current \bar{I}_{LD} is given by (D.2):

$$\bar{I}_{LD} = \frac{\bar{V}_{S1} - \bar{V}_{R1}}{Z_{1M} + Z_{1N}} \qquad (D.2)$$

To calculate the fault currents, the Thévenin equivalents of the sequence circuits are required. By analyzing the Figure D.1c, the prefault voltage at point F can be obtained from (D.3).

$$\bar{V}_F = \bar{V}_S - \bar{I}_{LD} \cdot Z_{1M} \qquad (D.3)$$

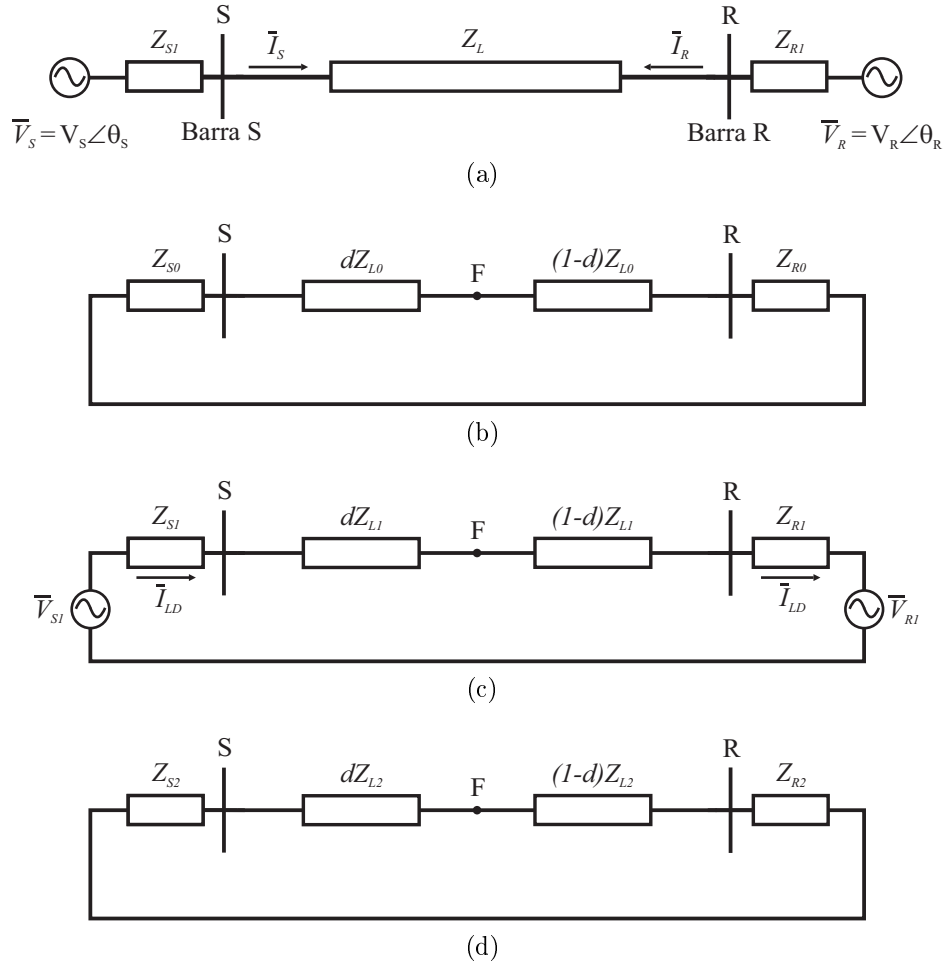


Figure D.1. Unifiliars diagrams. (a) Short line model. (b) Zero sequence diagram. (c) Positive sequence diagram. (d) Negative sequence diagram.

The equivalent impedances at the point of fault correspond to the parallel between Z_M and Z_N of the respective sequence circuits and can be calculated according to (D.4):

$$Z_0 = \frac{Z_{0M} \cdot Z_{0N}}{Z_{0M} + Z_{0N}} \quad Z_1 = \frac{Z_{1M} \cdot Z_{1N}}{Z_{1M} + Z_{1N}} \quad Z_2 = \frac{Z_{2M} \cdot Z_{2N}}{Z_{2M} + Z_{2N}} \quad (\text{D.4})$$

Equivalents are shown in Figure D.1. The connection between them depends on the type of short-circuit analyzed and allows the calculation of fault currents \bar{I}_{F1} , \bar{I}_{F2} and \bar{I}_{F0} at the fault location.

For steady state's evaluation of the fault, the voltage sources are removed and a current source, with a value identical to the fault current, is inserted in point F of each sequence circuit, resulting in the diagrams of Figura D.3.

In these circuits, identified by the superscript "CC", the contributions of each terminal to the pure fault current are represented. These components are calculated by current divider formula from the fault circuits of the Figura D.3. For this purpose, the current distributions

factors are shown in (D.5):

$$C_0 = \frac{Z_{0N}}{Z_{0M} + Z_{0N}} \quad C_1 = \frac{Z_{1N}}{Z_{1M} + Z_{1N}} \quad C_2 = \frac{Z_{2N}}{Z_{2M} + Z_{2N}} \quad (\text{D.5})$$

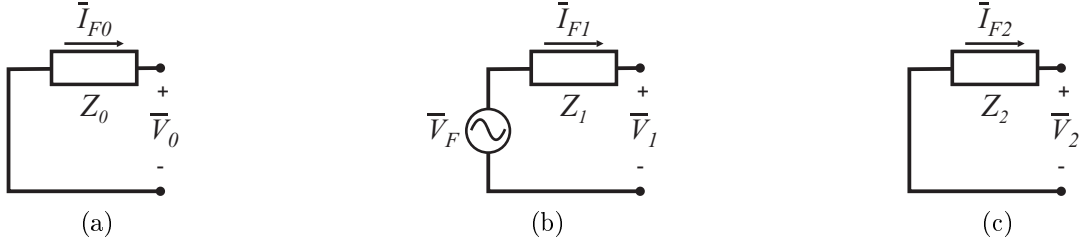


Figure D.2. Thévenin equivalents. (a) Zero sequence. (b) Positive sequence. (c) Negative sequence.

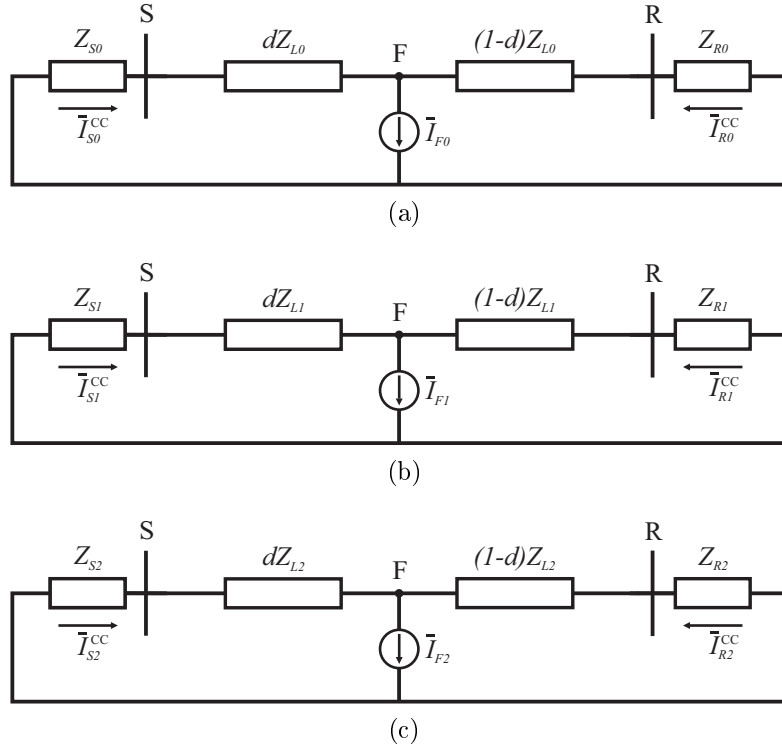


Figure D.3. Sequence circuits during a fault. (a) Zero sequence. (b) Positive sequence. (c) Negative sequence.

Thus, pure fault contributions are acquired according to (D.6):

$$\bar{I}_{S0}^{CC} = C_0 \cdot \bar{I}_{F0} \quad \bar{I}_{R0}^{CC} = (1 - C_0) \cdot \bar{I}_{F0} \quad (\text{D.6a})$$

$$\bar{I}_{S1}^{CC} = C_1 \cdot \bar{I}_{F1} \quad \bar{I}_{R1}^{CC} = (1 - C_1) \cdot \bar{I}_{F1} \quad (\text{D.6b})$$

$$\bar{I}_{S2}^{CC} = C_2 \cdot \bar{I}_{F2} \quad \bar{I}_{R2}^{CC} = (1 - C_2) \cdot \bar{I}_{F2} \quad (\text{D.6c})$$

The only pre-fault component corresponds to \bar{I}_{LD} , present only in the positive sequence of each terminal. Therefore, the total contribution of the positive sequence is the sum of these

two plots, while the remaining sequences are composed only of the missing portion, as shown in (D.7):

$$\bar{I}_{S0} = C_0 \cdot \bar{I}_{F0} \qquad \bar{I}_{R0} = (1 - C_0) \cdot \bar{I}_{F0} \qquad (\text{D.7a})$$

$$\bar{I}_{S1} = C_1 \cdot \bar{I}_{F1} + \bar{I}_{LD} \qquad \bar{I}_{R1} = (1 - C_1) \cdot \bar{I}_{F1} - \bar{I}_{LD} \qquad (\text{D.7b})$$

$$\bar{I}_{S2} = C_2 \cdot \bar{I}_{F2} \qquad \bar{I}_{R2} = (1 - C_2) \cdot \bar{I}_{F2} \qquad (\text{D.7c})$$

The conversion of the sequence contributions to the phase domain is done through the Fortescue transform, applying the transformation matrix [F] to the sequence currents, as indicated in (D.8):

$$\begin{bmatrix} \bar{I}_{SA} \\ \bar{I}_{SB} \\ \bar{I}_{SC} \end{bmatrix} = \begin{bmatrix} 1 & 1 & 1 \\ 1 & a^2 & a \\ 1 & a & a^2 \end{bmatrix} \cdot \begin{bmatrix} \bar{I}_{S0} \\ \bar{I}_{S1} \\ \bar{I}_{S2} \end{bmatrix} \qquad \begin{bmatrix} \bar{I}_{RA} \\ \bar{I}_{RB} \\ \bar{I}_{RC} \end{bmatrix} = \begin{bmatrix} 1 & 1 & 1 \\ 1 & a^2 & a \\ 1 & a & a^2 \end{bmatrix} \cdot \begin{bmatrix} \bar{I}_{R0} \\ \bar{I}_{R1} \\ \bar{I}_{R2} \end{bmatrix} \qquad (\text{D.8})$$

D.1 THREE-PHASE SHORT-CIRCUIT

The three-phase sequence fault currents are given by (D.9), in which the subscript 3φ indicates the three-phase short.

$$\bar{I}_{F1,3\varphi} = \frac{\bar{V}_F}{Z_1 + R_F} \qquad \bar{I}_{F2,3\varphi} = 0 \qquad \bar{I}_{F0,3\varphi} = 0 \qquad (\text{D.9})$$

Therefore, the contributions of each terminal result in (D.10):

$$\bar{I}_{S1} = C_1 \cdot \bar{I}_{F1,3\varphi} + \bar{I}_{LD} \qquad \bar{I}_{S2} = 0 \qquad \bar{I}_{S0} = 0 \qquad (\text{D.10a})$$

$$\bar{I}_{R1} = (1 - C_1) \cdot \bar{I}_{F1,3\varphi} - \bar{I}_{LD} \qquad \bar{I}_{R2} = 0 \qquad \bar{I}_{R0} = 0 \qquad (\text{D.10b})$$

Applying (D.8) to (D.10) leads to the three-phase phase currents presented in Tabela D.1.

Table D.1. Three-phase short-circuit Currents.

Currents at terminal S	Currents at terminal R
$\bar{I}_{SA} = C_1 \cdot \bar{I}_{F1,3\varphi} + \bar{I}_{LD}$	$\bar{I}_{RA} = (1 - C_1) \cdot \bar{I}_{F1,3\varphi} - \bar{I}_{LD}$
$\bar{I}_{SB} = a^2 C_1 \cdot \bar{I}_{F1,3\varphi} + a^2 \bar{I}_{LD}$	$\bar{I}_{RB} = a^2 (1 - C_1) \cdot \bar{I}_{F1,3\varphi} - a^2 \bar{I}_{LD}$
$\bar{I}_{SC} = a C_1 \cdot \bar{I}_{F1,3\varphi} + a \bar{I}_{LD}$	$\bar{I}_{RC} = a (1 - C_1) \cdot \bar{I}_{F1,3\varphi} - a \bar{I}_{LD}$

D.2 SINGLE-PHASE SHORT-CIRCUIT: AG

The single-phase sequence fault currents are given by (D.11), in which the subscript 1φ designates the monophasic fault.

$$\bar{I}_{F1,1\varphi} = \frac{\bar{V}_F}{Z_1 + Z_2 + Z_0 + 3R_F} \quad \bar{I}_{F2,1\varphi} = \bar{I}_{F1,1\varphi} \quad \bar{I}_{F0,1\varphi} = \bar{I}_{F1,1\varphi} \quad (\text{D.11})$$

In this way, the contributions of each terminal can be obtained from (D.12)

$$\bar{I}_{S1} = C_1 \cdot \bar{I}_{F1,1\varphi} + \bar{I}_{LD} \quad \bar{I}_{S2} = C_2 \cdot \bar{I}_{F1,1\varphi} \quad \bar{I}_{S0} = C_{01} \cdot \bar{I}_{F1,1\varphi} \quad (\text{D.12a})$$

$$\bar{I}_{R1} = (1 - C_1) \cdot \bar{I}_{F1,1\varphi} - \bar{I}_{LD} \quad \bar{I}_{R2} = (1 - C_2) \cdot \bar{I}_{F1,1\varphi} \quad \bar{I}_{R0} = (1 - C_0) \cdot \bar{I}_{F1,1\varphi} \quad (\text{D.12b})$$

Applying the Fortescue transformation to the (D.12), the monophasic phase currents presented in the Tabela D.2 are arrived at.

Table D.2. Single-phase short-circuit Currents.

Currents at terminal S
$\bar{I}_{SA} = (C_0 + C_1 + C_2) \cdot \bar{I}_{F1,1\varphi} + \bar{I}_{LD}$
$\bar{I}_{SB} = (C_0 + a^2C_1 + aC_2) \cdot \bar{I}_{F1,1\varphi} + a^2\bar{I}_{LD}$
$\bar{I}_{SC} = (C_0 + aC_1 + a^2C_2) \cdot \bar{I}_{F1,1\varphi} + a\bar{I}_{LD}$
Currents at terminal R
$\bar{I}_{RA} = (3 - C_0 - C_1 - C_2) \cdot \bar{I}_{F1,1\varphi} - \bar{I}_{LD}$
$\bar{I}_{RB} = [1 - C_0 + a^2(1 - C_1) + a(1 - C_2)] \cdot \bar{I}_{F1,1\varphi} - a^2\bar{I}_{LD}$
$\bar{I}_{RC} = [1 - C_0 + a(1 - C_1) + a^2(1 - C_2)] \cdot \bar{I}_{F1,1\varphi} - a\bar{I}_{LD}$

D.3 PHASE-TO-PHASE SHORT-CIRCUIT: BC

The two-phase fault sequence currents are calculated by means of (D.13), where the subscript $2, \varphi$ indicates the two-phase short.

$$\bar{I}_{F1,2\varphi} = \frac{\bar{V}_F}{Z_1 + Z_2 + R_F} \quad \bar{I}_{F2,2\varphi} = -\bar{I}_{F1,2\varphi} \quad \bar{I}_{F0,2\varphi} = 0 \quad (\text{D.13})$$

Then follows in (D.14) the contributions from each terminal:

$$\bar{I}_{S1} = C_1 \cdot \bar{I}_{F1,2\varphi} + \bar{I}_{LD} \quad \bar{I}_{S2} = -C_2 \cdot \bar{I}_{F1,2\varphi} \quad \bar{I}_{S0} = 0 \quad (\text{D.14a})$$

$$\bar{I}_{R1} = (1 - C_1) \cdot \bar{I}_{F1,2\varphi} - \bar{I}_{LD} \quad \bar{I}_{R2} = -(1 - C_2) \cdot \bar{I}_{F1,2\varphi} \quad \bar{I}_{R0} = 0 \quad (\text{D.14b})$$

Applying (D.8) to (D.14) gives the two-phase phase currents shown in Tabela D.3.

Table D.3. phase-to-phase short-circuit Currents.

Currents at terminal S
$\bar{I}_{SA} = (C_1 - C_2) \cdot \bar{I}_{F1,2\varphi} + \bar{I}_{LD}$
$\bar{I}_{SB} = (a^2 C_1 - a C_2) \cdot \bar{I}_{F1,2\varphi} + a^2 \bar{I}_{LD}$
$\bar{I}_{SC} = (a C_1 - a^2 C_2) \cdot \bar{I}_{F1,2\varphi} + a \bar{I}_{LD}$
Currents in terminal R
$\bar{I}_{RA} = (C_2 - C_1) \cdot \bar{I}_{F1,2\varphi} - \bar{I}_{LD}$
$\bar{I}_{RB} = [a^2(1 - C_1) - a(1 - C_2)] \cdot \bar{I}_{F1,2\varphi} - a^2 \bar{I}_{LD}$
$\bar{I}_{RC} = [a(1 - C_1) - a^2(1 - C_2)] \cdot \bar{I}_{F1,2\varphi} - 2\bar{I}_{LD}$

D.4 PHASE-TO-PHASE-TO-GROUND SHORT-CIRCUIT: BCT

The sequence currents for the phase-to-phase-to-ground fault are given by (D.15):

$$\begin{aligned}\bar{I}_{F1,2\varphi-T} &= \frac{\bar{V}_F}{Z_1 + \frac{R_F}{2} + [Z_2 + \frac{R_F}{2}] \cdot D} \\ \bar{I}_{F2,2\varphi-T} &= -\bar{I}_{F1,2\varphi-T} \cdot D \\ \bar{I}_{F0,2\varphi-T} &= -\bar{I}_{F1,2\varphi-T} \cdot (1 - D)\end{aligned}\tag{D.15}$$

where:

$$D = \frac{Z_0 + \frac{R_F}{2} + 3R_G}{Z_0 + Z_2 + 3R_G + R_F}\tag{D.16}$$

where R_G corresponds to the ground resistance, R_F to the resistance between the affected phases and the subscribed $2\varphi - T$ identifies the BCT fault. Thus, the contributions of each terminal result in (D.17).

$$\bar{I}_{S1} = C_1 \cdot \bar{I}_{F1,2\varphi-T} + \bar{I}_{LD} \qquad \bar{I}_{R1} = (1 - C_1) \cdot \bar{I}_{F1,2\varphi-T} - \bar{I}_{LD}\tag{D.17a}$$

$$\bar{I}_{S2} = -C_2 \cdot \bar{I}_{F1,2\varphi-T} \cdot D \qquad \bar{I}_{R2} = -(1 - C_2) \cdot \bar{I}_{F1,2\varphi} \cdot D\tag{D.17b}$$

$$\bar{I}_{S0} = -C_0 \cdot \bar{I}_{F1,2\varphi-T} \cdot (1 - D) \qquad \bar{I}_{R0} = -(1 - C_0) \cdot \bar{I}_{F1,2\varphi-T} \cdot (1 - D)\tag{D.17c}$$

Applying Fortescue's transform to (D.17), one arrives at the monophasic phase currents presented in Tabela D.4.

Table D.4. Biphasic-earth short current

Currents at terminal S	
\bar{I}_{SA}	$= [-C_0(1 - D) + C_1 - C_2D] \cdot \bar{I}_{F1,2\varphi-T} + \bar{I}_{LD}$
\bar{I}_{SB}	$= [-C_0(1 - D) + a^2C_1 - aC_2D] \cdot \bar{I}_{F1,2\varphi-T} + a^2\bar{I}_{LD}$
\bar{I}_{SC}	$= [-C_0(1 - D) + aC_1 - a^2C_2D] \cdot \bar{I}_{F1,2\varphi-T} + a\bar{I}_{LD}$
Currents at terminal R	
\bar{I}_{RA}	$= [-(1 - C_0)(1 - D) + (1 - C_1) - (1 - C_2)D] \cdot \bar{I}_{F1,2\varphi-T} - \bar{I}_{LD}$
\bar{I}_{RB}	$= [-(1 - C_0)(1 - D) + a^2(1 - C_1) - a(1 - C_2)D] \cdot \bar{I}_{F1,2\varphi-T} - a^2\bar{I}_{LD}$
\bar{I}_{RC}	$= [-(1 - C_0)(1 - D) + a(1 - C_1) - a^2(1 - C_2)D] \cdot \bar{I}_{F1,2\varphi-T} - a\bar{I}_{LD}$